Fortschritt-Berichte VDI

VDI

Reihe 3

Verfahrenstechnik

Dipl.-Ing. Christian Redepenning,
Aachen

Nr. 955

Pinch-based Methods for Absorption and Extraction Process and Solvent Screening

Pinch-basierte Methoden für Absorptions- und Extraktions-Prozess- und Lösungsmittelscreening

Pinch-based Methods for Absorption and Extraction Process and Solvent Screening

---

Pinch-basierte Methoden für Absorptions- und Extraktions-Prozess- und Lösungsmittelscreening

Von der Fakultät für Maschinenwesen der
Rheinisch-Westfälischen Technischen Hochschule Aachen
zur Erlangung des akademischen Grades
eines Doktors der Ingenieurwissenschaften
genehmigte Dissertation vorgelegt von

Christian Redepenning

Berichter: Universitätsprofessor Dr.-Ing. Wolfgang Marquardt
Universitätsprofessor Dr.-Ing. André Bardow

Tag der mündlichen Prüfung: 20.12.2017

Fortschritt-Berichte VDI

Reihe 3

Verfahrenstechnik

Dipl.-Ing. Christian Redepenning,
Aachen

Nr. 955

Pinch-based Methods for Absorption and Extraction Process and Solvent Screening

Pinch-basierte Methoden für Absorptions- und Extraktions-Prozess- und Lösungsmittelscreening

Redepenning, Christian
Pinch-based Methods for Absorption and Extraction Process and Solvent Screening
Pinch-basierte Methoden für Absorptions- und Extraktions-Prozess- und Lösungsmittelscreening
Fortschr.-Ber. VDI Reihe 3 Nr. 955. Düsseldorf: VDI Verlag 2018.
206 Seiten, 62 Bilder, 30 Tabellen.
ISBN 978-3-18-395503-9, ISSN 0178-9503,
€ 71,00/VDI-Mitgliederpreis € 63,90.

Keywords: shortcut method – extraction – absorption – rectification – process design – solvent screening – conceptual design

This thesis introduces shortcut methods for the conceptual design of absorption and extraction columns. The simplified design relies on the existence of so-called pinch points which indicate vanishing thermodynamic driving force in general counter-current devices, and therefore allow for direct conclusions on energy-efficient operation at minimum energy or solvent demand. In particular, this thesis introduces the first mathematically-sound description of the pinch-based model for general counter-current separation columns. Reliable solution procedures are introduced and implemented to solve the shortcut model in a fully automated manner. The potential of the novel methods is illustrated by three case studies. Several thousand of solvents are screened for absorption and extraction processes under the consideration of multiple separation units, heat-integration as well as optimization of the operating point.

Bibliographische Information der Deutschen Bibliothek
Die Deutsche Bibliothek verzeichnet diese Publikation in der Deutschen Nationalbibliographie; detaillierte bibliographische Daten sind im Internet unter www.dnb.de abrufbar.

Bibliographic information published by the Deutsche Bibliothek
(German National Library)
The Deutsche Bibliothek lists this publication in the Deutsche Nationalbibliographie (German National Bibliography); detailed bibliographic data is available via Internet at www.dnb.de.

D 82 (Diss. RWTH Aachen University, 2017)

ISSN 0178-9503
ISBN 978-3-18-395503-9

Vorwort

Die hier vorliegende Arbeit entstand während meiner Zeit von Januar 2011 bis Januar 2017 als wissenschaftlicher Mitarbeiter der Aachener Verfahrenstechnik - Prozesstechnik, der RWTH Aachen.
Mein Dank gilt zuerst meinem Doktorvater, Herrn Professor Dr.-Ing. Wolfgang Marquardt für die Förderung und Unterstützung in einer wechselhaften Zeit am Lehrstuhl. Besonders herausstellen möchte ich meinen Dank für seine gute Ideen, aber auch für viele kritische Fragen, welche diese Arbeit und mich besser gemacht haben.
Weiterhin danke ich Herrn Professor Dr.-Ing. André Bardow für die Übernahme des Konferats und die sehr bereichernde Zusammenarbeit mit ihm und seinem Team. Hervorheben möchte ich dabei die Unterstützung durch Kai Leonhard, Jan Scheffczyk und Christian Jens, ohne die diese Arbeit so nicht möglich gewesen wäre. Außerdem gilt mein Dank Professor Alexander Mitsos Ph.D. und seinem Team, wodurch mir die Transferphase vom Lehrstuhl für Prozesstechnik zur Systemverfahrenstechnik sehr leicht fiel.
Dankbar hervorheben möchte ich auch die Unterstützung von Dominik Bongartz, Tobias Ploch, Moll Glass, Adrian Caspari, Sebastian Recker, Mirko Skiborowski, Andreas Harwardt und Franca Janssen, welche mir Verbesserungsideen zu Manuskripten und Dissertation gegeben haben, oder stets für fachlichen Austausch herhielten und so zum Gelingen dieser Arbeit beitrugen. Arno Saxena hat mich geduldig in die Welt der Programmierung und Softwareentwicklung eingeführt, wofür ich ihm sehr dankbar bin. Dankbar betonen möchte ich auch die Unterstützung aller Studenten durch HiWi-Tätigkeiten und studentische Abschlussarbeiten. Besonderer Dank gilt dabei Lukas Mertens, Daniel Penner und Matthias Hoffmann für ihre Unterstützung. Danken möchte ich meinen Bürokollegen Arno Saxena, Moll Glass, Jennifer Puschke und Jeff Cumpston für eine angenehme Zeit.
Zuletzt gilt mein besonderer Dank meinen Eltern, Ulrike und Karl-Heinz, und meinen Brüdern, Robert und Felix.
Ich habe meine Zeit am Lehrstuhl nie als langweilige Büroarbeit empfunden. Für eine aufregende und großartige Zeit bin ich meinen Bürokollegen, Studenten, allen Mitarbeitern des Lehrstuhls, meinen Forschungspartnern, Professor Bardow, Professor Mitsos und Professor Marquardt sehr dankbar.

Aachen, im Sommer 2018 *Christian Redepenning*

Contents

Notation

Variables

A	absorption factor
C	total number of components
CC	cooling costs
e	eigenvector
h	enthalpy
HC	heating costs
K	phase equilibrium
M	additional stages
N	total number of stages
O	additional stages
OC	operating costs
S	stripping factor
SC	solvent costs
V	vapor flow rate
L	liquid flow rate
n	stage
p	pressure
p	set of pinch equations
Q	energy duty

T	temperature
u	set of variables
x	liquid composition
y	vapor composition
w	null vector

Greek letters

ε	small distance
γ	activity coefficient
λ	eigenvalue
μ	length of eigenvector
ν	length of eigenvector
ϕ	recovery factor
σ	desired purity of selected component
ξ	continuation variable

Superscripts

E	extract phase
L	liquid phase
R	raffinate phase
V	gaseous phase

Subscripts

A	absorption section
D	distillate
d	device

i	component
j	component
k	start of recurrence (stage number)
m	stage number
n	stage number
o	stage number
N	last stage
P	pinch
S	stripping section
1	first stage

Acronyms

DFG	German research foundation
BMFB	federal ministry of education and research
EnMS	energy management system
MESH	mass, equilibrium, summation, and enthalpy equations
MINLP	mixed integer non-linear programming
IPCC	intergovernmental panel on climate change
PSE	process systems engineering
TMFB	tailor-made fuels from biomass

Kurzfassung

In dieser Dissertation werden neue Näherungsverfahren für die Auslegung von Absorptions- und Extraktionskolonnen vorgestellt. Für die vereinfachte Auslegung wird ein energieeffizienter Betriebspunkt angestrebt, wofür sogenannte Pinch-Punkte herangezogen werden, die in Gegenstrom-Apparaten stets bei verschwindender thermodynamischer Triebkraft auftreten. Analogien zwischen Pinch-Punkten und sogenannten Fixpunkten nichtlinearer, dynamischer Systeme werden ausgenutzt, um erstmalig das Pinch-basierte Modell für allgemeine Gegenstromkolonnen mathematisch fundiert herzuleiten. Hieraus folgt dann konsequent die Anwendung für adiabate Absorptionskolonnen und isotherme Extraktionskolonnen. Die neuen Modelle weisen dabei einen kleineren Approximationsfehler auf als etablierte Näherungsverfahren, die nicht auf Pinch-Punkten beruhen. Außerdem erlaubt die hergeleitete mathematische Formulierung sogar die systematische Verbesserung der Schätzung bis zur Genauigkeit der rigorosen Lösung, womit ebenso der Übergang von der Pinch-basierten Schätzung zur rigorosen Lösung erstmalig aufgezeigt wird. Ein wesentlicher Baustein der neuen Methoden ist die automatisierte Auswertung durch die Entwicklung geeigneter Initialisierungsstrategien. Nicht nur Extraktions- und Absorptionskolonnen können so zuverlässig ausgewertet werden, sondern sogar komplexe Prozesse bestehend aus mehreren Trennapparaten unter Berücksichtigung von Wärmeintegration sowie Betriebspunktoptimierung. Das Potential der neuen Methoden wird anhand eines automatisierten Screenings von mehreren Tausend Lösungsmitteln für Absorptions- und Extraktionsprozesse veranschaulicht. Drei Fallstudien werden untersucht: Zwei Fallstudien behandeln Absorptionsprozesse, zum einen für die Abtrennung von Kohlenstoffdioxid und zum anderen für die Abtrennung von Dimethyl ether jeweils aus Gasgemischen, und eine Fallstudie einen Extraktionsprozess für die Abtrennung von Aceton, Butanol und Ethanol aus wässrigem Medium. Identifiziert werden neue, energieeffiziente Lösungsmittel und die zugehörigen optimierten Prozesse.

Abstract

This thesis introduces novel shortcut methods for the conceptual design of absorption and extraction columns. The simplified design relies on the existence of so-called pinch points which indicate vanishing thermodynamic driving force in general counter-current devices, and therefore allow for direct conclusions on energy-efficient operation at minimum energy or solvent demand. Analogies between pinch points and fixed points of non-linear dynamical systems are exploited to derive for general counter-current columns the first mathematically-sound description of a pinch-based model. The application to adiabatic absorption and isothermal extraction columns follows consequently. The novel pinch-based model shows a smaller deviation than established shortcut methods which do not rely on pinch points. In contrast to all existing shortcut methods, the mathematically sound formulation of the model even allows the systematic reduction of the approximation error to the accuracy of a rigorous model. The mathematically sound formulation also allows to systematically derive the rigorous solution from the pinch-based estimate. Key feature of the novel shortcut methods is the automated evaluation which is accomplished by tailored initialization procedures. Not only absorption and extraction columns can be evaluated in a fully automated manner, but even complex processes which combine multiple devices and involve heat-integration as well as optimization of the operating point. The potential of the novel methods is illustrated by screening thousands of solvents for absorption and extraction processes. Three case studies are investigated: Two absorption processes for the separation of carbon-dioxide and dimethyl ether from gaseous mixtures, as well as one extraction process for the separation of acetone, butanol, and ethanol from aqueous solution. Novel, energy-efficient solvents and their optimal process configurations are identified.

Chapter 1

Introduction

Energy efficiency is stimulating engineering research more and more. Today the obvious economic concern is amplified by the omnipresent effects of global warming. While the temperature increase has tripled in the last half of the past century (Hansen, 2006), predictions of the IPCC (Intergovernmental Panel on Climate Change) forecast a temperature rise between one and seven degree within this century (IPCC, 2007). The scientific evidence presented by the IPCC indicates overwhelmingly the responsibility of human industrialization which calls for immediate measures. Thus, if current prosperity is to be maintained, in order to reduce the overall energy consumption and resulting greenhouse gas emissions, energy efficiency is acknowledged as the most effective and economic lever to sustainably lower the effects of global warming (IPCC, 2007).

Worldwide, Germany has the seventh largest total primary energy consumption (data retrieved for 2014 from U.S. Energy Information Administration (2017)). While the largest consumers China and the United-States already require forty percent of the total worldwide primary energy demand, Germany is responsible for a share of up to three percent (cf. Figure 1.1). The latest study of the German Federal Statistical Office shows that the largest part of the German energy consumption is caused by its industry. The German chemical industries thereby account for the highest share of thirty-one percent of the industrial energy consumption (Statistisches Bundesamt, 30.10.2015). Obviously, the chemical industries have an urging demand for energy-efficiency innovations, and any improvement will directly have a significant impact on the overall German or even worldwide energy consumption.

In chemical engineering, there are two well acknowledged concepts to improve the en-

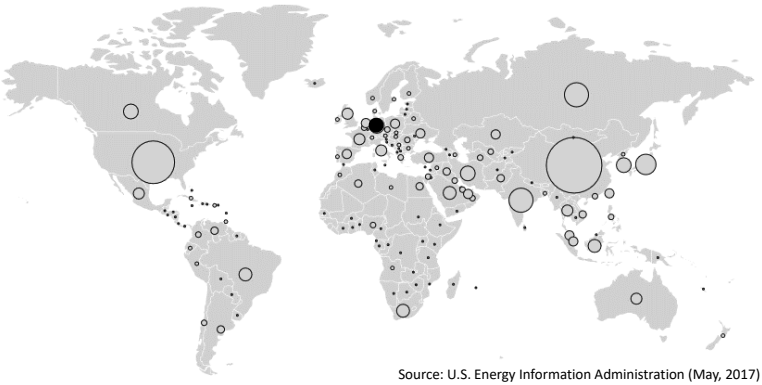

Figure 1.1.: Total primary energy consumption worldwide. Image and data retrieved from U.S. Energy Information Administration (2017). Size of circles represent the in energy consumption for each country.

ergy efficiency of a production process: Process analysis and process synthesis. In process analysis, existing processes are analyzed to find energetic bottlenecks and opportunities for improvement. In process synthesis, new processes are designed based on novel innovations in the fields of chemistry or engineering or based on renewable resources. Both concepts are complex. While the analysis problem can build on a given process structure and available data, often not every performance indicator can be measured directly and usually a large amount of data needs to be evaluated.. The synthesis of a new process is in general even more complex than process analysis because the best process structure to establish a dedicated purpose is unknown *a priori*. Thus, not only more than one alternative process option needs to be considered, but each of these alternatives needs to be analyzed to identify the best process option.

From a Process Systems Engineering (PSE) perspective, process analysis and process synthesis are related, because the analysis of existing processes is the inverse problem to the process synthesis of a novel process (cf. Klatt & Marquardt (2009)). Figure 1.2 illustrates the design approach for process analysis, which starts based on the actual chemical plant, and the inverse design approach for process synthesis, which starts from the separation task represented by desired products or available educts. A powerful tool to tackle both challenges, process analysis and process synthesis, is computer-aided design, which

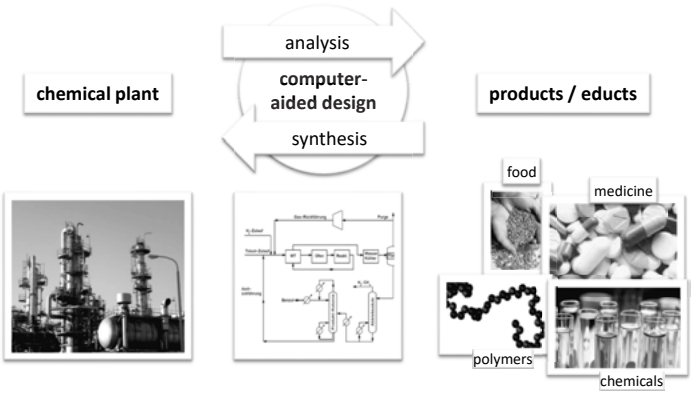

Figure 1.2.: Design approach for process analysis and process synthesis. Computer-aided process design contributes to the challenges of both approaches.

demands for tools or methods to predict appropriate performance targets and to allow for a preferably automated and computer-aided evaluation of the large amount of data or process alternatives.

As a consequence of the significance of chemical industries for Germany's overall energy consumption, the German government actively supports application and research on methods for process analysis and process synthesis. Examples are legal instruments which enforce the chemical industries to install Energy Management Systems (EnMSs) to monitor their energy consumption (ISO 50001, Bundesministerium für Umwelt, Naturschutz und Reaktorsicherheit (2012)), as well as research projects to overcome persistent challenges. Two projects motivated the research outlined in this work. The project Energy Efficiency Management funded by the Federal Ministry of Education and Research (BMBF) focused on new methodologies for process analysis, while the project Tailor-Made Fuels from Biomass (TMFB) funded by the German Research Foundation (DFG) as part of the German excellence initiative focused on process synthesis. The ambitions of these projects and their contribution to the fields of process analysis and synthesis are briefly summarized in the following.

The research project Energy Efficiency Management reviewed existing EnMSs (Bunse et al., 2011; Dörr et al., 2013; Drumm et al., 2013; Kicherer et al., 2007; Saling et al., 2002) and outlined improvements (Drumm, 2014). EnMSs allow to monitor the efficiency of a process by analyzing its energy consumption. Energy loss, e.g., between dynamic and

static operation, is observed and can enable immediate actions to minimize costs, increase competitiveness, and reduce waste or greenhouse gas emissions. While the actual energy demand of a process can be determined by on-line measurements, comparison between processes of different types is difficult, because a consistent reference is not established. Such a reference could be represented by operation at minimum energy demand. If the actual energy consumption is compared to the minimum energy demand of a process, direct conclusions on the energy efficiency are possible. Establishing minimum energy demand as a reference allows to compare processes of different types regarding their energy efficiency. However, while the actual operation at minimum energy demand is infeasible, minimum energy is difficult to measure in the analyzed process. Instead, computation by model-based computer-aided design tools is necessary.

The research project TMFB has the ambition to establish environmental viable fuel alternatives to compete with existing fossil-based fuel candidates (Marquardt et al., 2010). Despite all environmental advantages, a process for the new fuel candidate has to be at least equally or even more efficient than processes for existing fuel candidates in order to prevail. While existing processes have benefited from improvements for decades, e.g., through EnMS initiatives, the new processes directly have to exploit all potentials to be competitive, including sophisticated methods of heat integration, intensification of the process, and the selection of optimal solvents. Furthermore, for the design of a new, bio-based fuel, only soft constraints are available regarding possible educts or desired products, which have to meet certain environmentally friendly properties. This gives rise to a large number of alternative products, educts, and processes. Therefore, success of the TMFB research project is closely related to the development of an efficient strategy to cope with the large number of alternatives. Again, comparison of processes of different types by a consistent reference is required, which can suggest minimum energy demand for this purpose. However, for this classical problem of process synthesis, where many alternatives need to be compared, the challenge is not only about consistency of the reference, but also about efficiency of its computation, which needs to be simple to allow for a preferably automated and computer-aided evaluation.

Minimum energy demand, which is obviously an interesting performance target for both process analysis and synthesis, is related to vanishing thermodynamic driving force. The thermodynamic driving force, and this is one key point which carries throughout this thesis, vanishes in characteristic locations, which are referred to as pinch points. These pinch points can allow for direct conclusions on an operation at minimum energy demand. Instead of solving complex process models, the mere observation of the existence of pinch points can be sufficient for a full evaluation. As a consequence of this simplification,

pinch-based methods are not only an interesting reference, but their simple nature meets in particular the challenges of process analysis and synthesis where the automated evaluation of large amounts of process data or number of alternatives is demanded. However, despite these advantages, the current lack of appropriate pinch-based methods for most process devices still prevents their broad application.

The focus of this thesis is research on pinch-based methods and their application to popular industrial processes such as rectification, extraction, and absorption processes. Existing methods to overcome the challenges of process analysis and synthesis are covered by the research field of conceptual process design. Conceptual process design methods can range from simple heuristic rules for the identification of preliminary ideas up to complex optimization-based calculations using rigorous models. In order to illustrate relevance and value of pinch-based methods to the field of conceptual process design, existing methods are briefly reviewed in Section 1.1. The simple but thermodynamically valid nature of pinch-based methods can be a valuable link between first ideas generated by heuristic rules and detailed calculations. Such a framework, which acknowledges the potential of pinch-based methods, is discussed in Section 1.2. Shortcomings of existing pinch-based methods are touched. As a result of these shortcomings, scope of this thesis is defined in Section 1.3. Structure and outline follow in Section 1.4.

1.1 Conceptual process design

Process analysis and synthesis play an important role for the energy efficient design of chemical processes. The process analysis has to cope with large amount of data or highly integrated processes where complicated interactions need to be identified. In process synthesis the challenges of process analysis are amplified by the large number of alternatives which need to be compared. The large amount of data, the complicated interactions, as well as the large number of alternatives are just some of many strong arguments which urgently demand for systematic guidelines or frameworks to accomplish a successful conceptual process design.

Research on frameworks supporting a systematic and an expedient work-flow play an important role in conceptual process design. One comprehensive framework, which has inspired best practice in Process Systems Engineering, is represented by the hierarchical framework of Douglas (1985, 1988, 1995). Different levels of detail are introduced as illustrated in Figure 1.3. The design starts with fundamental decisions on dedicated educts, products, and type of operation (level 0), followed by the generation of a simple flowsheet structure (level 1 - level 4), towards a detailed, cost-optimal flowsheet covering sophis-

ticated methods of heat integration (level 5). Between the low and the high level, each additional level shows more and more details, and thus increases incrementally the complexity of the design problem. Similarly, the framework can be applied to process analysis by starting at a high level and following the inverse work-flow to identify, for example, energetic bottlenecks or process interactions.

The original framework of Douglas is very general and intended for the application to chemical processes of different types. Both experience and knowledge on state-of-the art methods strongly influence the outcome of the final design. There is, in fact, no guarantee that the final design is optimal. In order to constantly update existing guidelines with the state-of-the art methods, and in order to improve the outcome of the design, selected works address different challenges and innovations in the field of conceptual process de-

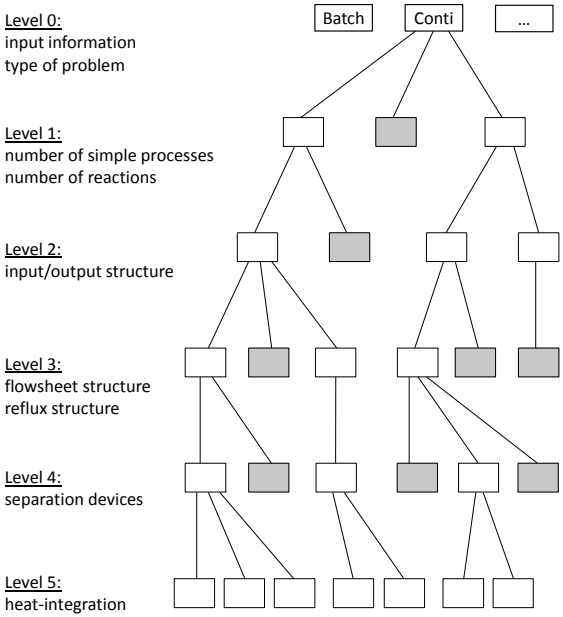

Figure 1.3.: Hierarchical framework of Douglas (1985, 1988, 1995). Different levels of detail are introduced: On a low level, process tasks are summarized and focus lies on their interactions. On a high level, the process is described in all its complexity to determine the performance. Adapted from Douglas (1988).

sign. Examples are the simultaneous optimization-based design of reaction and separation processes (Recker, Skiborowski, Redepenning & Marquardt, 2015), the synthesis of heat exchanger networks (Furman & Sahinidis, 2004; Morar & Agachi, 2010), the intensification of hybrid separation processes (Babi et al., 2016; Lutze et al., 2010; van Gerven & Stankiewicz, 2009), the efficient optimization of large and complex processes (Dowling & Biegler, 2015), the design of bio-refineries (Fatih Demirbas, 2009; Sanders et al., 2012; Yuan et al., 2013), or general recommendations for an energy-efficient design (Barnicki & Siirola, 2004; Grossmann & Guillén-Gosálbez, 2010; Siirola, 1996; Westerberg, 2004; Yuan & Chen, 2012). Pinch-based methods and their integration into conceptual process design is also addressed by the work of (Marquardt et al., 2008) which is discussed in detail in Section 1.2.

All conceptual design frameworks share in some way the idea of incremental refinement spanning from different levels of detail. Their goal is to identify, step-by-step, the best process alternative. Broadly speaking, three important steps can be isolated: The first step has to identify feasible and promising alternatives. Then, in the second step, an appropriate mathematical model needs to be derived to allow for a computer-aided evaluation. Finally, in the last step, different alternatives represented by, for example, different operating conditions or different process structures, need to be compared by modern optimization techniques. Each of these three steps, the identification of alternatives, the modeling of the process by rigorous models, and finally the performance assessment by optimization techniques requires dedicated methods which are briefly discussed in the following subsections.

1.1.1 Identification of alternatives

In the early phase of conceptual process design, identification of alternatives has a large impact on the outcome of the final design. Fundamental decisions on the general type of process, i.e., batch or continuous, or on the necessary unit operations and their interactions, are made in this phase (cf. Figure 1.3, level 0). Therefore, identification of alternatives is one of the most important and can as well be on of the the most creative tasks in conceptual process design demanding both experience and expert knowledge. As creativity is, of course, difficult to teach or train and a company can be naive if it solely relies on their own experts and their established knowledge, there are attempts to manifest experience and expert knowledge by guidelines and heuristic rules.

Prominent heuristic rules used for decision making are based on thermodynamic mixture properties which directly provide insights into a mixture and thus information on the

applicability of unit operations (Jaksland et al., 1995). Examples are the existence of miscibility gaps which is mandatory for liquid-liquid separations, boiling temperatures which indicate applicability of distillative separations, or presence of azeotropes which can in turn complicate distillative separations. These rules are summarized in decision diagrams and thereby contribute to an expedient design workflow (Barnicki & Fair, 1990, 1992).

Existing heuristic rules are available for all fields of chemical engineering. A comprehensive summary can be found in the book of Harmsen (2013). Dedicated rules address the selection of unit operations (Barnicki & Fair, 1990, 1992), the design of separation sequences (Nadgir & Liu, 1983; Rong, 2014), methods of heat integration (Dowidat et al., 2016; Umeda et al., 1979)), selection of solvents (Brunet & Liu, 1993), or case-based decision making (Pajula et al., 2001). The rapid improvements of computer technology fostered the development of intelligent systems (Stephanopoulos & Han, 1996), which is currently revitalized using artificial intelligence (AI) techniques (Mohd Ali et al., 2015).

Software applications are available to support decision making by heuristic rules, e.g., heuristics to support process design decisions, PROSYN®[1] (Kravanja & Grossmann, 1990, 1993), heuristics on the design of bio-processes, Jacaranda[2] (Steffens et al., 1999, 2000), or integration of property prediction and process design, ICAS[3] (Eden et al., 2002; Gani, 2004; Gani et al., 1997, 2005; Kongpanna et al., 2016).

One major limitation of guidelines and heuristic rules is that they can only provide a qualitative evaluation. Rules can contradict each other and under certain circumstances, exceptions may apply. For example, usually the low relative volatility of a component indicates an energy-intensive rectification, whereas in cases where a high product purity is desired, rectification could still be the best separation alternative. In fact, the full complexity of a separation device such as rectification cannot be captured by one single heuristic rule alone. As pointed out, competing or contradicting rules demand for multi-objective design, which ultimately demands careful balancing of these rules (Papadopoulos & Linke, 2006).

Hardly any design is developed without some expert knowledge, heuristic rule, or guideline to constrain the almost infinite number of alternative process options, configurations, or operating points. While superficiality by heuristic rules is appreciated in an early phase of the design where many alternatives are compared, there is always the risk that unconventional alternatives are discarded. In consequence, the quality of the final design strongly depends on truthfulness, precision, and careful application and combination of

[1] PROSYN®: www.process-design-center/prosyn.html
[2] Jacaranda: www.ucl.ac.uk/ ucecesf/jacaranda.html
[3] Integrated Computer Aided System: www.capec.kt.dtu.dk/Software/ICAS-and-its-Tools

heuristic rules, but accurate calculation of a performance target can only be accomplished using rigorous process models in a following step.

1.1.2 Rigorous models

The alternatives derived in early phases of conceptual process design need to be evaluated and compared based on calculations with accurate models. So-called rigorous models provide a detailed picture of a chemical process or device by an accurate modeling of the most important physical, chemical, and thermodynamic phenomena involved. So far, rigorous models are available for all types of unit operations, and, as recently pointed out in a review by Cremaschi (2015), over the past years these models have become one of the most important tools in conceptual process design.

A rigorous model usually describes all controlling phenomena by mass, equilibrium, summation, and enthalpy (MESH) equations (Kister, 2008). One complex task of the modeling process is the accurate thermodynamically-sound representation of phase equilibria. Usually, separations such as rectification, absorption, and extraction are influenced by transport limitations. Therefore, these separations ideally need to be described as mass-transfer rate-based operations, using what has become known as nonequilibrium or rate-based models (Mohanty, 2000; Taylor et al., 2003). Mass transfer phenomena can be described by different levels of complexity, starting with simple efficiencies up to the two-film diffusion model with Maxwell-Stefan correlations (Krishna & Wesselingh, 1997). Not only does this complex modeling usually require dedicated experiments, in addition detailed knowledge of the geometry of the final device is needed. Often, this effort cannot be afforded and is also not required in the early phase of conceptual process design. Instead, all diffusion-controlled phenomena are ignored which simplifies the modeling of the equilibrium and allows to delay the choice of the geometry of the device. Thermodynamic equilibrium is assumed for each separation stage by using so-called equilibrium-based models. Different types of equilibrium-based models are available, which as well allow for different complexity ranging from simple polynomials auch as the Porter equation up to complex molecularly-sound structure correlations such as PC-SAFT (see, e.g., Pfennig (2004); Poling et al. (2001)).

For the solution of rigorous models, all MESH equations are combined into a mathematical problem. The complexity of such a mathematical problem is indicated by the total number and non-linearity of the set of MESH equations. For example, the simple rectification column with N stages which can be used to separate a mixture with C components usually requires $N*(2*C+4)$ equations (Kister, 2008). Although the total number

of equations could be different depending on how the MESH equations are written, it is obvious that the number of stages and even more the number of components have a large impact on the complexity of such a problem. Therefore, separation devices with many stages for mixtures with many components quickly lead to complex mathematical problems with large sets of non-linear equations. Usually, these problems are then solved by local numerical algorithms which benefit from an accurate initial solution (Amaran et al., 2014). The systematic derivation of a sufficiently accurate initial solution is obviously important in order to successfully solve such a problem in a reasonably short period of time. However, only little work is available on the systematic initialization by appropriate solution procedures (Kim et al., 2010; Kossack et al., 2006). Therefore, the fully automated solution of such rigorous models is still not established.

Rigorous models are implemented in commercial process simulators such as AspenPlus®[1] or gPROMS®[2], CHEMCAD[3], or ChemSep[4], which allow to solve flowsheets with multiple separation and reaction units. Large chemical companies often have their own process simulator, e.g., VtPLAN at Covestro or CHEMASIM at BASF. The simulation engines can be applied directly to solve large flowsheets with many devices involving mixtures with many components and complex thermodynamics.

1.1.3 Optimization techniques

Competing alternatives are generally represented by different operating conditions as well as different flowsheet structures. The alternatives could be evaluated sequentially by enumeration, which is, for instance, established for the evaluation of zeotropic mixtures by rectification (Agrawal, 1996; Harwardt et al., 2008; Pleşu et al., 2015). Often, however, enumeration is not possible when iterative calculations are required or the number of combinations gets too high. Then, the problem can be mathematically formulated as a mixed integer non-linear programming (MINLP) problem (Grossmann & Ruiz, 2012; Trespalacios & Grossmann, 2014), where continuous variables can represent different operating conditions and integer variables refer to active or inactive flowsheet interconnections. Optimization-based approaches are applied to solve these problems, which draws the attention to problem formulation techniques (Grossmann, 2002; Trespalacios & Grossmann, 2014) as well as to available numerical optimization algorithms (Amaran et al., 2014).

Alternative flowsheet structures described by active or inactive interconnections are re-

[1] AspenPlus®: www.aspentech.com/products/engineering/aspen-plus
[2] gPROMS®: www.psenterprise.com/products/gproms
[3] CHEMCAD: www.chemstations.com
[4] ChemSep: www.chemsep.org

ferred to as superstructure (Barnicki & Siirola, 2004). Some prominent superstructure formulations are state-task networks, state-equipment networks, resource-task networks, generalized modular networks, unit-operation-port-stock networks, or group-contribution based networks (Cremaschi, 2015; Fahmi et al., 2014). Examples for superstructure formulations can be found throughout conceptual process design, e.g., for the optimal design of heat exchanger networks (Klemeš & Kravanja, 2013; Kong et al., 2016), for the optimal configuration of rectification columns (e.g., (Caballero, 2015; Kossack et al., 2006; Krämer et al., 2009)), for the identification of optimal process alternatives subject to heat integration (Caballero & Grossmann, 2014; Yang et al., 2012), for the identification of promising reaction pathways (Ulonska et al., 2016; Voll & Marquardt, 2012), for the identification of optimal heat exchanger networks (Chen et al., 2015), or for superstructure optimization of alternative process intensification techniques of a hybrid absorption-rectification process (Lee et al., 2016).

Algorithms are distinguished as to whether they provide a local or global search for an optimal solution. Local optimal solutions usually benefit from short calculation time but require good initial guesses to avoid accidentally finding non-optimal solutions (Floudas, 1999, 2000; Floudas et al., 2005; Kallrath, 2000, 2005; Viswanathan & Grossmann, 1990). Instead, globally optimal solutions can be guaranteed, e.g., by BARON[1] (Tawarmalani & Sahinidis, 2005) or ANTIGONE[2], (Misener & Floudas, 2014)), but large-scale non-linear problems demand tight bounds on the variables and usually involve high computational effort (Floudas et al., 2005). Solution with any of these approaches bears the risks that alternatives are excluded. With local algorithms, solutions may be excluded if the algorithm fails, which could not only be caused by actual infeasibility of the problem but also by inaccurate initial guesses. Global algorithms exclude alternatives, if too tight bounds are provided by the user whereas too wide bounds would result in too long calculation times. Alternatively, the combination of both types of algorithms with meta-heuristics in evolutionary or genetic algorithms has the potential to overcome some of these shortcomings (Grossmann & Biegler, 2004), however, bounds are still required and there is no guarantee that the globally optimal solution is identified. The limitations of all approaches fostered the development of novel multi-scale optimization techniques including approaches such as surrogate models (Henao & Maravelias, 2011) and derivative-free optimization (Caballero & Grossmann, 2008).

In conclusion, optimization techniques have the potential to identify the best design. However, the accuracy of an initial solution and the size of the problem have a strong

[1] branch-and-reduce optimization navigator
[2] algorithms for continous/integer global optimization of nonlinear equations

impact on both calculation time and reliability of the final solution. Therefore, careful pre-selection of promising alternatives, identification of an accurate initial solution, and determination of proper bounds is a crucial part of conceptual process design.

1.2 The pinch-based design approach

When reviewing the methods available for conceptual process design, there is no single method which can solve all problems associated with this task alone. A combination of methods for the generation of first ideas by heuristic rules and the final optimization with rigorous models is necessary. Methods for the generation of first ideas usually achieve low accuracy, but are easy to use. Rigorous models, on the other hand, can achieve good accuracy, but are difficult to solve. As the discrepancy regarding complexity and accuracy between heuristic rules and rigorous models is large, in order to bridge this gap in conceptual design, the application of shortcut methods, which are simple but provide reasonable accuracy, is promising.

A framework which acknowledges the potential of shortcut methods for an efficient ranking and pre-selection of alternatives envisaged by Marquardt et al. (2008) is depicted in Figure 1.4. The framework starts at the left with a given process task. In the first step, possible alternatives are generated by literature review, heuristics, or rules of thumb. The generated alternatives are then evaluated with the help of shortcut calculations in the second step. As the shortcuts already allow to determine a performance target, many alternatives can typically be discarded after the shortcut step. The results of the most promising alternatives are then exported to the optimization with rigorous models which finally determines the cost-optimal process.

Shortcut methods are central for this framework. Classical and well-known shortcut methods, such as the methods of Underwood (1949) or Kremser (1930), combine simplicity with a moderate level of detail which can otherwise only be provided by a rigorous model. The substantial drawback of these classical shortcut methods is, however, the uncertain quality of their approximation and thus resulting lack of confidence in their performance assessment. Alternatively, shortcut methods can be improved by introducing the pinch point. The pinch, which represents vanishing thermodynamic driving force, occurs in any counter-current device in case an infinite time for the heat and mass transport can be assumed, for instance represented by infinitely large heat-exchanger area or infinitely extended separation column sections. Vanishing thermodynamic driving force finally allows direct conclusions on the minimum energy demand representing a favorable operating point for many processes. As a consequence, the concept of pinch-based meth-

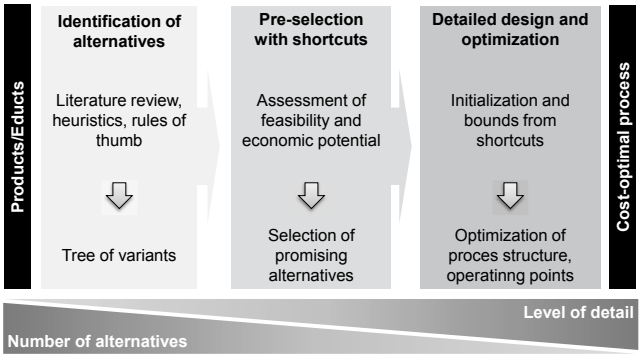

Figure 1.4.: Conceptual process design framework using shortcut methods. Figure adapted from Marquardt et al. (2008).

ods is well-known in conceptual process design, for example for the design of rectification columns (McCabe & Thiele, 1925) or heat exchanger networks (Linnhoff & Hindmarsh, 1983).

The concept of pinch-based methods in comparison to classical shortcut methods without a pinch and rigorous models is schematically illustrated for a general counter-current column section in Figure 1.5. According to classical shortcut methods, the separation behavior within one column section is approximated by correlations (Kremser, 1930), while only one set of MESH equations is used to balance the first and the last stage of each section. In a rigorous model, on the other hand, each stage is covered by the set of MESH equations (Kister, 2008). As a compromise, the pinch can serve as an additional sampling point for the shortcut calculation. When using one additional stage, the pinch-based shortcut approximation can be expected to improve the estimation which is also reported in multiple studies (Bausa, 2001; Brüggemann & Marquardt, 2011b; Harwardt, 2013). On the other hand, the pinch-based model is still simple compared to the rigorous model, because only two sets of MESH equations are required, one set to balance the pinch and one set to balance the first and the last stage. Therefore, regarding simplicity and accuracy, the compromise offered by pinch-based shortcut methods complements perfectly with the tasks of conceptual process design in Figure 1.4 where accurate but simple methods are needed to evaluate a large number of alternatives and make strategic design decisions.

An overview on the most sophisticated pinch-based shortcut methods for rectification, extraction, and absorption, is given in Table 1.1. For rectification columns, the most ad-

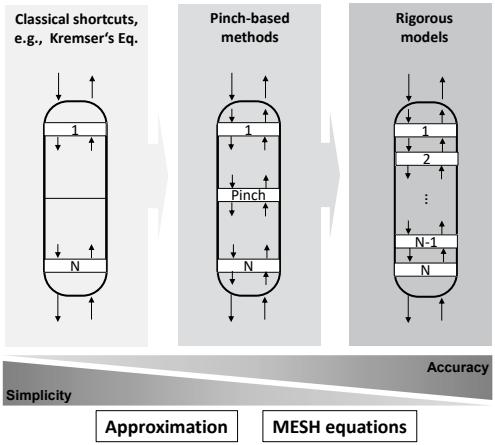

Figure 1.5.: Pinch-based shortcut compared to classical shortcut without a pinch and rigorous model for a counter-current column. The pinch serves as additional sampling point which improves the calculation. A good compromise regarding simplicity and accuracy can be expected.

vanced method is the rectification body method (RBM, Bausa et al. (1998)). There are other alternative pinch-based methods available for rectification columns and a brief review can be found in Chapter 4.1.3. However, only the RBM combines both a simple approximation concept with a systematic solution strategy. The RBM has also been extended to rectification coupled with decantation (Bausa & Marquardt, 2000), rectification with sidestreams (von Watzdorf et al., 1999), complex rectification columns (von Watzdorf et al., 1999), rectification coupled with reaction (Lee et al., 2003), extractive rectification columns (Brüggemann & Marquardt, 2004), and batch distillation columns (Espinosa et al., 2005).

The RBM and similar methods for rectification columns only require the complete specification of all feed and product streams, and then allow to estimate the minimum energy demand for arbitrary mixtures. No limitation regarding number of components or thermodynamic property modeling is necessary. In contrast, pinch-based methods for extraction or absorption columns are not only hard to find, but assume simplifications of the thermodynamic behavior and are effectively limited to ternary mixtures. A detailed discussion on existing shortcut methods for absorption columns is provided in Chapter 2 and for extrac-

Table 1.1.: Representative pinch-based shortcut methods for the design of rectification, extraction, and absorption columns.

unit operation	literature	limitation
rectification	Bausa et al. (1998)	• full specification of outlet compositions required • heuristic detection of tangential pinch points
extraction	Minotti et al. (1998), Hunter & Nash (1935)	• ternary mixtures • isothermal
absorption	Kister (2008)	• ternary mixtures • no condensation of gas carrier and solvent condensation

tion columns in Chapter 3. In short, for extraction columns there is the graphical method of Hunter & Nash (1935) which assumes an isothermal separation and an algebraic interpretation has been presented by Minotti et al. (1998). While the assumption of an isothermal separation is mostly valid for liquid-liquid extraction, in gas-liquid separations such as absorption often a strong temperature gradient is observed. In order to consider a temperature gradient along the column section but still allow for a graphical interpretation, condensation of the carrier gas and evaporation of the solvent can be ignored (Kister, 2008), which is, however, often inaccurate.

The limitations of pinch-based methods for devices other than rectification columns can be surprising at first sight. After all, the column sections for rectification, absorption, and extraction columns are described by a similar set of MESH equations which should therefore allow for a similar approximation. The reasons, however, which explain why the promising concept of the RBM has not been transferred to other devices such as extraction and absorption can be found in persistent limitations of the RBM. When reviewing the RBM closely, two shortcomings can be isolated which have both still not been resolved: The detection of tangential pinch points, and the necessary definition of outlet compositions prior to the calculation.

Tangential pinch points are a frequent phenomena caused by non-ideal thermodynamics

which can occur in both rectification as well as extraction and absorption separations. Although there exists an algebraic approach to model tangential pinch points by bifurcation analysis (Levy & Doherty, 1986), the RBM employs heuristic rules to avoid the complicated modeling procedure. In the original contribution, Bausa et al. (1998) suggested an angle criterion which was improved later in the thesis of Brüggemann (2005) by a so-called pinch reachability check. A model-based integration of the tangential pinch into the RBM, for example by bifurcation analysis, has not yet been considered.

Outlet compositions need to be fully specified for the application of the RBM in order to determine minimum energy demand. In contrast, when using a rigorous model, all outlet compositions are calculated. A degrees of freedom analysis of the rigorous model of a rectification column (cf. Doherty (2008)) and the RBM reveals that for a mixture with C components the RBM requires $C-2$ specifications in addition to the specifications required by a rigorous model. Thus, the separation task approximated by the RBM inherently demands overspecification when mixtures with more than two components are investigated. As a consequence, the user has to choose outlet compositions which have to agree with both the assumption of an infinite number of stages and with the approximated minimum energy demand. If, however, the user chooses outlet compositions which disagree with any of these assumptions, then large deviations in the predicted minimum energy demand may result as illustrated in the thesis of Skiborowski (2015).

For the estimation of feasible outlet compositions, the RBM can be combined with so-called feasibility tests. The most prominent tests include the method of Rooks et al. (1998), an interpretation of the ∞/∞-analysis as suggested by Ryll et al. (2012), and the method for the calculation of the pitchfork distillation boundary (PDB) by Brüggemann & Marquardt (2011a). All these methods assume an infinite number of stages which agrees with the assumption of a pinch-based shortcut such as the RBM. On the other hand, a different energy demand is assumed which, however, only has an influence if the composition of the outlets are in fact controlled by the employed energy demand. For all zeotropic and most azeotropic separations, the outlets are not controlled by the employed energy demand and these feasibility tests therefore provide identical and accurate results. Only in case of azeotropic mixtures with separation boundaries, the outlet compositions are in fact controlled by the employed energy demand (Widagdo & Seider, 1996). The method of Rooks et al. (1998) and the ∞/∞-analysis assume an infinitely large energy demand, and the PDB a low energy demand defined by the presence of a pitchfork bifurcation. In conclusion, when outlet compositions are controlled by the employed energy demand, none of the existing feasiblity tests accurately predicts feasible outlet compositions and their estimations can in consequence lead to the large deviations in the predicted minimum

energy demand by the RBM (cf. Skiborowski (2015)).

These two shortcomings are also relevant for the pinch-based design of absorption and extraction columns. Tangential pinch points are frequently occurring phenomena in extraction and absorption systems, and identical with the impact of the energy demand on outlet compositions for rectification, for extraction and absorption the solvent flow rate always has an impact on outlet compositions. The heuristic rules or work-arounds developed over the past decades for the design of rectification columns have apparently been impossible to apply for the design of absorption and extraction columns, because according to the summary of pinch-based methods in Table 1.1 existing pinch-based methods for extraction and absorption are limited to ternary mixtures and simplified thermodynamic modeling. Hence, there is a need to first establish a consistent pinch-based model for general counter-current column sections. A mathematically-sound model has to inherently cover tangential pinch points, determine outlet compositions, and finally has to apply to all types of counter-current separations.

1.3 Scope of this thesis

Pinch-based shortcut methods are well-known tools for the conceptual process design. While in the last decades most research efforts on pinch-based methods have focused on the design of rectification columns, some limitations remained unsolved such as the detection of tangential pinch points and the the calculation of outlet compositions without any heuristic rule or work around. In consequence, the extension of pinch-based methods to different fields of application stagnated, and shortcut methods for the design of absorption or extraction columns are limited to ternary mixtures and simplified thermodynamic modeling. All of these limitations can be related to the lack of a consistent pinch-based model for general counter-current separation columns.

Ambition of this thesis is to derive a consistent pinch-based model for general counter-current columns. Such a model has the potential to overcome existing shortcomings. Furthermore, the novel model has the potential to provide valuable insight to assess and reduce the inaccuracy inherently caused by the applied simplification. Such a concept, which is not accomplished for any type of shortcut method, could close the gap in conceptual process design between shortcut estimation and rigorous calculation. The model is investigated for case studies from adiabatic absorption and isothermal extraction. For theses case studies, the shortcut method can serve as a screening tool, which, according to the challenges associated with the application of shortcut methods in conceptual process design, demands for automated evaluation. To this end, this work investigates solution procedures

which provide a solution to the pinch-based models in a fully automated manner.

Nowadays, process alternatives are often evaluated by using heuristic rules because these rules allow for an automated evaluation. While the envisaged solution procedures for pinch-based methods could directly allow for an automated screening of single separation devices, their combination with existing pinch-based methods for rectification columns and heat-integration leads to a screening of complex separation processes, which is highlighted in this thesis. In conclusion, this thesis envisions a pinch-based screening for absorption and extraction processes which can only be accomplished by a consistent pinch-based model and its reliable automation.

1.4 Outline and structure

Chapter 2 begins with a comparison of classical shortcut methods and rigorous models for the conceptual design of absorption columns. As a consequence of the identified shortcomings, a novel pinch-based model is derived for general adiabatic counter-current columns. The model covers rigorous thermodynamics. No simplifications regarding phase equilibrium, heat effects, or the number of components are required. Tangential pinch points and the states of all outlet streams are simultaneously covered when calculating an operation at minimum solvent demand. Classical shortcut predictions without accounting for a pinch are significantly outperformed by the novel shortcut model, which – in addition – can be gradually refined to any desired accuracy. Integration into a stepwise procedure results in reliable solutions. The performance of the procedure in terms of speed and prediction quality is highlighted by screening several thousands of solvent candidates for two case studies with up to seven components.

The novel pinch-based model for adiabatic absorption carries over to isothermal extraction columns. In Chapter 3, existing shortcut methods and their limitations for the conceptual design of extraction columns are reviewed, before the modifications of the novel pinch-based model are discussed. While existing pinch-based models for extraction columns are limited to ternary mixtures, the novel model has no constrains regarding the number of components, it is more accurate than shortcut methods without a pinch, and it even allows the gradual reduction of deviation caused by the prediction error to any degree of desired accuracy. The stepwise solution procedure takes into account the constrains of isothermal liquid-liquid separations. The pinch-based screening of several thousands of solvent candidates for two case-studies validates the performance of the novel method.

While existing methods for the screening of solvents for absorption and extraction rely

on thermodynamic properties such as the activity coefficients at infinite dilution, the novel pinch-based shortcut methods allow for a screening based on the performance of the actual separation device. In Chapter 4, existing pinch-based methods for rectification columns and heat integration are combined with the novel pinch-based methods for absorption and extraction. The pinch-based methods perfectly complement, and thus allow for a comprehensive flowsheet evaluation based on minimum energy demand. Three case studies are investigated: Two absorption processes, one for the absorption of carbon-dioxide and the other for the absorption of dimethyl ether, and one extraction process for the recovery of aceton, butanol, and ethanol from aqueous solution. Several thousands of solvents are screened, and novel solvents are selected based on optimized process performance.

Chapter 5 introduces the software architecture developed during this work. The new prototypes for the pinch-based design of absorption and extraction columns are integrated into an existing software framework for the thermodynamic analysis and the pinch-based design of rectification columns. The methods can be conveniently accessed from MATLAB or C♯ to allow for further application. Recommendations for further research are given in Chapter 6. Conclusions are finally presented in the last Chapter 7.

1.5 Previous publication of results

The results discussed in this thesis originate from the research performed by the author at Aachener Verfahrenstechnik – Process Systems Engineering, RWTH Aachen University. The following results related to this thesis have been published previously by the author and his colleagues:

- Parts of the pinch-based shortcut method for adiabatic absorption columns discussed in Chapter 2 have been published by Redepenning & Marquardt (2016) in the *American Institute of Chemical Engineers Journal*.
- Parts of the pinch-based shortcut method for isothermal extraction columns discussed in Chapter 3 have been published by Redepenning, Recker & Marquardt (2016) in the *American Institute of Chemical Engineers Journal*. The journal contribution generalizes previous work published by Redepenning, Skiborowski & Marquardt (2013) as a conference proceedings in the book series *Computer Aided Chemical Engineering*.
- The results discussed in Chapter 4 build on a software framework for the estimation of thermodynamic property parameters which is part of a joint cooperation with the Chair of Technical Thermodynamics, RWTH Aachen University. Parts of the

method have been described by Scheffczyk, Redepenning, Jens, Winter, Leonhard, Marquardt & Bardow (2016b) in the *Chemical Engineering Research and Design*.

- On the integration of nonequilibrium modeling and pinch-based shortcut methods in Chater 6.3 an extended abstract published by Redepenning, Penner & Marquardt (2014) is available in *Chemie Ingenieur Technik*.

Chapter 2

Pinch-based shortcut method for the design of adiabatic absorption columns

Absorption processes are a mature technology routinely employed in the chemical industries for the separation of gaseous mixtures. Usually, absorption processes combine two separation columns. In the first column, a solvent absorbs one or more solutes selectively from a gaseous feed mixture, while in the second column solutes are separated from the solvent, which is recycled to the absorption column (Kister, 2008).

The design of an absorption process involves the identification of optimal operating conditions such as pressure, temperature, number of separation stages, and optimal solvent. In general, the performance of both the absorption and desorption column must be taken into account during the conceptual design of an absorption process. Superstructure optimization, where a mixed-integer non-linear programming (MINLP) problem covers all alternatives and operating points, has the potential to determine the optimal design directly (Dowling & Biegler, 2015; Trespalacios & Grossmann, 2014). However, large superstructures are still challenging to solve efficiently and reliably with today's optimization algorithms (Amaran et al., 2014).

Alternatively, in the early phase of conceptual process design, when many alternative processes (Marquardt et al., 2008), solvents (Burger et al., 2015), and operating points (Peschel et al., 2012) need to be compared, often representative performance indicators are attractive for a comparison. Since the vaporization of the solvent in the solvent recovery column mostly determines the energy demand of the process, operation at minimum solvent demand represents a favorable operating point.

For the calculation of minimum solvent demand, two techniques are employed in engineering practice: A rigorous model is solved with a sufficiently large number of stages modeled by mass, equilibrium, summation, and enthalpy (MESH) equations (Köhler et al., 1995). This approach can be computationally demanding when many stages are necessary and mixtures with many components are investigated. Alternatively, shortcut calculations are applied, but the approximating nature of any shortcut method causes inaccuracies.

In the next section, a comparison of existing techniques for the calculation of minimum solvent demand motivates the need for a novel shortcut model, which is derived subsequently. The novel shortcut model is then discussed for several distinctive modes of operation. A step-by-step solution procedure establishes quick and reliable determination of a model solution. Applicability is demonstrated by a fully automated screening of thousands of solvent for industrial examples with up to seven components. Conclusions are finally given in the last section.

2.1 Comparison of rigorous and established shortcut model

Shortcut methods for the calculation of minimum solvent demand have been available for a long time. One of the first and still relevant method was proposed by Kremser (1930). As the accuracy of shortcut methods can be poor, rigorous models are often preferred. Rigorous models are, however, not the best choice in the early phase of conceptual design when quick and robust calculations are desirable (Marquardt et al., 2008).

To review existing techniques, the separation of ethylene-oxide (EO) from argon (AR) with water (W) used as a solvent serves as an illustrating case study. Usually, the interfacial mass transfer is kinetically controlled. Such transport limitations are, however, strongly influenced by diffusion phenomena, which can only be described by complex rate-based models fitted to dedicated experimental data. This effort can often not be justified in the early phase of conceptual process design. Alternatively, equilibrium-based models are employed in this work. The distribution coefficient is modeled by Henry's law for argon and Antoine's extended equation for ethylene-oxide and water. Non-ideality of the binary mixture of ethylene-oxide and water is covered by activity coefficients described by the NRTL model (cf. Appendix B for a summary of model equations). Reactions such as the hydration of ethylene-oxide to ethylene glycol are ignored. The mixture and type of split are chosen such that all operating points required for the discussion can be applied.

2.1.1 Rigorous model

A schematic of an isobaric and adiabatic absorption column is illustrated in Figure 2.1. In the counter-current arrangement, the gaseous feed (V_{N+1}) and the lean solvent (L_0) enter the column on opposite ends. The liquid (L) and gaseous (V) streams, which are described by flow rates (L or V), compositions ($\mathbf{x}$ or $\mathbf{y}$), and temperatures (T) for each stage (n) flow in opposite directions. In a rigorous model (cf. Kister (2008)), the set of MESH equations for all separation stages (N) and components (C) can be written as an implicit stage-to-stage recurrence:

$$\begin{aligned} 0 &= L_0 x_{0,i} + V_{n+1} y_{n+1,i} - V_1 y_{1,i} - L_n x_{n,i}, \\ &\qquad i = 1,...,C, \quad n = 1,...,N, \end{aligned} \tag{2.1}$$

$$0 = y_{n,i} - K_{n,i} x_{n,i}, \qquad i = 1,...,C, \quad n = 1,...,N, \tag{2.2}$$

$$0 = 1 - \sum_{i=1}^{C} x_{n,i}, \qquad n = 1,...,N, \tag{2.3}$$

$$0 = 1 - \sum_{i=1}^{C} y_{n,i}, \qquad n = 1,...,N, \tag{2.4}$$

$$\begin{aligned} 0 &= L_0 h_0^{\mathrm{L}} + V_{n+1} h_{n+1}^{\mathrm{V}} - V_1 h_1^{\mathrm{V}} - L_n h_n^{\mathrm{L}}, \\ &\qquad n = 1,...,N. \end{aligned} \tag{2.5}$$

The distribution coefficients ($\mathbf{K}_n$) and the enthalpies of the liquid and gaseous phases (h^{L}, h^{V}) are functions of compositions, pressure, and temperature,

$$\begin{aligned} K_{n,i} &= f(\mathbf{x}_n, \mathbf{y}_n, p, T_n), \\ &\qquad i = 1,...,C, \quad n = 1,...,N, \end{aligned} \tag{2.6}$$

$$h_n^{\mathrm{L}} = f(\mathbf{x}_n, p, T_n), \qquad n = 0,...,N, \tag{2.7}$$

$$h_n^{\mathrm{V}} = f(\mathbf{y}_n, p, T_n), \qquad n = 1,...,N+1. \tag{2.8}$$

which are given by appropriate thermodynamic models. In principle, any thermodynamic model can be employed when appropriate data are available.

Finally, the required solvent to feed ratio can be calculated, if one additional specification, e.g., the desired purity of one solute in the product gas, σ, is specified

$$y_{1,j} = \sigma, \qquad j \in \{1,...,C\}. \tag{2.9}$$

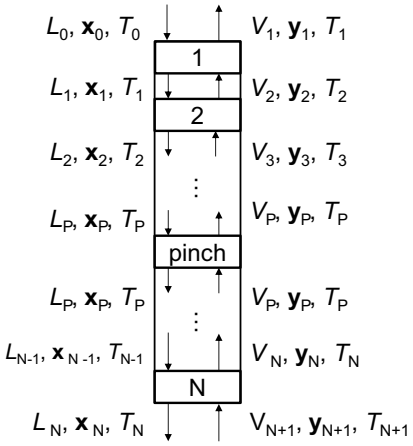

Figure 2.1.: Schematic of an adiabatic counter-current absorption column. Rigorous calculation is based on a finite number of separation stages N, while minimum solvent demand involves an infinite number of stages ($N = \infty$).

Table 2.1.: Specifications for the illustrating case study. Adiabatic and isobaric absorption at 10 MPa is assumed. The desired purity of ethylene-oxide in cleaned gas is set to 1 mol-%.

concentration	$\mathbf{y}_{N+1}$	$\mathbf{x}_0$	temperature	
argon	0.5	0	T_0	373K
ethylene-oxide	0.5	0	T_{N+1}	373K
water	0	1		

Table 2.1 provides a set of specifications for the illustrating case study. Pressure, compositions and temperatures of both the feed and the solvent streams are given. The desired purity of ethylene-oxide in the cleaned gas is set to $y_{1,\mathrm{EO}} = 1$ mol-%, and $N = 20$ separation stages are found to be sufficient to properly approximate minimum solvent demand with the RADFRAC separation module of AspenPlus®.

Figure 2.2 shows the vapor compositions of the stage-to-stage recurrence in a ternary diagram (left) and along the column (right). Between separation stages 9 and 19 the com-

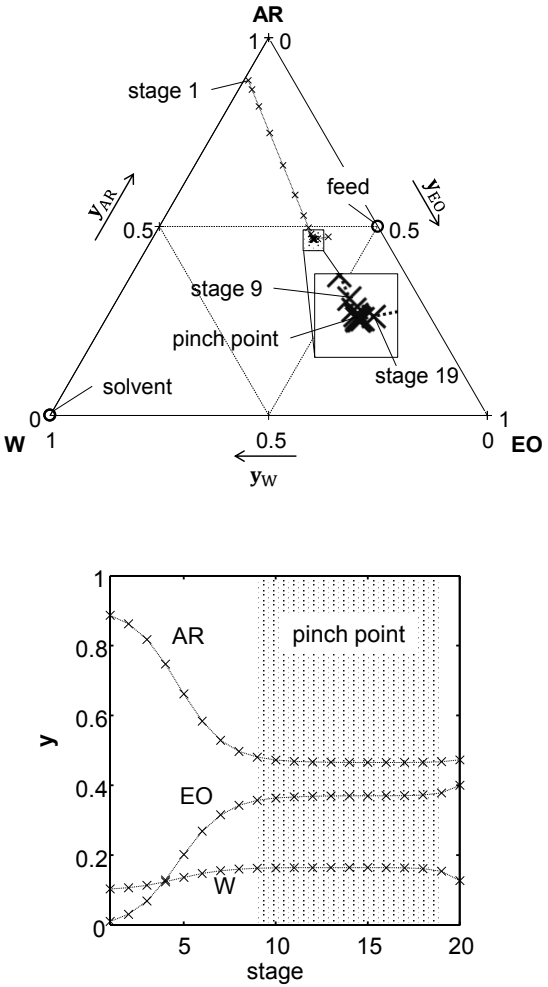

Figure 2.2.: Stage-to-stage recurrence with vapor compositions (**y**) in ternary diagram (top) and along the column (bottom). The existence of a pinch indicates minimum solvent demand.

positions are almost constant. This zone, where thermodynamic driving force is low, indicates a pinch. The existence of a pinch is a well-known indicator for minimum solvent operation (Köhler et al., 1995).

Minimum solvent operation requires an infinite number of separation stages (Köhler et al., 1995). Only a sufficiently large number of separation stages allow to predict minimum solvent operation with sufficient accuracy. The rigorous model is therefore not only incapable of the rigorous prediction of minimum solvent operation, but also comes along with other well-known difficulties: If a mixture with many components or complex thermodynamic behavior is considered, and if only inaccurate initial guesses are available, the solution of the rigorous model can be difficult. Moreover, for the calculation of minimum solvent demand, many stages must be considered which increases the number of equations and hence the computational effort. Alternatively, shortcut calculations can be considered to overcome these drawbacks.

2.1.2 Established shortcut models

Shortcut models in general intend to simplify the set of MESH equations by some approximation. To this end, Kremser (1930) introduced recovery factors ($\phi_{\mathrm{A},i}$, $\phi_{\mathrm{S},i}$) to approximately relate the states of the first and the last stage by the overall mass balances,

$$\begin{aligned} 0 = {} & L_0 x_{0,i}(1-\phi_{\mathrm{S},i}) + V_{\mathrm{N}+1} y_{\mathrm{N}+1,i}\phi_{\mathrm{A},i} \\ & - V_1 y_{1,i} - L_{\mathrm{N}} x_{\mathrm{N},i}, \\ & i = 1,...,C-1. \end{aligned} \tag{2.10}$$

The principle assumption for this type of shortcut model is that the recovery factors can be described by so-called absorption and stripping factors ($\tilde{A}_i$, $\tilde{S}_i$),

$$\phi_{\mathrm{A},i} = \frac{\tilde{A}_i - 1}{\tilde{A}_i^{\mathrm{N}+1} - 1}, \qquad i = 1,...,C-1, \tag{2.11}$$

$$\phi_{\mathrm{S},i} = \frac{\tilde{S}_i - 1}{\tilde{S}_i^{\mathrm{N}+1} - 1}, \qquad i = 1,...,C-1, \tag{2.12}$$

which are defined as

$$\tilde{A}_i = A_{n,i} = \frac{L_n}{K_{n,i} V_n}, \qquad i = 1,...,C-1, \tag{2.13}$$

$$\tilde{S}_i = S_{n,i} = \frac{1}{A_{n,i}}, \qquad i = 1,...,C-1. \tag{2.14}$$

For an infinite number of stages, the recovery factors simplify to

$$\phi_{\mathrm{A},i} = \begin{cases} 0, & \tilde{A}_i \geq 1, \\ 1-\tilde{A}_i, & \tilde{A}_i < 1, \end{cases} \qquad i = 1,...,C-1, \tag{2.15}$$

$$\phi_{\mathrm{S},i} = \begin{cases} 0, & \tilde{S}_i \geq 1, \\ 1-\tilde{S}_i, & \tilde{S}_i < 1, \end{cases} \qquad i = 1,...,C-1. \tag{2.16}$$

For non-negligible heat-effects, Edmister (1957) modified the absorption and stripping factors by introducing averages between the first and the last stage:

$$\tilde{A}_i = \sqrt{A_{\mathrm{N},i}(A_{1,i}-1)+0.25}-0.5, \quad i = 1,...,C-1, \tag{2.17}$$

$$\tilde{S}_i = \sqrt{S_{\mathrm{N},i}(S_{1,i}-1)+0.25}-0.5, \quad i = 1,...,C-1. \tag{2.18}$$

Alternative averaging functions were proposed recently by Bahadori & Vuthaluru (2010). The equation of Kremser (1930) has received attention for the evaluation of complex column configurations (Kamath et al., 2010) and the assessment of hybrid absorption-desorption processes (Notz et al., 2011).

The established shortcut model for absorption columns relies on the correlations of Kremser (1930) and Edmister (1957). It combines the approximations (2.10), (2.15)-(2.18), and the MESH equations (2.1), (2.5) for $n = \mathrm{N}$, (2.2)-(2.4) for $n = 1$ and $n = \mathrm{N}$ to relate feed, solvent, and outlet streams. One design specification, i.e., the desired purity of the solute, is provided by Eq. (2.9) in addition.

Table 2.2 summarizes the results determined with the shortcut correlation and with a rigorous model for a desired purity $y_{1,\mathrm{EO}} = 1\,\mathrm{mol\text{-}\%}$. The solvent to feed ratio computed by the shortcut and the rigorous model deviate by 22 %. This deviation is large which can make the comparison of process alternatives based on the shortcut model incorrect. For

Table 2.2.: Results for shortcut and rigorous calculations. Specifications are summarized in Table 2.1. The rigorous model uses twenty stages and the shortcut model is based on correlations of Kremser (1930) and Edmister (1957).

comp.	$\mathbf{y}_1$	$\mathbf{x}_N$	flow ratio		temperature	
shortcut						
AR	0.703	0.004	L_0/V_{N+1}	6.87	T_1	405K
EO	**0.010**	0.069	V_1/V_{N+1}	0.67	T_N	373K
W	0.287	0.928	L_N/V_{N+1}	7.19		
rigorous						
AR	0.887	0.000	L_0/V_{N+1}	8.83	T_1	374K
EO	**0.010**	0.053	V_1/V_{N+1}	0.56	T_{20}	381K
W	0.103	0.947	L_{20}/V_{N+1}	9.27		

screening and pre-selection during the early phase of conceptual design improved shortcut calculations are consequently required.

When shortcut calculations are based on minimum solvent demand, the quality of the approximation can be improved by integrating the pinch into the model. At the pinch, thermodynamic driving forces vanish and the compositions entering and leaving the pinch stage are constant (cf. Figure 2.1: $\mathbf{y}_P = \mathbf{y}_{P+1}$). Conservation of mass and energy allows to describe the pinch (P) by the equations

$$0 = V_{N+1} y_{N+1,i} - V_P y_{P,i} - L_N x_{N,i} + L_P x_{P,i}, \quad i = 1, ..., C, \tag{2.19}$$

$$0 = V_{N+1} h^V_{N+1} - V_P h^V_P - L_N h^L_N + L_P h^L_P, \tag{2.20}$$

which assume thermodynamic equilibrium of entering and leaving streams at the pinch.

There has been only little work on pinch-based shortcut methods for absorption columns. In particular, two-dimensional diagrams can be constructed to identify the minimum solvent demand for ternary mixtures (Kister, 2008). The approach requires negligible vaporization of the solvent and condensation of the carrier gas. If heat effects are negligible and isothermal behavior can be assumed, a shortcut method originally developed for isothermal extraction columns (Burger et al., 2016; Minotti et al., 1996) carries over to absorption columns. Besides the simplifying assumptions, both methods are limited to ternary mixtures. Consequently, their application to industrial processes often involving

more than three components and mixtures with strong heat effects is not possible.

Hence, there is a need for a pinch-based shortcut method for absorption columns separating gaseous mixtures with an arbitrary number of components and with non-ideal thermodynamic behavior.

2.2 Pinch-based shortcut model

The pinch is central to the concept of the novel shortcut introduced in this section. In the following, two algebraically sound approximations, one extending from the first stage to the pinch and one from the pinch to the last stage, are derived. These approximations, combined with sets of MESH equations to balance the first stage, the last stage, and the pinch, provide the basic pinch-based shortcut model. After the derivation of the basic model, an approach is presented which allows a gradual reduction of the approximation error to any degree of desired accuracy.

2.2.1 Basic model

The stage-to-stage recurrence in Eqs. (2.1)-(2.5) is a non-linear, discrete, and distributed system, which is generally referred to a a non-linear discrete dynamical system. At the pinch, $n = \mathrm{P}$, all compositions, temperatures, and flow-rates on two adjacent stages are identical, e.g., for the composition of the liquid phases $\mathbf{x}_{\mathrm{P}+1} = \mathbf{x}_{\mathrm{P}}$ can be written. Hence, the pinch is a fixed point of the discrete dynamical system. The implicit function theorem allows to linearize the non-linear equations (2.1)-(2.5) at the pinch (Poellmann et al., 1994). Then, the first order differential $\frac{\partial \mathbf{x}_{\mathrm{n}+1}}{\partial \mathbf{x}_{\mathrm{n}}}$ can be calculated as a $(C-1)\times(C-1)$ matrix. If the difference quotient approximation,

$$\left.\frac{\partial \mathbf{x}_{\mathrm{n}+1}}{\partial \mathbf{x}_{\mathrm{n}}}\right|_{\mathrm{P}} \approx \frac{\mathbf{x}_{n+1}-\mathbf{x}_{\mathrm{P}}}{\mathbf{x}_{n}-\mathbf{x}_{\mathrm{P}}}, \tag{2.21}$$

is pragmatically assumed to hold not only at stages n, $n+1$ close to the pinch P, but at any stages n, $n+1$, a linear approximate solution for the course of stage compositions can be derived (cf. Appendix A) as

$$x_{n,i} = x_{\mathrm{P},i} + \sum_{j=1}^{C-1} c_j \lambda_j^{n-k} \mathbf{e}_j, \qquad i = 1,\ldots,C-1. \tag{2.22}$$

The eigenvectors $\mathbf{e}_j$ and eigenvalues λ_j of the matrix $\frac{\partial \mathbf{x}_{n+1}}{\partial \mathbf{x}_n}$ are determined at the pinch for $n = \mathrm{P}$ (cf. Appendix A). The weights c_j could only be determined from Eq. (2.22) directly, if a composition $\mathbf{x}_k$ was known on some stage $n = k$. Then, if the weights are known, the course of compositions of the liquid phase $\mathbf{x}_n$ for all stages n in the column could be calculated from Eq. (2.22).

Since the pinch constrains progress of stage-to-stage calculations, the linear approximation is employed in the following to estimate the course of the stage compositions starting from both sides of the column towards the pinch. Starting at the first stage ($k = 1$),

$$\begin{aligned} x_{n,i} &= x_{\mathrm{P},i} + \sum_{j=1}^{C-1} \mu_j \lambda_j^{n-1} \mathbf{e}_j, \\ i &= 1,...,C-1, \quad n = 1,2,...,\infty, \end{aligned} \tag{2.23}$$

is obtained, and starting at the last stage ($k = \mathrm{N}$),

$$\begin{aligned} x_{n,i} &= x_{\mathrm{P},i} + \sum_{j=1}^{C-1} \nu_j \lambda_j^{n-\mathrm{N}} \mathbf{e}_j, \\ i &= 1,...,C-1, \quad n = \mathrm{N},\mathrm{N}-1,...,\mathrm{N}-\infty, \end{aligned} \tag{2.24}$$

is obtained. Because the compositions on stages 1 and N are not known *a priori* in the absorption column, values for the weights μ_j and ν_j cannot be determined directly from Eqs (2.23) and (2.24) only. Instead, qualitative information on the weights is derived subsequently.

Feasible separation at minimum solvent flow rate requires a stage-to-stage trajectory connecting the first stage with the last stage. As the pinch has to occur within the column section for an infinite number of stages, that pinch is touched by the stage-to-stage trajectory. Thus, for the recurrence (2.23) starting at the first stage, convergence to the pinch has to be established for an increasing number of stages, i.e.,

$$\lim_{n\to\infty} \mathbf{x}_n \stackrel{!}{=} \mathbf{x}_{\mathrm{P}}, \tag{2.25}$$

which, according to Eq. (2.23), requires

$$\lim_{n\to\infty} \mu_j \lambda_j^{n-1} \stackrel{!}{=} 0, \qquad j = 1,...,C-1. \tag{2.26}$$

For non-reactive mixtures, all eigenvalues λ_j for $j = 1,...,C-1$ are real, positive, and

distinct (Doherty, 1985),

$$0 < \lambda_1 < ... < \lambda_{C-1} < \infty. \tag{2.27}$$

Depending on their values, four situations can be distinguished: The eigenvalues in the set can be smaller than unity, greater than unity, smaller and greater than unity, or, one eigenvalue equals unity, while the remaining are smaller or greater than unity. Each situation causes different behaviors of the individual terms in Eq. (2.26):

$$\lim_{n\to\infty} \lambda_j^{n-1} = (0,...,0)^{\mathrm{T}}, \quad 0 < \lambda_1 < ... < \lambda_{C-1} < 1, \tag{2.28}$$

$$\lim_{n\to\infty} \lambda_j^{n-1} = (\infty,...,\infty)^{\mathrm{T}}, \quad 1 < \lambda_1 < ... < \lambda_{C-1} < \infty \tag{2.29}$$

$$\lim_{n\to\infty} \lambda_j^{n-1} = (0,...,\infty)^{\mathrm{T}}, \quad 0 < \lambda_1 < ... < 1 < ... < \lambda_{C-1} < \infty, \tag{2.30}$$

$$\lim_{n\to\infty} \lambda_j^{n-1} = (0,...,1,...,\infty)^{\mathrm{T}}, \quad 0 < \lambda_1 < ... < \lambda_j = 1 < ... < \lambda_{C-1} < \infty. \tag{2.31}$$

Eigenvalues smaller than unity lead to converging behavior while eigenvalues greater than unity result in diverging behavior. Hence, eigenvectors referring to convergent behavior are called stable eigenvectors, and eigenvectors referring to divergent behavior unstable eigenvectors. When one eigenvalue equals unity, the behavior is inconclusive and the corresponding eigenvector is called a neutral eigenvector (Sandefur, 1990).

As a consequence, each weight μ_j in Eq. (2.26), which refers to a divergent behavior according to Eqs. (2.28)-(2.31), needs to be zero, which constrains the solution of Eq. (2.23) to

$$x_{n,i} = x_{\mathrm{P},i} + \sum_{\substack{j=1,\\ \lambda_j \leq 1}}^{C-1} \mu_j \lambda_j^{n-1} e_{j,i} \qquad i = 1,...,C-1. \tag{2.32}$$

In particular, for a given composition of the first stage ($n = 1$) the solution is

$$x_{1,i} = x_{\mathrm{P},i} + \sum_{\substack{j=1,\\ \lambda_j \leq 1}}^{C-1} \mu_j e_{j,i} \qquad i = 1,...,C-1. \tag{2.33}$$

Only weights μ_j for each stable and neutral eigenvector ($\lambda \leq 1$) need to be considered.

For the second approximation which starts from the last stage, Eq. (2.24), an approximate solution can be derived accordingly. Again, convergence to the pinch is assumed for an infinite number of stages but in the opposite direction which then is a decreasing number of stages, i.e.,

$$\lim_{n\to-\infty} \mathbf{x}_n \stackrel{!}{=} \mathbf{x}_\mathrm{P}. \tag{2.34}$$

According to the discussion for the first approximation on the behavior due to the eigenvalues, Eq. 2.28-2.31, we obtain

$$x_{\mathrm{N},i} = x_{\mathrm{P},i} + \sum_{\substack{j=1,\\ \lambda_j \geq 1}}^{C-1} \nu_j e_{j,i}, \qquad i = 1,...,C-1. \tag{2.35}$$

For this approximation, only weights ν_j for each unstable and neutral eigenvector ($\lambda \geq 1$) need to be considered.

In conclusion, the shortcut model combines the set of MESH equations for the first stage, the last stage, and the pinch point, Eqs. (2.1), (2.5) for $n = \mathrm{N}$, (2.2)-(2.4) for $n \in \{1, \mathrm{N}, \mathrm{P}\}$, (2.19)-(2.20). For an approximation, linear solutions for the path from the first stage to the pinch, Eq. (2.33), and from the pinch to the last stage, Eq. (2.35), are used.

Eigenvalues classify the pinch: If stable eigenvectors, Eq. (2.28), are present, the pinch is unstable, if only unstable eigenvectors, Eq. (2.29), are present, the pinch is stable, or, if only stable and unstable eigenvectors, Eq. (2.30), are present, the pinch is a saddle pinch (Krause, 1999). The type of pinch also determines the number of weights μ_j and ν_j. For a stable, unstable, or saddle pinch, the total number of weights μ_j and ν_j is $C-1$, and the basic shortcut model can be solved for given specifications according to Table 2.1 for all flow rates, compositions, temperatures, and weights.

A fourth type of pinch occurs if one eigenvalue equals unity, Eq. (2.31). Then, the model has a total number of C weights, μ_j and ν_j, and one additional constraint is required. The stable or unstable pinch merges with a saddle in a saddle-node bifurcation. This type of pinch is referred to as saddle-node or tangential pinch (Krause, 1999; Levy & Doherty, 1986). It is described by the constraint

$$\lambda_j = 1, \qquad j \in \{1,...,C-1\}. \tag{2.36}$$

The shortcut model with a saddle-node pinch combines the constraint, Eq. (2.36), with

the model equations for the stable, unstable, or saddle pinch, Eqs. (2.1), (2.5) for $n = \mathrm{N}$, (2.2)-(2.4) for $n \in \{1, \mathrm{N}, \mathrm{P}\}$, (2.9), (2.19)-(2.20), (2.33), and (2.35).

2.2.2 Improved shortcut model

The approximations employed by the basic shortcut model presented in the previous section assume linearity by Eq. (2.21) of the non-linear stage-to-stage equations (2.1)-(2.5). Thus, the approximation in Eq. (2.22) is always accurate close to the pinch. However, if the rigorous solutions of a stage-to-stage recurrence shows a curved, non-linear, course (cf. Figure 2.2), inaccuracy grows when the distance between a stage and the pinch increases.

For thermodynamically ideal mixtures (ideal liquid and gaseous phase, constant molar overflow), Levy et al. (1985) showed that an approximation for the stage-to-stage recurrence, Eqs. (2.1)-(2.5), is, in fact, a linear set of equations. Then, the linear approximations in Eqs. (2.33) and (2.35) are accurate representations of the course of a rigorous non-linear stage-to-stage recurrence.

For non-ideal mixtures, the assumption of a linear stage-to-stage recurrence is widely recognized and usually leads to good results (Bausa et al., 1998; Krämer et al., 2011b; Levy et al., 1985). There have been attempts to improve the accuracy, but none can be applied in a fully automated manner to a multi-component mixture separations (Krämer et al., 2011b; Urdaneta et al., 2002). In consequence, the applicability of all existing shortcut approaches is limited due to the uncertain quality of their approximation and thus the resulting lack of confidence in their performance assessment.

In order to overcome this shortcoming, the novel basic shortcut model concept is used as a starting point to prepare a method which gradually reduces the approximation error. The approximation error is caused by the non-ideality of the mixture, which causes curvature of the stage-to-stage trajectory. Therefore, when using a linear approximation according to the basic shortcut model, the approximation error is more dominant for an increasing distance between the stage of interest and the pinch. While the non-ideality of the mixture cannot be ignored without losing information about the thermodynamic behavior, the distance of the approximation can be reduced by including additional stages in the shortcut model.

Consequently, M additional stages are included in the shortcut model by Eqs. (2.1), (2.5) for $n = 1, 2, ..., M$, (2.2)-(2.4) for $n = 2, 3, ..., 1 + M$, if the recurrence starts at the first stage, or, starting at the last stage, O additional stages are included such that Eqs. (2.1)-(2.5) are used for $n = \mathrm{N} - 1, ..., \mathrm{N} - O$. The approximations, Eqs. (2.33) and (2.35), then

only extend between the pinch and the stage closest to the pinch, $n = 1+M$ or $n = \mathrm{N}-O$,

$$x_{1+M,i} = x_{\mathrm{P},i} + \sum_{\substack{j=1,\\ \lambda_j \leq 1}}^{C-1} \mu_j e_{j,i}, \qquad ,i = 1,....,C-1, \tag{2.37}$$

$$x_{\mathrm{N}-O,i} = x_{\mathrm{P},i} + \sum_{\substack{j=1,\\ \lambda_j \geq 1}}^{C-1} \nu_j e_{j,i}. \qquad i = 1,....,C-1. \tag{2.38}$$

Each additional stage (i.e., increasing M and O) gradually improves the accuracy, because the dominance of the approximation, and thus the approximation error introduced by Eq. (2.21), is reduced.

2.3 Analysis of the shortcut model

The shortcut model is in the following illustrated for the separation of argon, ethylene-oxide, and water, which was introduced previously (cf. Table 2.1). In the following, solutions of the shortcut model are studied for three different purities σ, each resulting in a model with a stable, saddle-node, or saddle pinch point. To improve readability of the discussed phenomena, an enlarged detail of the ternary diagram of Figure 2.2 is used.

2.3.1 Stable pinch

The sample separation has a stable pinch point when a purity of ethylene-oxide of about $y_{1,\mathrm{EO}} = 46\,\text{mol-\%}$ is specified. The results for this split are summarized in Table 2.3. The model determines outlet flow ratios $V_1/V_{\mathrm{N}+1}$ and $L_{\mathrm{N}}/V_{\mathrm{N}+1}$, outlet compositions $\mathbf{y}_1$ and $\mathbf{x}_{\mathrm{N}}$, and outlet temperatures T_1 and T_{N}, as well as a minimum solvent to feed ratio $L_0/V_{\mathrm{N}+1}$. Figure 2.3 visualizes the results in an enlarged detail of the ternary diagram. The three stages employed by the shortcut model are marked as circles. Open circles mark the composition of the first and last stage, $\mathbf{y}_1$ and $\mathbf{y}_{\mathrm{N}}$, and the filled circle the composition of the pinch $\mathbf{y}_{\mathrm{P}}$. When the separation experiences a stable pinch, the pinch is located at the last stage, $\mathbf{y}_{\mathrm{P}} = \mathbf{y}_{\mathrm{N}}$. Stable eigenvectors are depicted as arrows pointing towards the pinch point. This pinch has only stable eigenvectors which characterize a stable pinch.

One feature of this type of pinch, as shown in the following, is that the result of the shortcut model is an accurate representation of an operation at minimum solvent demand. On the one hand, the approximation extending from the first stage to the pinch allows to

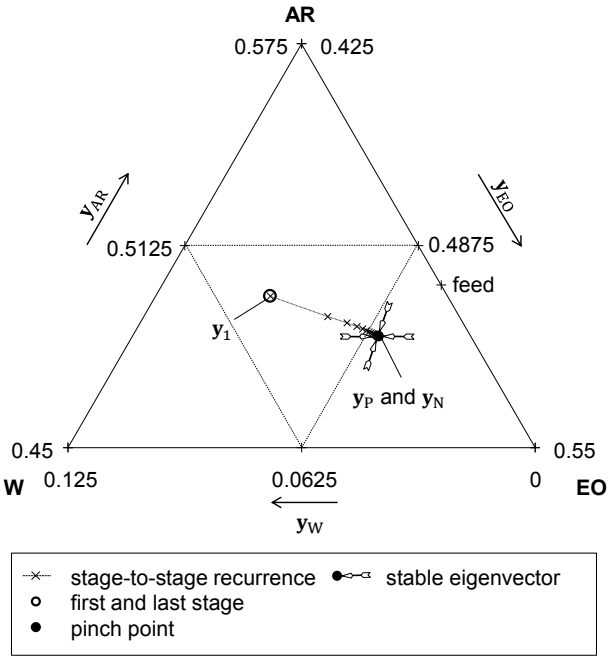

Figure 2.3.: Stable pinch point situation with results for the shortcut and rigorous model.

calculate all $C-1$ weights μ_j explicitly from the $C-1$ equations (2.33). Thus, since the information by the weights has no further relevance for the outlet compositions, flow rates, or for the minimum solvent demand, the equations could be omitted. On the other hand, without any unstable eigenvector, the second approximation extending from the pinch to the last stage, Eq. (2.35), reads as

$$x_{N,i} = x_{P,i}, \qquad i = 1,...,C-1. \tag{2.39}$$

Hence, the composition of the last stage is located at the pinch which is calculated accurately. In consequence, when one approximation could be omitted and the other is accurate, the calculated result of the shortcut model is an accurate representation of the minimum solvent operation.

Table 2.3.: Results of the shortcut and rigorous model when a stable pinch controls the separation. For a stable pinch, no approximation is required. Therefore, results by the shortcut agree with results by a rigorous model when a sufficient number of stages is assumed.

comp.	$\mathbf{y}_1$	$\mathbf{x}_N$	flow ratio		temperature	
shortcut and rigorous						
AR	0.495	0.000	L_0/V_{N+1}	0.17	T_1	354K
EO	**0.460**	0.214	V_1/V_{N+1}	1.00	T_{N+1}	342K
W	0.045	0.786	L_N/V_{N+1}	0.17		

For a comparison, the stage-to-stage trajectory calculated by a rigorous model with twenty stages is depicted with crosses connected by a dotted line. Starting at the first stage, the pinch is approached while separation progress gradually vanishes. For a sufficient number of stages, no deviation between the rigorous and the shortcut model can be observed.

2.3.2 Saddle-node pinch

The sample separation experiences a saddle-node pinch for an ethylene-oxide concentration of $y_{1,EO} = 35\,\text{mol-}\%$ in the product gas. A saddle-node pinch occurs if a stable pinch merges with a saddle pinch. In consequence, a behavior referring to both the saddle and stable pinch can be observed in the ternary diagram in Figure 2.4. The region where the stage-to-stage recurrence experiences stable behaviour is indicated as a shaded area, and the region with saddle behavior is left blank. The regions are separated by the direction of the remaining stable eigenvectors, which is referred to as separatrix (Krause, 1999). In the region with stable behavior, the rigorous stage-to-stage recurrence converges to the direction of the neutral eigenvector, which is indicated as a black dashed line. In contrast, in the region with saddle behavior, a stage-to-stage recurrence can diverge and weights ν_j, which refer to diverging eigenvalues $\lambda_j < 1$, are zero. This part of the stage-to-stage recurrence is approximated with the direction of the neutral eigenvector.

For a comparison, the rigorous stage-to-stage recurrence with thirty stages is depicted as crosses connected by a dotted line. The rigorous stage-to-stage recurrence starts almost at the estimated first stage of the shortcut, converges to the direction of the neutral eigenvector while thermodynamic driving force vanishes, and ends close to last stage predicted by the shortcut. The results for this operating point are summarized in Table 2.4. The short-

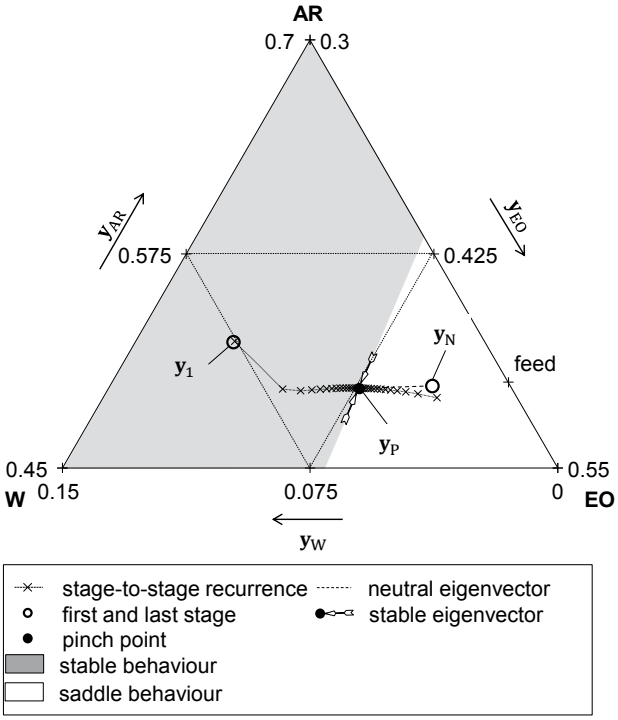

Figure 2.4.: Saddle-node pinch with results for the shortcut and rigorous model. Shaded area refers to stable behavior of the stage-to-stage recurrence; blank area to saddle behavior.

cut result deviates slightly from the rigorous result, e.g., in terms of the solvent to feed ratio by 1 %. The deviation is caused by the slight curvature of the rigorous stage-to-stage recurrence between the pinch and the last stage.

2.3.3 Saddle pinch

The third sample separation experiences a saddle pinch for a purity of ethylene-oxide in the cleaned gas of about $y_{1,\mathrm{EO}} = 1\,\mathrm{mol\text{-}\%}$. Figure 2.5 displays the results of the shortcut

Table 2.4.: Results of the shortcut and rigorous model when saddle-node pinch point controls the separation. Rigorous solutions are obtained with thirty stages.

comp.	$\mathbf{y}_1$	$\mathbf{x}_\infty$	flow ratio		temperature	
shortcut						
AR	0.524	0.000	L_0/V_{N+1}	1.19	T_1	381K
EO	**0.350**	0.135	V_1/V_{N+1}	0.95	T_∞	352K
W	0.126	0.865	L_∞/V_{N+1}	1.23		
rigorous						
AR	0.523	0.000	L_0/V_{N+1}	1.17	T_1	381K
EO	**0.350**	0.136	V_1/V_{N+1}	1.00	T_{20}	351K
W	0.127	0.864	L_{30}/V_{N+1}	1.22		

model for this type of pinch in a ternary diagram. The pinch has stable and unstable eigenvectors indicating a saddle. The part of the stage-to-stage recurrence approaching the pinch from the first stage is approximated with the stable eigenvector, and the part towards the last stage with the unstable eigenvector.

The results for the shortcut model are summarized in Table 2.5. This operating point has previously been discussed in the introduction and results obtained for rigorous and existing shortcut calculations are reproduced from Table 2.2.

For comparison, a rigorous stage-to-stage recurrence with twenty stages is depicted in Figure 2.5. Both parts of the stage-to-stage recurrence are approximated, and the slight curvature of the rigorous recurrence causes the deviation between the shortcut and the rigorous results, e.g., in terms of the solvent to feed ratio about 3 %. In comparison to existing shortcut correlations, the approximation error by the pinch-based shortcut model is more than seven times smaller.

2.3.4 Improved shortcut model

The accuracy of the shortcut model can be improved by adding additional separation stages to the basic shortcut model by Equations (2.37) and (2.38). This is illustrated for the operating point investigated in the last subsection when the purity of about $y_{1,EO}$=1 mol-% is desired.

Figure 2.6 depicts the solvent to feed ratio calculated with the shortcut model when additional separation stages are added step-by-step to the shortcut model. When no addi-

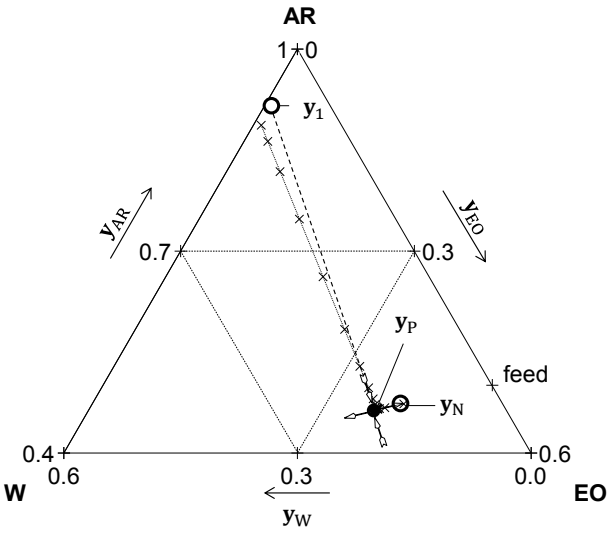

Figure 2.5.: Saddle pinch situation with results for the shortcut and rigorous models. Refer to Figure 2.4 for a description of the symbols.

tional separation stages are used ($M = 0$, $O = 0$), the results summarized in Table 2.5 are achieved. Then, an improvement is pursued in two phases: In the first phase, ten additional separation stages are added step-by-step to the approximation extending from the first stage to the pinch point, Eq. (2.37) until $M = 10$, followed by a second phase, when two additional separation stages are added to the approximation from last stage to the pinch point, Eq. (2.38) until $O = 2$. Both extensions result in an asymptotic improvement, because each additional stage reduces the distance to the pinch. The refinement is stopped, when a separation stage is sufficiently close to the pinch.

The solution of the improved shortcut model with four additional separation stages (A in Figure 2.6, $M = 4$) is illustrated in Figure 2.7. Each additional stage is marked as a cross, and the crosses are connected with a solid line. The necessary approximation from the fourth additional stage to the pinch point is marked as a dashed line. Since this step is close to the asymptote in Figure 2.6, further stages will approach the pinch point along this dashed line.

Figure 2.8 shows the solution of the improved shortcut model with a total of twelve

Table 2.5.: Results of the pinch-based shortcut model when a saddle controls the separation. Results obtained for rigorous and classical shortcut calculations are reproduced from Table 2.2.

comp.	$\mathbf{y}_1$	$\mathbf{x}_N$	flow ratio		temperature	
shortcut						
AR	0.915	0.000	L_0/V_{N+1}	9.06	T_1	365K
EO	**0.010**	0.052	V_1/V_{N+1}	0.55	T_N	382K
W	0.075	0.948	L_N/V_{N+1}	9.52		
classical shortcut						
AR	0.703	0.004	L_0/V_{N+1}	6.87	T_1	405K
EO	**0.010**	0.069	V_1/V_{N+1}	0.67	T_N	373K
W	0.287	0.928	L_N/V_{N+1}	7.19		
rigorous						
AR	0.887	0.000	L_0/V_{N+1}	8.83	T_1	374K
EO	**0.010**	0.053	V_1/V_{N+1}	0.56	T_{20}	381K
W	0.103	0.947	L_{20}/V_{N+1}	9.27		

additional stages (B in Figure 2.6). Ten additional stages are employed to improve the approximation from the first stage to the pinch ($M = 10$), and two to improve the approximation from the last stage to the pinch ($O = 2$). The results of the improved shortcut agree with the rigorous approach (cf. Figure 2.2 and Table 2.2). Nevertheless, the rigorous model requires a high number of stages to overcome the low driving force close to the pinch, whereas the shortcut model with additional stages relies on the direction of the eigenvectors to approximate the behavior in the vicinity of the pinch. An accurate representation of the rigorous result is already obtained when the calculated solvent to feed ratio is sufficiently close to the asymptote in Figure 2.6. E.g., in total three additional stages are sufficient to achieve fairly accurate results; two additional stages to improve the approximation extending from the first stage to the pinch point, and one additional stage to improve the approximation extending from the pinch point to the last stage.

2.4 Solution of the shortcut model

The solution procedure suggested in this work solves the shortcut model in two phases: The first phase identifies a feasible solution at the lower bound of the solvent to feed ratio

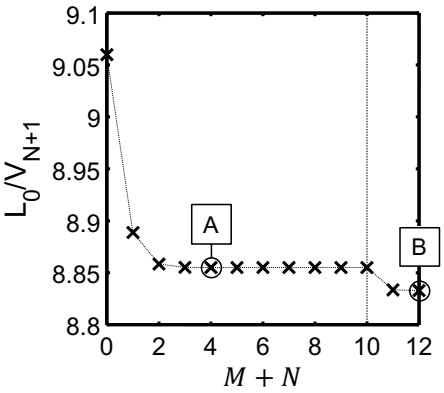

Figure 2.6.: Solvent to feed ratio subject to the stepwise refinement of the approximations by adding additional stages M and N. Asymptotic improvement is observed. Situation A is illustrated in Figure 2.7, situation B in Figure 2.8.

L_0/V_{N+1}. This represents not yet the solution for a desired design specification such as purity of a value product in the cleaned gas, but the operation with the lowest solvent to feed ratio to just achieve a pinch-based separation. Beginning with the solution at the lower bound of the solvent to feed ratio, the second phase employs continuation techniques in order to find the solution for any desired design specification.

2.4.1 Identification of feasible initial solution

At the lower bound of the solvent to feed ratio, the last stage, where the feed enters the column, dries out. The liquid flow rate is zero, i.e.,

$$L_N = 0. \tag{2.40}$$

This simplifies the pinch equations, Eqs. (2.19) and (2.20), to

$$0 = V_{N+1} y_{N+1,i} - V_P y_{P,i} + L_P x_{P,i}, \quad i = 1,...,C, \tag{2.41}$$

$$0 = V_{N+1} h^V_{N+1} - V h^V_P - L_P h^L_P. \tag{2.42}$$

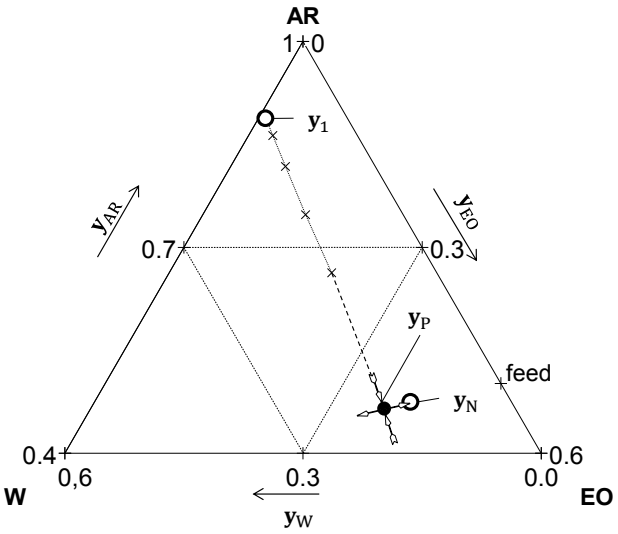

Figure 2.7.: Situation A of refinement in Figure 2.6. Four additional separation stages improve the approximation from first stage to pinch point. Refer to Figure 2.4 for a description of the symbols.

Usually, the shortcut model covers simultaneously the pinch equations and the integral balances of the column, Eqs. (2.1)-(2.5) for $n = \mathrm{N}$. At the lower bound, however, both sets of equations can be solved independently.

An initial solution for the non-linear set of equations is easily identified when the feed is at boiling temperature. Then, the vapor compositions at the pinch, the first stage, and the last stage are equal to the composition of the feed ($\mathbf{y}_\mathrm{F} = \mathbf{y}_\mathrm{P} = \mathbf{y}_1 = \mathbf{y}_\mathrm{N}$), and the solvent to feed ratio is zero. In contrast, when the feed stream is overheated, the solvent to feed ratio is greater than zero and the simplified set of pinch equations can have multiple solutions.

For distillation, the multiplicity of pinch point solutions has been extensively discussed in literature. Since the set of simplified pinch equations, Eqs. (2.2)-(2.4) for $n = \mathrm{P}$, (2.41), (2.42), of an absorption column section is identical to the set of pinch equations of a distillation column section, the algorithm originally proposed for distillation columns (Bausa, 2001; Bausa et al., 1998) can be applied to find all pinch points. Continuation techniques are employed for a rigorous calculation of all pinch lines which comprise the locus of all

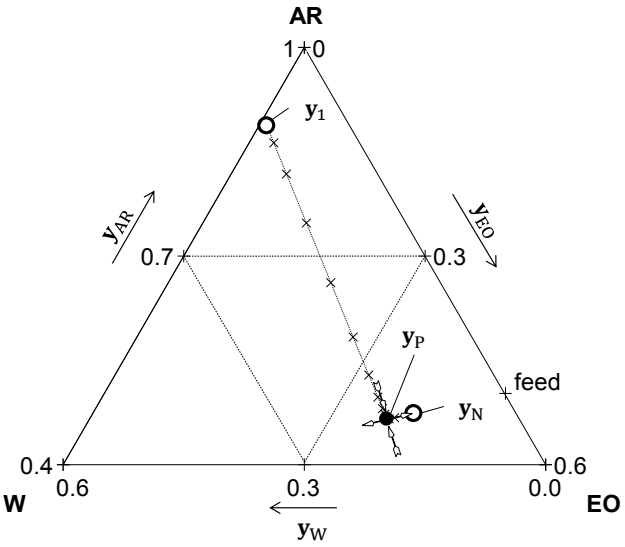

Figure 2.8.: Situation B of refinement in Figure 2.6. Ten additional stages improve the approximation from first stage to pinch point, two additional stages from last stage to pinch point. Refer to Figure 2.4 for a description of the symbols.

pinch points for all possible reflux ratios (Bausa et al., 1998; Felbab, 2012). For distillation, pinch lines can be interpreted as functions of the reflux ratio which start in all pure components or azeotropes for an infinite reflux. In comparison, for absorption, pinch lines are interpreted as functions of the temperature of the feed stream, which start in all pure components or azeotropes for an infinite temperature. The (infinitely) large temperature or reflux ratio have, of course, no physical meaning, but allow to find reliably all possible initial solutions by a systematic continuation.

For the lower bound of the solvent to feed ratio, in the ternary diagram in Figure 2.9 pinch solutions are depicted for different compositions and as a function of the feed temperature. Two types of pinch lines occur which are marked as dotted and dashed lines and refer to stable and saddle pinch points respectively. Depending on the stability, saddle pinch points are marked as triangles, and stable pinch points as squares. One dotted line is located on the edge representing the binary mixture of argon and ethylene-oxide, and a second line, which has dotted and dashed parts, connects the pure water vertex with the

azeotrope close to pure ethylene-oxide. When the feed is introduced at boiling temperature, the pinch is located at the composition of the feed and has identical temperature. When, however, the temperature of the feed stream is increased above boiling temperature, initial pinch solutions at the lower bound of the solvent to feed ratio recede from the feed composition towards singular points of the mixture such as pure components or azeotropes.

For each exemplary temperature, one saddle and two stable pinch points occur. Since the purpose of the separation is the absorption of ethylene-oxide from the feed, the pinch with lowest fraction of ethylene-oxide is selected. For the desired temperature of 373 K, the identified initial pinch solution is marked with a circle.

2.4.2 Continuation of the shortcut model

If the design specification by Eq. (2.9) is not considered, one-dimensional solution branches can be determined with continuation techniques. The branches are determined with a predictor-corrector continuation algorithm (Choi et al., 1996; Jiménez-Islas et al., 2013).

The correction step requires repetitive calculation of eigenvalues, eigenvectors, and their derivatives, which is time-consuming and can be numerically difficult (Beyn et al., 2011). Instead, eigenvalues and eigenvectors can be treated as parameters in the correction step, which are updated using the eigenvectors from the previous iterate of the continuation. This yields sufficiently accurate results as long as a small step-size is used during the continuation.

For the continuation of the saddle-node model, Brüggemann & Marquardt (2004) suggest to replace the saddle-node model constraint, Eq. (2.36). When a saddle-node pinch occurs, the set of pinch equations, Eqs. (2.2)-(2.4) for $n = \mathrm{P}$, (2.19)-(2.20), is singular (Levy et al., 1985). Thus, when the set of pinch equations are abbreviated as $\mathbf{0} = \mathbf{p}$, and the variables at the pinch point as $\mathbf{u} = (L_\mathrm{P}, V_\mathrm{P}, \mathbf{x}_\mathrm{P}^\mathrm{T}, \mathbf{y}_\mathrm{P}^\mathrm{T}, T_\mathrm{P})^\mathrm{T}$, the saddle-node pinch can be computed from

$$\mathbf{0} = \nabla_\mathbf{u}\mathbf{p}^\mathrm{T}\mathbf{w}, \tag{2.43}$$

$$0 = \mathbf{w}^\mathrm{T}\mathbf{w} - 1, \tag{2.44}$$

where $\mathbf{w}$ is a null vector of $\nabla_\mathbf{u}\mathbf{p}^\mathrm{T}$ (Beyn et al., 2002). Prior to the continuation with this constraint, the vector $\mathbf{w}$ is initialized with the neutral eigenvector of $\nabla_\mathbf{u}\mathbf{p}^\mathrm{T}$.

With these preliminaries, the method can be summarized as follows: Continuation starts

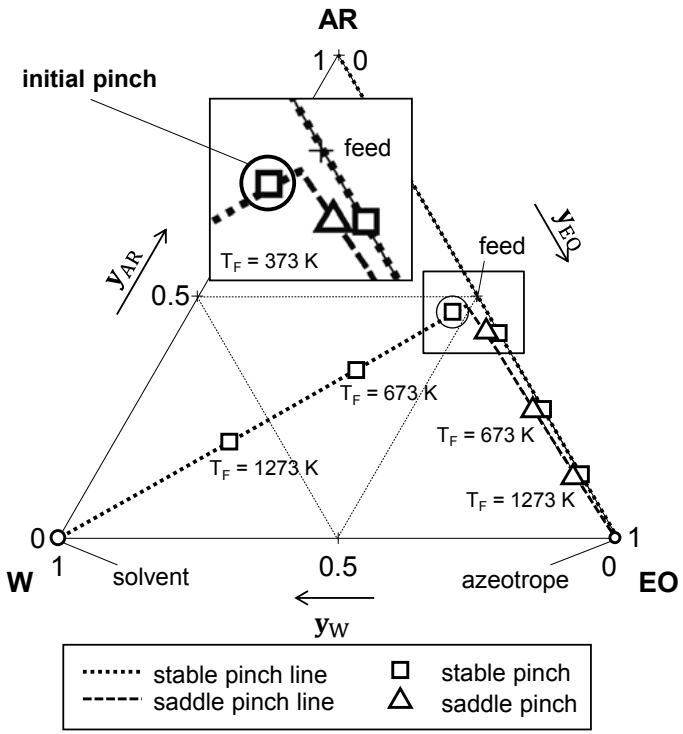

Figure 2.9.: Lines indicate all possible initial pinch point solutions. Solutions for various temperatures of the feed stream are depicted. The relevant initial pinch shows the lowest fraction of ethylene-oxide in the cleaned gas for the specified temperature of 373 K.

at the lower bound of the solvent to feed ratio. During the continuation, eigenvalues and their corresponding weights, ν_j or μ_j, are monitored to switch between models either referring to a saddle-node pinch or to a stable, unstable, or saddle pinch. The model with a saddle-node pinch is identified when one eigenvalue equals unity, while the model with a stable, unstable, or saddle pinch is identified when the weight corresponding to the neutral eigenvector, ν_j or μ_j for $\lambda_j = 1$, is zero. Finally, when the desired design specification by Eq. (2.9) is achieved, continuation stops.

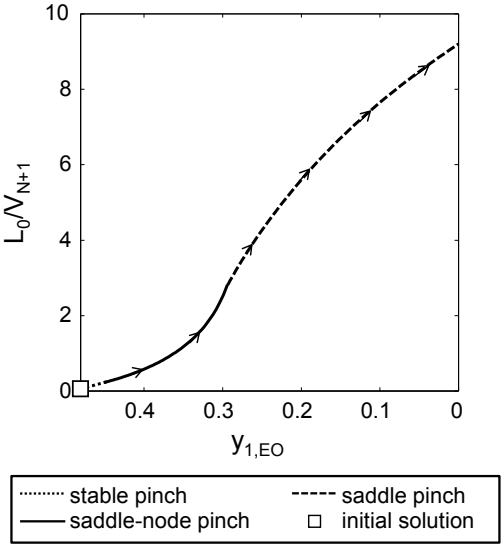

Figure 2.10.: Solvent to feed ratio during the continuation. Continuation starts at the lower bound of solvent to feed ratio, and stops when ethylene-oxide is fully absorbed from feed gas stream. Arrows indicate the direction of the continuation.

The solution procedure assumes that only one unique pinch, which is tracked by the continuation, controls the separation. This assumption agrees with observations for the middle section of extractive distillation columns where also only one unique pinch is relevant for the separation (Brüggemann & Marquardt, 2004; Knapp & Doherty, 1994; Petlyuk et al., 2015). Due to the analogy between an absorption column and a middle section of an extractive distillation column, the conclusions can carry over to absorption columns. Inconsistencies in this assumption for absorption columns could be identified by validating the solution with the improved shortcut model. So far, however, such inconsistencies of the solution procedure could not be observed.

Figure 2.10 illustrates the continuation for the model variable solvent to feed ratio subject to varying product gas specifications during the continuation. Continuation starts at

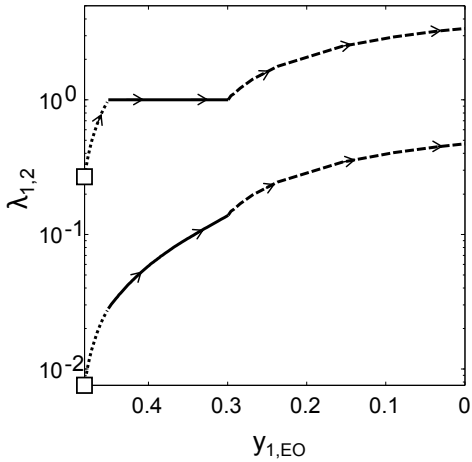

Figure 2.11.: Eigenvalues during the continuation. The eigenvalues allow to distinguish between different shortcut models during the continuation. Arrows indicate the direction of the continuation. Refer to Figure 2.10 for a description of the symbols.

the lower bound of the solvent to feed ratio. The solvent to feed ratio increases while the concentration of ethylene-oxide decreases. Different types of pinch points and according models are indicated as dotted, continuous, and dashed parts of the solution branch for stable, saddle-node, and saddle pinch points.

The models are selected according to the size of the eigenvalues. Figure 2.11 shows the values for the two eigenvalues occurring for varying product gas during the continuation. At the beginning of the continuation, the model referring to a stable pinch applies because all eigenvalues are smaller than unity. When the largest eigenvalue equals unity, the model referring to a saddle-node pinch applies until the weight ν_j, which refers to the neutral eigenvector $\lambda_j = 1$, is zero. Finally, the model referring to a saddle pinch is described by one eigenvalue smaller than unity and one greater than unity.

2.5 Ilustrating case studies

Applicability of the novel method to multi-component mixture separations is highlighted by means of four examples with up to seven components. The example are taken from literature (Peschel et al., 2012; Sun & Smith, 2013; Zhang et al., 2015) and evaluate the absorption of (I.) ethylene-oxide with water, of (II.) dimethyl-ether with methanol, of (III.) carbon-dioxide with water, and of (IV.) carbon-dioxide with methanol. Similar operating points are investigated with different thermodynamic models. The vapor pressure is described by Antoine's extended equation, except for the supercritical gases (hydrogen, nitrogen, argon, ethylene, oxygen, methane, carbon-dioxide, carbon-monoxide), which are described by Henry's law. Non-ideality of the liquid-phase is covered with the NRTL-model for the binary mixtures of dimethyl-ether and water, and of ethylene-oxide and water.

The results for all case studies are summarized in Table 2.6. The specifications are marked in bold and results represent a solution by the basic shortcut model without additional stages. Calculation time on a standard Intel(R) Core(TM) i3-4150 3.5 GHz personal computer is determined. It covers all steps of the method which are implemented in C/C++.

As a benchmark, operation at minimum solvent demand is calculated on the one hand with a rigorous (RIG) model with the RADFRAC module in AspenPlus®, and on the other hand with the established shortcut correlations (COR) introduced by Kremser (1930) and Edmister (1957). The key idea of the solution procedure — the initialization at the lower bound of the solvent to feed ratio, the continuation of the model until the desired design specification is reached — is also implemented to reliably solve established shortcut models. The results obtained from these established techniques are summarized in Table 2.7. For ease of comparison, the calculated solvent to feed ratio determined by the rigorous (RIG) and the established shortcut (COR) models are also shown in the right column of Table 2.6.

Existing shortcut correlations deviate from the rigorous results in terms of the solvent to feed ratio at least by 10 %, and for the absorption of ethylene-oxide with water even by up to 24 %. In contrast, the novel pinch-based shortcut model is for all investigated examples below 16 %.

The results of the novel pinch-based shortcut method can be improved up to any desired accuracy by adding additional stages to the shortcut model. This leads to results identical to rigorous calculations, which ultimately allows to identify minimum solvent operation accurately, within seconds, and reliably. No manual iteration is required.

Table 2.6.: Summary of shortcut results for the investigated examples. Specifications for feed and solvent stream and desired purity in cleaned gas are marked bold. For a comparison, solvent to feed ratio calculated with the rigorous (RIG) model and with existing shortcut correlations (COR) are shown.

case study	component	$\mathbf{y}_{N+1}$	$\mathbf{x}_0$	T_{N+1} (K) T_0 (K) p (MPa)	L_0/V_{N+1} V_1/V_{N+1} L_N/V_{N+1}	$\mathbf{y}_1$	$\mathbf{x}_N$	T_1 (K) T_N (K)	CPU (s)	$(L_0/V_{N+1})_{RIG}$ $(L_0/V_{N+1})_{COR}$
	argon	**0.36**	**0**	**303**	0.793	0.366	0.000	306	3.5	0.814
	oxygen	**0.05**	**0**	**303**	0.982	0.051	0.000	307		0.616
	methane	**0.09**	**0**	**2**	0.810	0.092	0.001			
I.	carbon-dioxide	**0.05**	**0**			0.050	0.001			
	ethylene	**0.43**	**0**			0.437	0.024			
	ethylene-oxide	**0.02**	**0**			**0.001**	0.024			
	water	**0**	**1**			0.002	0.880			
	argon	**0.002**	**0**	**303**	0.986	0.003	0.000	150	2.2	0.849
	methane	**0.002**	**0**	**223**	0.653	0.003	0.000	286		0.646
	hydrogen	**0.461**	**0**	**3.5**	1.333	0.701	0.002			
II.	nitrogen	**0.003**	**0**			0.005	0.000			
	carbon-dioxide	**0.442**	**0**			**0.001**	0.256			
	carbon-monoxide	**0.190**	**0**			0.287	0.002			
	methanol	**0**	**1**			0.000	0.740			
	argon	**0.002**	**0**	**303**	0.958	0.003	0.001	254	2.7	1.022
	methane	**0.002**	**0**	**223**	0.658	0.003	0.000	285		0.918
	hydrogen	**0.461**	**0**	**3.5**	1.30	0.700	0.000			
III.	nitrogen	**0.003**	**0**			0.005	0.000			

	carbon-dioxide	**0.342**	**0**			**0.001**	0.263				
	carbon-monoxide	**0.190**	**0**			0.288	0.000				
	water	**0**	**1**			0.000	0.737				
	hydrogen	**0.7**	**0**	**303**	1.307	0.863	0.004	280	1.7		1.150
	carbon-monoxide	**0.01**	**0**	**303**	0.804	0.012	0.000	313			0.977
IV.	carbon-dioxide	**0.22**	**0**	**3**	1.503	0.122	0.081				
	dimethyl-ether	**0.07**	**0**			**0.001**	0.046				
	methanol	**0**	**1**			0.002	0.868				

Table 2.7.: Summary of results determined with a rigorous model and existing shortcut correlations of Kremser (1930) and Edmister (1957). The specifications for the examples are summarized in Table 2.6.

		rigorous					**correlations**			
case study	component	L_0/V_{N+1} V_1/V_{N+1} L_N/V_{N+1}	$\mathbf{y}_1$	$\mathbf{x}_N$	T_1 (°C) T_N (°C)	stages	L_0/V_{N+1} V_1/V_{N+1} L_N/V_{N+1}	$\mathbf{y}_1$	$\mathbf{x}_N$	T_1 (°C) T_N (°C)
I.	argon	0.814	0.366	0.000	31	**100**	0.616	0.366	0.000	40
	oxygen	0.982	0.051	0.000	34		0.984	0.051	0.000	29
	methane	0.814	0.092	0.000			0.633	0.092	0.000	
	carbon-dioxide		0.050	0.000				0.050	0.006	
	ethylene		0.437	0.001				0.437	0.001	
	ethylene-oxide		**0.001**	0.023				**0.001**	0.030	
	water		0.002	0.976				0.004	0.968	
II.	argon	0.849	0.003	0.000	-48	**20**	0.646	0.003	0.000	27
	methane	0.654	0.003	0.000	9		0.614	0.003	0.000	6
	hydrogen	1.195	0.701	0.002			1.032	0.690	0.036	
	nitrogen		0.005	0.000				0.005	0.000	
	carbon-dioxide		**0.001**	0.286				**0.001**	0.331	
	carbon-monoxide		0.288	0.002				0.294	0.009	
	methanol		0.000	0.710				0.005	0.623	
III.	argon	1.022	0.003	0.000	-46	**20**	0.918	0.003	0.000	14
	methane	0.658	0.003	0.000	14		0.658	0.003	0.000	9
	hydrogen	1.364	0.700	0.002			1.260	0.700	0.000	
	nitrogen		0.007	0.000				0.005	0.000	

	carbon-dioxide		**0.001**	0.250					**0.001**	0.271	
	carbon-monoxide		0.288	0.000					0.288	0.000	
	water		0.000	0.749					0.000	0.729	
IV.	hydrogen	1.150	0.851	0.004	30	**100**		0.977	0.838	0.004	81
	carbon-monoxide	0.816	0.012	0.000	37			0.830	0.0115	0.000	30
	carbon-dioxide	1.334	0.129	0.086				1.148	0.132	0.009	
	dimethyl-ether		**0.001**	0.051					**0.001**	0.060	
	methanol		0.007	0.858					0.0174	0.839	

2.6 Screening of solvents

Existing concepts for the screening of solvents are usually restricted to the evaluation of thermodynamic properties such as the solubility or the loss of solvent (Kister, 2008; Masurel et al., 2015). Alternatively, the pinch-based method can be used. Reliable evaluation, which is required for the automated screening of solvents, is thereby accomplished by the suggested solution procedure. Therefore, in contrast to conventional methods for the screening of solvents, the new approach finally facilitates the automated screening of a large number of solvent candidates by evaluating the actual separation device.

In order to illustrate the possible range of application, two examples are investigated. The first example investigates the well-known absorption of carbon-dioxide (cf. Burger et al. (2015); Papadopoulos et al. (2016); Stavrou et al. (2014)) and the second example the absorption of dimethyl ether, where so far no solvent screening has been performed, although a recent simulation study indicates that physical absorption can be a competitive alternative (Zhang et al., 2015) to the conventional separation by rectification sequences (Clausen et al., 2010). The composition and state of feed and solvent streams is applied according to Table 2.6.

Parameters for the thermodynamic interactions between each solvent component and the mixture are determined by COSMO-RS (Klamt, 1995) and the group contribution method of Benson & Buss (1958). Details on the generation of property parameters are provided in Chapter 4.1.2. The thermodynamic models are summarized in Appendix B. Potential solvent candidates are taken from the COSMObase[1] database. In total, 4,121 solvent candidates are investigated.

The performance of the absorption column is evaluated for all of these solvent candidates. By using parallelization, which can be applied easily, calculation time is short. Figure 2.12 shows the results for the absorption of carbon-dioxide, and Figure 2.13 the results for the absorption of DME. For each solvent candidate, the solvent to feed ratio (L_0/V_{N+1}) and the concentration of the value component in the liquid stream ($\mathbf{x}_N$) are shown. Both curves show an asymptotic behavior. Large solvent to feed ratio leads to low concentrations of the value component in the loaded liquid stream and low solvent to feed ratios lead to high concentrations. Therefore, a low solvent to feed ratio is not only preferred because smaller devices can be used, but also because the value component is concentrated in the liquid stream. Top scoring candidates using minimum solvent to feed ratio as the ranking criteria are given in Table 2.9.

[1] COSMObase: http://www.cosmologic.de/products/cosmobase.html

Many of the solvents in the databank cannot be applied directly because operational constrains such as toxicity, stability, viscosity, or risk of explosion are not considered, but need to be included in an extension of this study. However, the large-scale screening can already be used to benchmark solvent candidates already suggested in literature (Bonet et al., 2015; Frank, 2008; Oudshoorn et al., 2009). More than 100 candidates were collected and their performance is shown by black crosses in Figures 2.12 and 2.13 Four top scoring solvent candidates in terms of solvent to feed ratio are recommended in Table 2.8 and 2.9, respectively.

In conclusion, the screening of thousands of solvents proves robustness of the suggested solution procedure. A quick screening of a large number of solvents is possible, which allows to benchmark existing, well-known solvents, and to identify new, promising alternatives. The pinch-based screening already distinguishes itself from conventional screening which only relies on the evaluation of thermodynamic properties. However, several studies strongly indicate, that solvents solvents should not be selected only based on the evaluation of the absorption column (Papadopoulos & Linke (2005); Scheffczyk, Redepenning, et al. (2016b)), but solvent recovery as well as other additional devices required for an absorption process need to be included in the evaluation. This next level of screening solvents is established in Chapter 4.

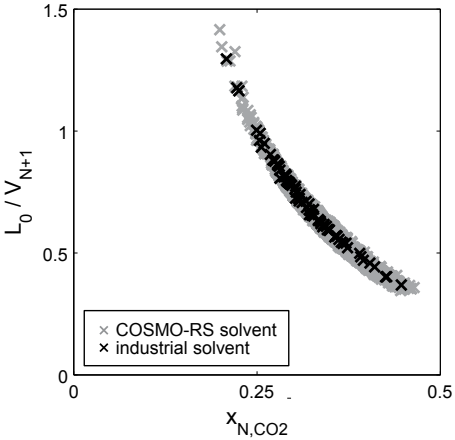

Figure 2.12.: Solvent-to-feed ratio (L_0/V_{N+1}) subject to the concentration of carbon-dixode (CO_2) in the liquid stream for 4,121 solvent candidates.

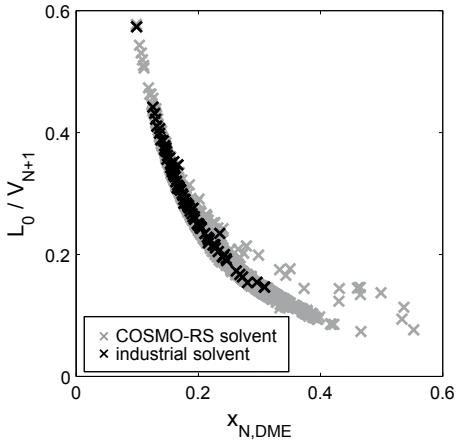

Figure 2.13.: Solvent-to-feed ratio (L_0/V_{N+1}) subject to the concentration of dimethyl-ether (DME) in the liquid stream for 4,121 solvent candidates.

Table 2.8.: Selected results for the screening of solvents. 4,121 solvents are evaluated. Concentrations are given in the order argon / methane / hydrogen / nitrogen / carbon-dioxide / carbon-monoxide / solvent. Specifications are according to Table 2.6, case study III. and IV

rank	solvent name	CAS	$\frac{L_0}{V_{N+1}}$	$\frac{V_1}{V_{N+1}}$ $\frac{L_N}{V_{N+1}}$	$\mathbf{y}_1$ $\mathbf{x}_N$	T_1 (°C) T_N (°C)
top scoring candidates						
1	pyranthrene	191-13-9	0.35	0.58	0.003/0.003/0.775/0.004/0.001/0.214/0.000	226
				0.77	0.000/0.001/0.015/0.001/0.446/0.086/0.001	267
2	digeranyl-ether	31147-36-1	0.35	0.59	0.003/0.002/0.753/0.005/0.001/0.236/0.000	227
				0.76	0.001/0.001/0.023/0.000/0.448/0.067/0.002	267
3	ethyl-linolenate	1191-41-9	0.35	0.59	0.003/0.002/0.745/0.005/0.001/0.244/0.000	226
				0.76	0.001/0.001/0.024/0.000/0.451/0.059/0.002	267
industrial solvents						
38	oleyl-alcohol	143-28-2	0.37	0.60	0.003/0.002/0.731/0.005/0.001/0.258/0.000	226
				0.76	0.001/0.001/0.025/0.000/0.447/0.044/0.002	267
193	1-hexadecene	629-73-2	0.40	0.60	0.003/0.002/0.737/0.005/0.001/0.252/0.000	229
				0.80	0.001/0.001/0.024/0.000/0.425/0.048/0.002	268
802	dodecanol	112-53-8	0.46	0.61	0.003/0.003/0.723/0.005/0.001/0.266/0.000	230
				0.84	0.000/0.001/0.020/0.000/0.404/0.032/0.001	270
937	dodecane	112-40-3	0.47	0.61	0.003/0.002/0.730/0.005/0.001/0.259/0.000	231
				0.86	0.001/0.001/0.022/0.000/0.395/0.038/0.002	271

Table 2.9.: Selected results for the screening of solvents. 4,121 solvents are evaluated. Concentrations are given in the order hydrogen / carbon-monoxide / carbon-dioxide / dimethyl-ether / solvent. Specifications are according to Table 2.6, case study II.

rank	solvent name	CAS	$\frac{L_0}{V_{N+1}}$	$\frac{V_1}{V_{N+1}}$ $\frac{L_N}{V_{N+1}}$	$\mathbf{y}_1$ $\mathbf{x}_N$	T_1 (°C) T_N (°C)
top scoring candidates						
1	4-methyl-1,2-benzenediol	452-86-8	0.02	0.93	0.754/0.011/0.234/0.001/0.000	326
				0.09	0.001/0.000/0.030/0.738/0.008	367
2	2,4-dihydroxybenzoicacid	89-86-1	0.02	0.93	0.754/0.011/0.234/0.001/0.000	333
				0.09	0.001/0.000/0.028/0.733/0.008	360
3	3-methylsalicylicacid	83-40-9	0.02	0.93	0.755/0.011/0.234/0.001/0.000	324
				0.10	0.001/0.000/0.034/0.723/0.010	364
industrial solvents						
237	3-hydroxytoluene	108-39-4	0.15	0.92	0.757/0.011/0.231/0.001/0.001	336
				0.22	0.006/0.000/0.032/0.308/0.308	336
240	4-methylphenol	106-44-5	0.15	0.92	0.757/0.011/0.231/0.001/0.001	335
				0.22	0.006/0.000/0.033/0.308/0.308	336
303	2,4-dimethylphenol	105-67-9	0.15	0.92	0.758/0.011/0.230/0.001/0.001	331
				0.23	0.007/0.000/0.035/0.296/0.296	335
495	dodecanol	112-53-8	0.17	0.91	0.765/0.011/0.223/0.001/0.001	305
				0.26	0.017/0.000/0.065/0.268/0.268	317

2.7 Conclusions

Existing shortcut concepts for absorption columns are improved by an accurate modeling of the pinch point. Minimum solvent demand could then be determined by exploiting the fixed point properties of the pinch. Four types of fixed point behavior are discussed. The number of eigenvalues greater or smaller than unity allow to distinguish between shortcut models referring to a stable, unstable, saddle-node, or a saddle pinch point. The novel shortcut outperforms existing shortcut methods in terms of accuracy in all investigated case studies. By adding additional separation stages to the shortcut model, the shortcut result can be improved to any desired accuracy. The proposed solution procedure reliably identifies the controlling model. Good computational performance can be achieved with a continuation algorithm which taps a wide range of applications. The performance of the solution procedure is illustrated for multiple examples including a fully automated screening of thousands of solvents.

The quick and reliable convergence of the proposed method to a favorable operation at minimum solvent demand allows for the fully automated comparison of operating points or a large number of solvents. Likewise, the reliable convergence combined with the improvement to any desired accuracy can directly be applied to initialize rigorous models, because the shortcut can determine bounds and initial values. In addition, the improvement poses a unique concept to determine an upper bound for the required number of separation stages which is suggested for further research in Chapter 6.2. The method directly provides insights into the investigated separation. For example, the initialization of the continuation according to Figure 2.9 determines the influence of the feed temperature on the design. Low temperatures lead to less solvent loss which supports the well-known observation that absorption favours low temperatures of the feed stream (Kister, 2008). Furthermore, each iterate of the continuation represents a feasible operation at minimum solvent demand according to Figure 2.10, and therefore allows direct conclusions on good operating conditions. The screening of solvents, illustrated by evaluating thousands of solvents in a fully automated manner, not only proves robustness of the suggested solution procedure, but can already be used to replace conventional selection of solvents by heuristic rules.

Finally, the shortcut method presents an innovative technology to bridge the gap in conceptual design between first ideas and detailed optimization. Initialization of rigorous models, pre-selection of promising separation alternatives, or screening of solvents can directly be addressed.

Chapter 3

Pinch-based shortcut method for the design of isothermal extraction columns

Solvent extraction is a promising separation alternative when distillation is difficult because of the low relative volatility, low concentration, or heat-sensitivity of a value component. Prominent examples therefore are the removal of aromatic compounds, the purification of waste streams, or the recovery of bio-molecules from a fermentation broth (Frank, 2008).

The selected solvent and the mixture to be processed exhibit a liquid-liquid phase split. Different solubility of one or more solutes serves as separating driving force. The recovery of solutes from the feed mixture can be improved when multiple separation stages are ordered in a counter-current arrangement. In general, additional separation stages reduce the solvent demand but increase the investment cost. Since the subsequent solvent recovery process determines economics, operation at or close to minimum solvent demand is often economically attractive, though a large or even infinite number of separation stages is required (Köhler et al., 1995).

The schematic of an isothermal extraction column is illustrated in Figure 3.1. The liquid feed ($L^{\mathrm{R}}_{\mathrm{N}+1}$) and solvent ($L^{\mathrm{E}}_{0}$) streams enter the column on opposite ends, and, on each stage, the raffinate (L^{R}_{n+1}) and the solvent-rich extract (L^{E}_{n}) streams are in a liquid-liquid equilibrium. In contrast to an adiabatic column, such as the absorption column discussed in the previous Chapter 2, no energy balance is required. The rigorous model, which covers all stages (N) and components (C), requires mass, equilibrium, and summation

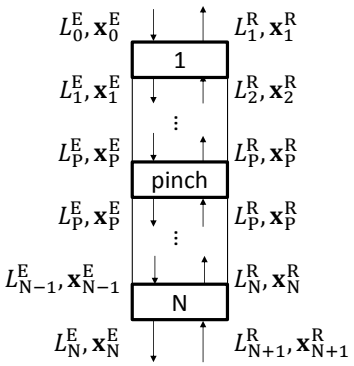

Figure 3.1.: Schematic of an isothermal counter-current extraction column. The rigorous model relies on a large number of stages, whereas an infinite number is assumed by the pinch-based shortcut.

(MES) equations which can be written as an implicit stage-to-stage recurrence:

$$0 = L_0^E x_{0,i}^E + L_{n+1}^R x_{n+1,i}^R - L_n^E x_{n,i}^E - L_1^R x_1^R, \quad i = 1,...,C, \quad n = 1,...,N, \tag{3.1}$$

$$0 = x_{n,i}^E - K_{n,i} x_{n,i}^R, \quad i = 1,...,C, \quad n = 1,...,N, \tag{3.2}$$

$$0 = 1 - \sum_{i=1}^{C} x_{n,i}^R, \qquad n = 1,...,N, \tag{3.3}$$

$$0 = 1 - \sum_{i=1}^{C} x_{n,i}^E, \qquad n = 1,...,N. \tag{3.4}$$

Usually, the liquid-liquid phase equilibrium (K_i) is kinetically controlled. Transport limitations are strongly influenced by the type of extractor device and depend on a number of diffusion-controlled phenomena such as rise, formation, and coalescence of drops (Mohanty, 2000). Therefore, an accurate description of interfacial mass transfer requires dedicated experiments and complex modeling, which can often not be afforded in the early phase of conceptual process design. Instead, diffusion-controlled phenomena are ignored and the choice of the extractor device is delayed, such that equilibrium-based models can

be employed (Frank, 2008; Marcilla et al., 1999). Phase equilibrium is then determined by activity coefficients γ_i,

$$K_{n,i} = \frac{\gamma_{n,i}(\mathbf{x}_n^{\mathrm{R}}, T)}{\gamma_{n,i}(\mathbf{x}_n^{\mathrm{E}}, T)}, \qquad i = 1,...,C, \qquad n = 1,...,N, \tag{3.5}$$

which are functions of compositions and temperature and can be described by appropriate thermodynamic models.

For a given number of separation stages N, temperature T, and compositions of the feed and solvent stream $\mathbf{x}_0^{\mathrm{E}}$ and $\mathbf{x}_{\mathrm{N}+1}^{\mathrm{R}}$, the minimum solvent-to-feed ratio $L_0^{\mathrm{E}}/L_{\mathrm{N}+1}^{\mathrm{R}}$ can be calculated by the rigorous model, Eqs. (3.1)-(3.4), if one additional specification, e.g., the desired purity σ of one component j in the cleaned raffinate stream

$$x_{1,j}^{\mathrm{R}} = \sigma, \qquad j \in \{1,...,C\}, \tag{3.6}$$

is provided.

If a sufficiently large number of separation stages is considered, the rigorous model predicts minimum solvent operation with sufficiently high accuracy. The rigorous model, however, involves well-known difficulties: If a mixture with many components is considered, and if only inaccurate initial guesses are available, the solution of the rigorous model is laborious. Moreover, since many stages must be considered for the calculation of minimum solvent demand, the number of MES equations and hence the computational effort is further increased. Alternatively, shortcut calculations can be applied to cut down the computational effort and to improve the robustness of the calculations. In general, shortcut calculations intend to simplify the set of MES equations by approximations, which leads to different concepts providing a diverse range of detail and quality.

Performance of a solvent is often investigated by evaluating thermodynamic properties of the mixture such as the activity coefficient at infinite dilution (Gmehling & Schedemann, 2014; Pretel et al., 1994; Schweitzer, 1988). However, thermodynamic properties can only provide a qualitative comparison between different solvents, but offer no information on outlet flow rates, compositions, or minimum solvent demand.

In case one single separation stage is assumed to approximate the separation apparatus (Bonet et al., 2015; Frank, 2008), product flow rates and compositions can be calculated. However, information on minimum solvent demand requires an infinite number of separation stages, which, in consequence, cannot be determined.

Alternatively, a shortcut model can be based on an integral balance of the separation column with the MES equations (3.1)-(3.4) for $n = N$ to determine outlet flow rates and

compositions, while correlations are employed to approximate the stage concentrations extending from the first to the last stage. A prominent representative for such an approach is the equation of Kremser (1930), which can be modified to tackle liquid-liquid separations (Smith & Brinkley, 1960).

Minimum solvent operation implies vanishing thermodynamic driving force within the column section, which refers to the existence of the pinch point. Consequently, integration of accurate pinch modeling has the potential to improve the shortcut calculation of minimum solvent demand. At the pinch, the vanishing thermodynamic driving force ($\mathbf{x}_{\mathrm{P}}^{\mathrm{E}} = \mathbf{x}_{\mathrm{P}+1}^{\mathrm{E}}$) allows to describe the pinch (P) by the set of pinch equations (cf. Figure 3.1),

$$\begin{aligned} 0 = L_0^{\mathrm{E}} x_{0,i}^{\mathrm{E}} + L_{\mathrm{P}}^{\mathrm{R}} x_{\mathrm{P},i}^{\mathrm{R}} - L_{\mathrm{P}}^{\mathrm{E}} x_{\mathrm{P},i}^{\mathrm{E}} - L_1^{\mathrm{R}} x_1^{\mathrm{R}}, \\ i = 1, ..., C. \end{aligned} \tag{3.7}$$

The pinch-based shortcut model therefore employs both the integral balance of the separation column given by the MES equations (3.1)-(3.4) for $n = N$, the design specification, Eq. (3.6), the liquid-liquid equilibrium, Eqs. (3.2)-(3.4) for $n \in \{1, N, \mathrm{P}\}$, and the pinch equations (3.7). In order to complete the pinch-based shortcut model, $C-2$ additional specifications are required which were originally represented by the large set of MES equations for all $n \in \{1, ..., N\}$, which are to be avoided.

For ternary mixtures, the pinch-based shortcut model has one degree of freedom. On the one hand, minimum solvent operation is tied to the existence of the pinch within the column section, i.e., if k is the value component,

$$x_{1,k}^{\mathrm{E}} \leq x_{\mathrm{P},k}^{\mathrm{E}} \leq x_{\mathrm{N},k}^{\mathrm{E}}, \qquad k \in \{1, ..., C\}. \tag{3.8}$$

On the other hand, the pinch constrains separation progress. Hence, in case of ternary mixtures, minimum solvent operation can be identified if the pinch just vanishes, either at the end of the column section ($\mathbf{x}_1^{\mathrm{E}} = \mathbf{x}_{\mathrm{P}}^{\mathrm{E}}$, or $\mathbf{x}_{\mathrm{N}}^{\mathrm{E}} = \mathbf{x}_{\mathrm{P}}^{\mathrm{E}}$) as a so-called product pinch, or within the column section as a so-called tangential pinch.

Graphical methods for the identification of minimum solvent operation are well-known for ternary mixtures (Burger et al., 2016; Hunter & Nash, 1935; Ruiz Beviá et al., 1984; Wankat, 2007). Key process variables are plotted in a two-dimensional diagram, e.g., the solvent flow rate as a function of the concentration of a component in the product stream. Then, minimum solvent operation is identified by visual inspection, in case the pinch just vanishes as a product or tangential pinch.

An algebraic approach for ternary mixtures is suggested by Minotti et al. (1996). A

continuation algorithm is employed to calculate composition and flow rate of the product and the pinch as a function of the solvent-to-feed ratio. Subsequently, the set of solutions is analyzed to find product or tangential pinch points in order to identify minimum solvent operation. Alternatively, maximization of the solvent-to-feed ratio subject to the existence of the pinch, Eq. (3.8), also identifies minimum solvent operation, if the pinch just vanishes (Krämer, 2012).

For mixtures with more than three components, the mere observation of the pinch cannot compensate for an approximation of the set of MES equations representing stages extending from the pinch to the first and the last stage. However, for isothermal liquid-liquid separations there is currently no concept available to provide a desired approximation, but shortcut methods for distillation or adiabatic absorption offer promising approaches. For instance, shortcut methods for distillative separations assume a linear path of stage compositions from one column end to the pinch. Alternative concepts to linearize the path lead to different methods for the pinch-based calculation of minimum reflux ratio (Bausa et al., 1998; Holland et al., 2004; Krämer et al., 2009; Levy et al., 1985; Lucia et al., 2008). Accurate results are achieved for thermodynamically ideal mixtures (ideal liquid and gas phase, constant molar overflow) (Levy et al., 1985). Since liquid-liquid equilibrium always involves non-ideal thermodynamic behavior, a possibly large approximation error is inevitable (Wallert, 2008).

In this chapter, the model previously developed for adiabatic absorption is modified to cover isothermal extraction, which leads to a novel pinch-based shortcut model for isothermal extraction columns. The set of non-linear model equations of the pinch-based shortcut model can have multiple solutions and thus requires careful initialization. Therefore, in the following section, a step-by-step solution procedure is established which reliably leads to a model solution. The procedure generalizes previous work of Redepenning et al. (2013) providing a method for arbitrary separations. Then, a fully automated screening of more than 3,500 solvents for the extraction of acetone, 1-butanol, and ethanol from a fermentation broth highlights the performance of the shortcut method. Conclusions are finally given in the last section.

3.1 Shortcut model

The stage-to-stage recurrence in Eqs. (3.1)-(3.4) is an instance of a non-linear discrete dynamical system. At the pinch, $n = \mathrm{P}$, the compositions on two adjacent stages are identical, i.e., $\mathbf{x}^{\mathrm{E}}_{\mathrm{P}+1} = \mathbf{x}^{\mathrm{E}}_{\mathrm{P}}$. Hence, the pinch is a fixed point of the discrete dynamical system. The implicit function theorem allows to differentiate the set of non-linear equations (3.1)-(3.4)

at the pinch point (Poellmann et al., 1994). The first-order differential $\frac{\partial \mathbf{x}^{\mathrm{E}}_{n+1}}{\partial \mathbf{x}^{\mathrm{E}}_{n}}$ is calculated as a $C \times C$ matrix. However, and this is the major difference compared to the pinch-based model for adiabatic absorption (cf., Chapter 2.2), only $C-2$ lines and rows of the matrix are independent, because isothermal liquid-liquid equilibrium is constrained by both the summation constraint and the specified temperature. Hence, the matrix provides $C-2$ independent eigenvectors $\mathbf{e}_j$ and eigenvalues λ_j, which allow to derive the general linear approximate solution (Poellmann et al., 1994; Redepenning & Marquardt, 2016) for the course of stage compositions starting at an arbitrary stage k as a linear combination of λ_j and $\mathbf{e}_j$ by considering the weights c_j,

$$x^{\mathrm{E}}_{n,i} = x^{\mathrm{E}}_{\mathrm{P},i} + \sum_{j=1}^{C-2} c_j \lambda_j^{n-k} e_{i,j}, \qquad i = 1,...,C-2. \tag{3.9}$$

Depending on the size of the eigenvalue, λ_j, the corresponding eigenvector,$\mathbf{e}_j$, is stable, if the eigenvalue is smaller than unity, unstable, if the eigenvalue is greater than unity, and neutral, if the eigenvalue equals unity (Sandefur, 1990).

Because the vanishing driving force at the pinch constrains progress of the stage-to-stage recurrence, the linear approximation is employed in the following to approximate the course of the stage compositions starting from both sides of the column towards the pinch. According to the basic pinch-based model suggested for adiabatic absorption columns (Chapter 2.2), neutral and stable eigenvectors represent the course starting at a stage $1+M$, $M \geq 0$,

$$x^{\mathrm{E}}_{1+M,i} = x^{\mathrm{E}}_{\mathrm{P},i} + \sum_{\substack{j=1,\\ \lambda_j \leq 1}}^{C-2} \mu_j e_{i,j}, \qquad i = 1,...,C-2, \tag{3.10}$$

while neutral and unstable eigenvectors represent the course starting at a stage $N-O$, $O \geq 0$,

$$x^{\mathrm{E}}_{\mathrm{N}-O,i} = x^{\mathrm{E}}_{\mathrm{P},i} + \sum_{\substack{j=1,\\ \lambda_j \geq 1}}^{C-2} \nu_j e_{i,j}, \qquad i = 1,...,C-2. \tag{3.11}$$

The basic shortcut model (BSM) assumes no additional stages ($M = 0$, $O = 0$). However, in this case, the linear approximations, Eqs. (3.10) and (3.11), are only accurate close to the pinch. If the actual path of stage-compositions is non-linear and the distance between the first or the last stage increases, the approximations show an error. The dis-

tance can, however, be decreased by adding additional stages, resulting in an improved shortcut model (ISM). Consequently, M additional stages can be introduced to the shortcut model comprising Eqs. (3.1) for $n = 1,...,M$, and (3.2)-(3.4) for $n = 2,...,M+1$, to improve the approximation of stage concentrations between the first stage and the pinch, Eq. (3.10). To improve the approximation of stage concentrations between the last stage and the pinch, Eq. (3.11), O additional stages can be introduced formulating Eqs. (3.1)-(3.4) for $n = \mathrm{N}-1,...,\mathrm{N}-O$. Each additional stage (i.e., increasing M and O) gradually improves the accuracy, because the distance to the pinch, and hence the approximation error, is reduced.

In conclusion, the pinch point is classified by the number of stable and unstable eigenvectors. If the pinch has only stable eigenvectors, the pinch is stable, if only unstable eigenvectors are present, the pinch is unstable, and if both stable and unstable eigenvectors occur, the pinch is a saddle. When a stable, unstable, or saddle pinch applies, the shortcut model combines the set of MES equations for the first stage, the last stage, and the pinch point, Eqs. (3.1) for $n = N$, Eqs. (3.2)-(3.4) for $n \in \{1, N, \mathrm{P}\}$, Eq. (3.7), the approximations which relate the first and the last stage with the pinch point, Eqs. (3.10) and (3.11), and one design specification, Eq. (3.6). The BSM ($M = 0$, $O = 0$) requires no additional equations, while the ISM requires a set of MES equations to cover additional stages by Eqs. (3.1) for $n = 1,...,M$, Eqs. (3.2)-(3.4) for $n = 2,...,M+1$, or by Eqs. (3.1)-(3.4) for $n = \mathrm{N}-1,...,\mathrm{N}-O$, respectively.

A fourth type of pinch occurs when one eigenvalue equals unity. The stable or unstable pinch merges with a saddle in a saddle-node bifurcation. This type of pinch is therefore referred to as saddle-node or tangential pinch (Levy & Doherty, 1986). It is described by the constraint

$$\lambda_j = 1, \qquad j \in \{1,...,C-2\}. \tag{3.12}$$

Hence, the shortcut model with a saddle-node pinch relies on this constraint and the model equations for the stable, unstable, or saddle pinch.

3.2 Solution of the shortcut model

The solution of the shortcut model is only possible if accurate initial guesses and the correct type of pinch are provided. In order to avoid trial-and-error calculations, which cannot guarantee a solution in a reasonably short period of time, a fully automated step-by-step solution procedure is suggested in the following.

The steps of the method are illustrated for the separation of the solutes o-xylene and toluene from n-heptane using propylene-carbonate as a solvent. The liquid-liquid equilibrium is described by the UNIQUAC model with parameters from literature (Salem et al., 1994). Figure 3.2 visualizes the investigated mixture in a quaternary diagram. The extract and raffinate phases are separated by a line, which comprises the locus of all critical points, and binodal surfaces represent the locations of compositions in an isothermal liquid-liquid equilibrium. Table 3.1 provides a set of specifications for the illustrating case study. Temperature, pressure, compositions of both the feed and solvent stream, as well as the desired purity of toluene in the cleaned raffinate stream are given. The mixture and type of split are chosen in such a way that all steps of the suggested method can be discussed.

Table 3.1.: Specifications for the illustrating case study. Isothermal extraction at 25°C is assumed.

component	$\mathbf{x}_{N+1}^{R}$	$\mathbf{x}_{0}^{E}$	σ
o-xylene	0.25	0	-
toluene	0.35	0	0
n-heptane	0.4	0	-
propylene-carbonate	0.0	1	-

3.2.1 Reduced shortcut model

In the first step, a reduced shortcut model (RSM) is solved, which ignores the approximation extending from the first stage to the pinch, Eq. (3.10), but assumes a fully specified composition of the first stage. Initially, a full recovery of all $C-2$ solutes l from the feed stream is assumed, i.e.,

$$x_{1,l}^{R} = 0, \qquad l = 1,...,C-2. \tag{3.13}$$

The specification of all solutes, Eq. (3.13), combined with summation and equilibrium equations, Eqs. (3.2)-(3.4) for $n = 1$, allows to calculate the composition at the first stage with a homotopy continuation algorithm (Bausa & Marquardt, 2000).

The RSM combines the set of MES equations covering the first stage, the last stage, and the pinch point, Eqs. (3.1) for $n = N$, Eqs. (3.2)-(3.4) for $n \in \{1, P, N\}$, Eq. (3.7), fea-

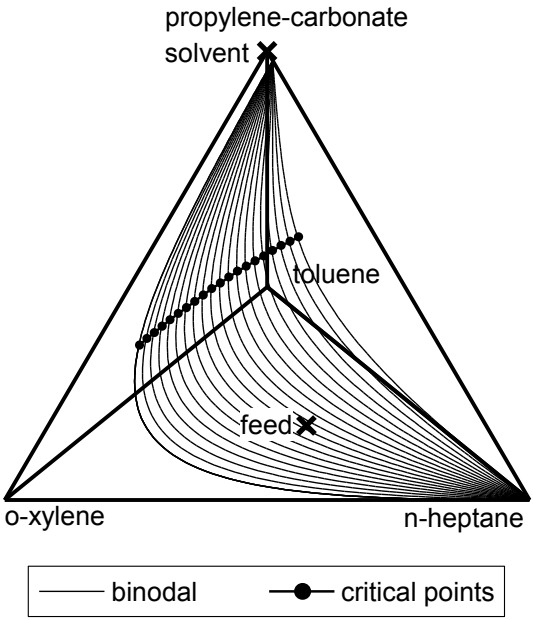

Figure 3.2.: Quaternary diagram for the mixture o-xylene, toluene, n-heptane, and propylene-carbonate. Crosses mark the compositions of the feed and the solvent stream.

sibility of the approximation extending from the pinch to the last stage, Eq. (3.11), and the specification of all solutes, Eq. (3.13). The RSM is further decomposed into two sub-models, RSM 1 and RSM 2, which allows to individually initialize and solve each sub-model. RSM 1 covers the first stage and the last stage with Eqs. (3.1) for $n = N$, (3.2)-(3.4) for $n \in \{1, N\}$, and Eq. (3.13), while RSM 2 covers the first stage and the pinch point with Eqs. (3.2)-(3.4) for $n \in \{1, \mathrm{P}\}$, Eq. (3.7), and Eq. (3.13). Both sub-models, RSM 1 and RSM 2, have only one degree of freedom and solutions are determined with a predictor-corrector continuation algorithm (Choi et al., 1996; Jiménez-Islas et al., 2013). Continuation reliably determines all solutions, if all one-dimensional solutions are continuously connected. In case isolated solutions occur, one initial point for each isolated solution branch is required.

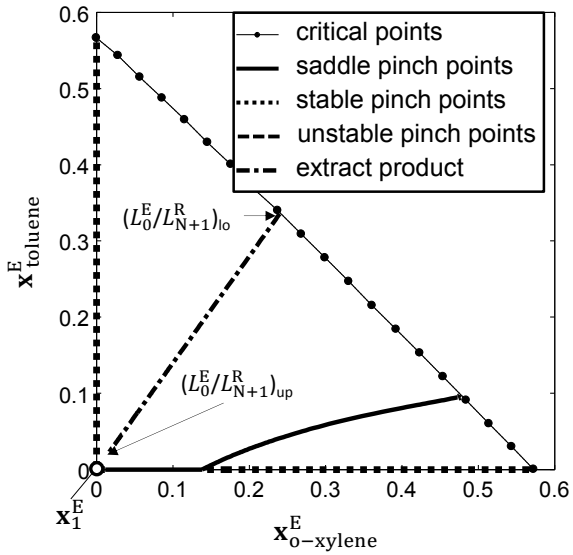

Figure 3.3.: Solutions for RSM 1 (dash-dotted line) and for RSM 2 (dotted, dashed, solid lines). RSM 1 provides solutions for the extract product $\mathbf{x}_N^E$. RSM 2 provides solutions for the pinch $\mathbf{x}_P^E$.

Figure 3.3 shows one-dimensional solution loci for both sub-models. The solutions of RSM 1 are depicted as dash-dotted line and are referred to as product of the extract. The upper bound of the solvent-to-feed ratio, $(L_0^E/L_{N+1}^R)_{up}$, serves as initial point for the continuation. At the upper bound, the extract and raffinate phase just separate and the raffinate flow rate is zero, $L_1^R/L_{N+1}^R = 0$, which is the initial solution for the continuation. Continuation stops at the edge of concentration range or the miscibility gap, which is typically described by a critical point, which is an actual point for ternary mixtures, a line for quarternary mixtures, and a multi-dimensional plane for mixtures with more than four components. The edge usually represents the lower bound of the solvent-to-feed ratio, $(L_0^E/L_{N+1}^R)_{lo}$.

The solutions of RSM 2 are referred to as pinch lines, which comprise the loci of all pinch points. In Figure 3.3, two types of pinch points occur, which are marked by solid

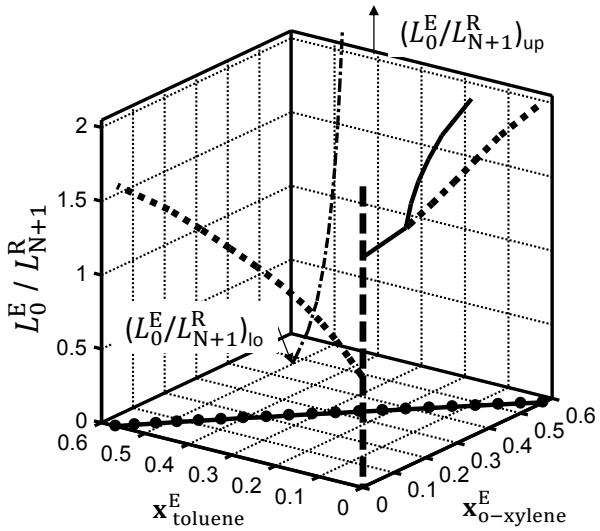

Figure 3.4.: Combined solutions for RSM 1 and for RSM 2. Refer to Figure 3.3 for a description of the symbols.

and dotted lines and refer to stable and saddle pinch points, respectively. Stable parts are located on the axis representing concentrations of toluene, and both saddle and stable parts, are located on the axis representing concentrations of o-xylene. The pinch line bifurcates and an additional line representing saddle pinch points starts. The continuation is initialized at the lower bound of the solvent to raffinate ratio, $L_0^E/L_1^R = 0$, when the composition of the pinch equals the composition of the first stage, $\mathbf{x}_P^E = \mathbf{x}_1^E$. For the designated operating point, all pinch solutions are reliably found, because all branches are connected with the initially specified composition of the first stage, $\mathbf{x}_1^E$.

The solutions of RSM 1 and RSM 2 are then combined in order to obtain one single set of solutions. This allows to depict both the compositions of the extract product and the compositions of the pinch points subject to the solvent-to-feed ratio in Figure 3.4. The compositions of the extract product recede from the line formed by critical points with increasing solvent-to-feed ratio, whereas pinch solutions show a converse behavior and

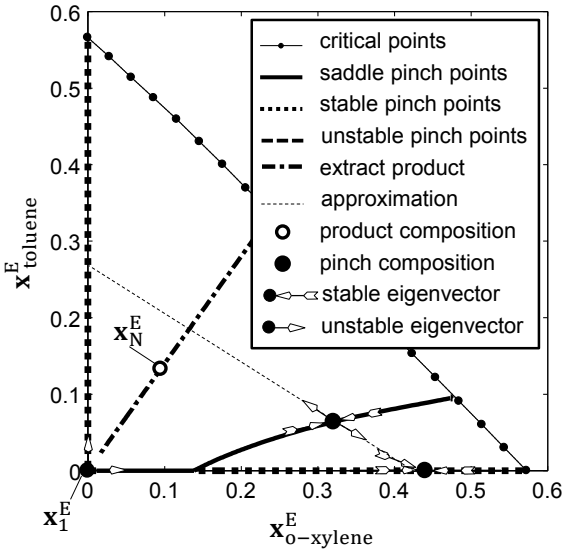

Figure 3.5.: At $L_0^{\mathrm{E}}/L_{\mathrm{N+1}}^{\mathrm{R}} = 1.95$, the unstable pinch provides a solution for the RSM.

approach the line formed by critical points. If a full recovery of all solutes from the feed is specified, Eq 3.13, an unstable pinch point occurs at the composition of the first stage, $\mathbf{x}_1^{\mathrm{E}}$, for all feasible solvent to feed ratios.

The feasible solutions of RSM can be identified from the combined set of solutions of RSM 1 and RSM 2. However, feasibility of the path of stage-to-stage compositions from the pinch to the extract product, Eq. (3.11), needs to be granted. For selected solvent-to-feed ratios $L_0^{\mathrm{E}}/L_{\mathrm{N+1}}^{\mathrm{R}}$, multiple pinch points can occur, leading to more than one possible solutions for RSM. This is illustrated in the following by comparing solutions for two different solvent to feed ratios, $L_0^{\mathrm{E}}/L_{\mathrm{N+1}}^{\mathrm{R}} = 1.95$ and $L_0^{\mathrm{E}}/L_{\mathrm{N+1}}^{\mathrm{R}} = 1.85$.

Figure 3.5 shows that three pinch points occur for $L_0^{\mathrm{E}}/L_{\mathrm{N+1}}^{\mathrm{R}} = 1.95$: An unstable pinch at the composition of the first stage, $\mathbf{x}_1^{\mathrm{E}}$, a stable pinch on the o-xylene axis, and a saddle pinch. The unstable eigenvector of the saddle approximates the path of the stage-to-stage compositions from the pinch to the last stage, which is indicated by a dashed line. The

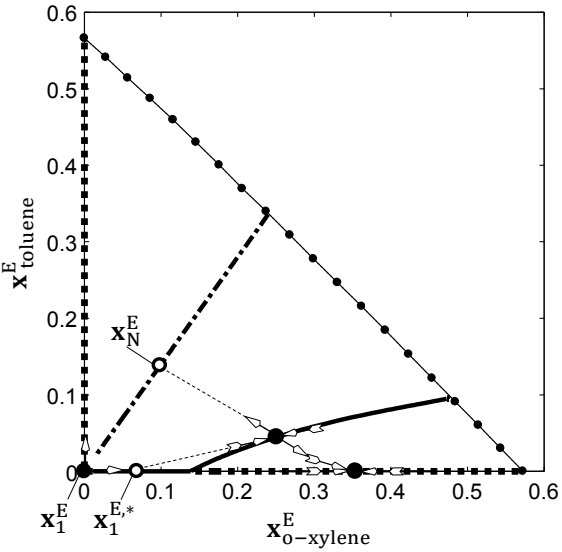

Figure 3.6.: At $L^E_0/L^R_{N+1} = 1.85$, both the saddle and unstable pinch provide a solution for the RSM.

approximation, Eq. (3.11), is infeasible, because it does not connect to the product composition of the extract, $\mathbf{x}^E_N$. Hence, infeasibility of the RSM is apparent when the saddle pinch is used. Alternatively, a feasible path from pinch to product can be obtained if the unstable pinch is chosen.

Figure 3.6 shows that the unstable pinch as well as the saddle pinch provide a solution for $L^E_0/L^R_{N+1} = 1.85$, because the saddle pinch connects with the composition of the last stage by Eq. (3.11). Likewise, the unstable pinch connects with the composition of the last stage, resulting in two candidate solutions of the RSM. Only one solution, however, can in fact be related to a feasible separation.

Close to the minimum solvent demand, the path of rigorous stage-to-stage compositions just touches pinch points (Köhler et al., 1995). According to Bausa et al. (1998), along this path, the number of stable eigenvectors must increase strictly monotonically to match the condition of increasing entropy production. Therefore, along the path of a stage-to-stage

trajectory, the pinch having the larger number of stable eigenvectors is located closer to the product of the opposite side, i.e., the extract product, and in consequence the eigenvectors of this pinch are likely to give the best approximation for the path to the extract product. For this separation the solution achieved with the saddle is used.

Having identified the controlling pinch for an initial composition of the first stage set by Eq. 3.13, in the next step of the method the composition of the first stage is updated, $\mathbf{x}_1^{\mathrm{E},*}$, using the approximation of the path from the first stage to the pinch, Eq. (3.10), the constraint for the desired purity, Eq. (3.6), and the liquid-liquid equilibrium, Eqs. (3.2)-(3.4) for $n = 1$.

While the previous composition of the first stage, $\mathbf{x}_1^{\mathrm{E}}$, and the new composition of the first stage, $\mathbf{x}_1^{\mathrm{E},*}$, deviate (cf. Figure 3.6), repetition of the previous steps of the procedure according to fixed-point iteration can be applied to obtain a better estimate for the composition of the first stage. Alternatively, since good initial guesses and the controlling pinch are already identified, a solution of the basic shortcut model with an appropriate numerical solver can be attempted directly. If no solution is found, repetitive execution of the solution procedure is required in order to improve initial guesses.

The presented steps of the solution procedure always allow to find a solution, provided all pinch points are reliably found by the continuation algorithm. So far, this condition is fulfilled if all solutions are connected with the initially specified composition of the first stage. However, this condition can be invalid if the pinch points need to be calculated for alternative compositions of the first stage, which is required when repetitive execution of the solution procedure is necessary. Such a condition and an appropriate method to find all solutions is discussed in the following section.

3.2.2 Initial solutions for the continuation

In the previous section, multiple solutions could be observed for the investigated case study. The solutions are distinguished by analyzing the stability of the pinch, which finally allows to identify the relevant solution. To this end, the preliminary calculation of all relevant pinch points is obviously required. The procedure which has been established so far, allows to find pinch points, if these points are connected by pinch lines with the composition of the first stage, $\mathbf{x}_1^{\mathrm{E}}$, specified according to Eq. 3.13. In the following, it is shown that pinch points can be isolated from the composition of the first stage which requires the extension of the procedure.

Figures 3.7 to 3.10 illustrate the behavior of pinch lines calculated by RSM 2 for different compositions of the first stage, $\mathbf{x}_1^{\mathrm{E}}$. The situation in Figure 3.7 has been investigated in

previous sections: All solutes are removed from the first stage according to Eq. 3.13, and all pinch lines are connected at bifurcation points. When the composition varies, i.e., a larger concentration of o-xylene about 1.8 mol-% is desired at the first stage ($x^{\mathrm{E}}_{1,\text{o-xylene}}$), pinch lines are calculated according to Figure 3.8. For this situation, all pinch lines just touch in one bifurcation point at the o-xylene-axis. In Figure3.9, if the concentration of o-xylene ($x^{\mathrm{E}}_{1,\text{o-xylene}}$) is increased to 2.5 mol-%, or in Figure 3.10, if the concentration of o-xylene is increased to 5 mol-%, one isolated pinch line occurs, which is not connected with the concentration of the first stage, $\mathbf{x}^{\mathrm{E}}_1$. These isolated pinch lines cannot be found by the procedure which has been established so far.

Previous works on pinch-based methods for quarternary extraction already mention the existence of isolated pinch lines (Minotti et al., 1996; Wallert, 2008). However, a systematic procedure for their calculation has not been discussed, and all existing methods are therefore effectively limited to ternary mixtures where this phenomena cannot occur, because all pinch points are simply located on the binodale curve. In the following, two different concepts for the calculation of isolated pinch lines are investigated and compared: The first approach is algebraically general, but proved to be numerically difficult to solve, the second approach is heuristic and relies on analogies to similar problems in vapor-liquid separations, but proved to be numerically robust.

Isolated solution branches are a general problem when continuation methods are applied. Often, isolated solution branches can be found by a continuation of higher-order bifurcations (Jiménez-Islas et al., 2013). The behavior of bifurcation points when different compositions of the first stage are applied can be observed in Figures 3.7 to 3.10. For this concept, higher-order bifurcations are tracked while the composition on the first stage is varied ($\tilde{\mathbf{x}}^{\mathrm{E}}_1$), e.g., from the initial specification according to Eq. 3.13, $\mathbf{x}^{\mathrm{E}}_1$, to an updated composition of the first stage, $\mathbf{x}^{\mathrm{E},*}_1$, according to

$$\tilde{x}^{\mathrm{E}}_{1,i} = x^{\mathrm{E}}_{1,i} + \xi\,(x^{\mathrm{E},*}_{1,i} - x^{\mathrm{E}}_{1,i}), \qquad i = 1,\ldots,C-2. \tag{3.14}$$

Higher-order bifurcation can be interpreted as tangential pinch points and have already been modeled by Eq. (3.12). The model for a continuation of those higher-order bifurcations finally combines the set of MES equations for the pinch, Eqs. (3.2)-(3.4) for $n \in \{1,\mathrm{P}\}$, Eq. (3.7) the variation of the composition of the first stage, Eq. (3.14), and the constraint for the saddle-node bifurcation, Eq. (3.12).

In Figure 3.11, the behavior of saddle-node bifurcations is depicted when the composition of the first stage is varied. For two exemplary compositions of the first stage, $\mathbf{x}^{\mathrm{E}}_1$ and $\mathbf{x}^{\mathrm{E},*}_1$, pinch lines with stable and saddle points are depicted in grey as dotted and solid lines. At the bifurcation, the stability of the pinch lines changes. The bifurcation locus

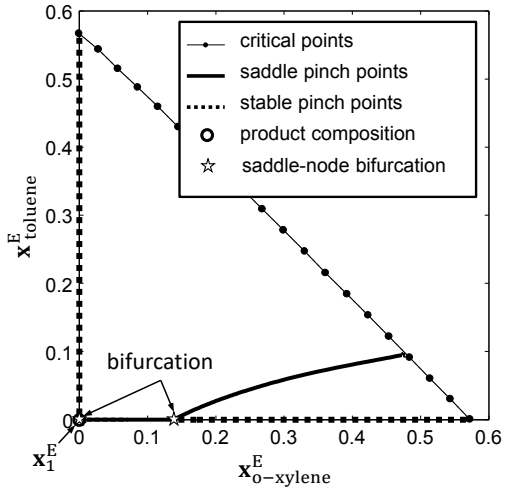

Figure 3.7.: All solutes removed, $x^{E}_{1,\text{o-xylene}}$ is 0 mol-%. Pinch lines are connected and thus found by the continuation of pinch points.

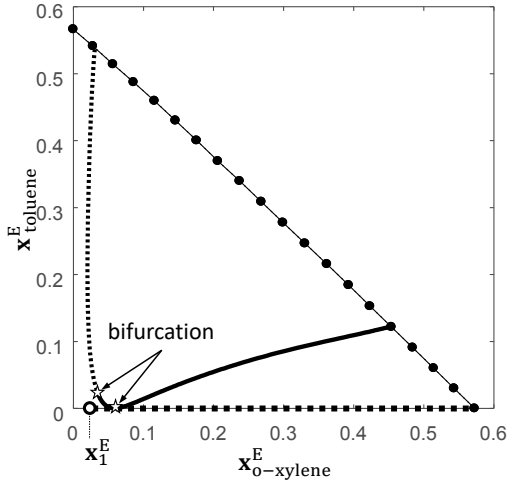

Figure 3.8.: Pinch lines calculated when $x^{E}_{1,\text{o-xylene}}$ is 1.8 mol-%. Pinch lines are just connected at the bifurcation on the o-xylene axis. Refer to Figure 3.7 for a description of the symbols.

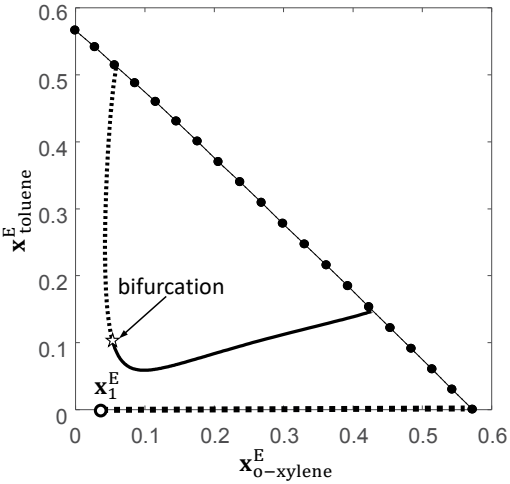

Figure 3.9.: Pinch lines calculated when $x^{E}_{1,\text{o-xylene}}$ is 2.5 mol-%. One pinch line is isolated. Figure 3.7 for a description of the symbols.

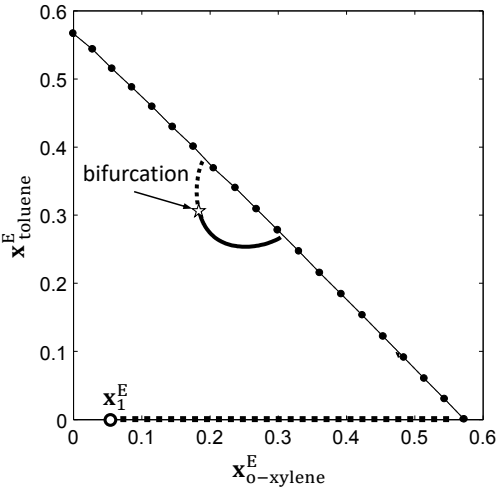

Figure 3.10.: Pinch lines calculated when $x^{E}_{1,\text{o-xylene}}$ is 5 mol-%. One pinch line is isolated. Figure 3.7 for a description of the symbols.

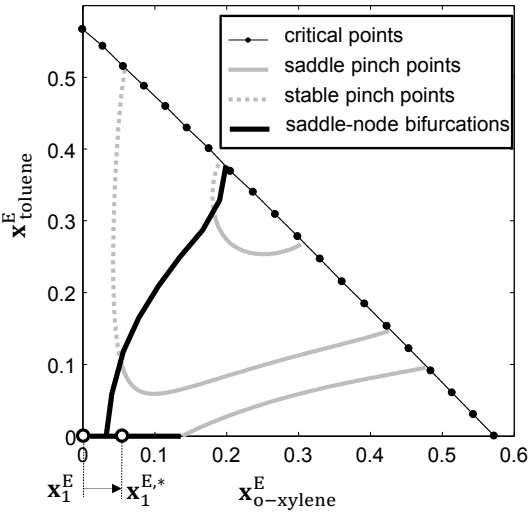

Figure 3.11.: Saddle-node bifurcations for varied composition of the first stage, $\tilde{\mathbf{x}}_1^{\mathrm{E},*}$. Pinch lines on the o-xylene and toluene axes are not depicted for a better readability.

bifurcates itself on the o-xylene axis. The continuation of bifurcation points traces isolated pinch points, which are not connected with the composition of the first stage, $\mathbf{x}_1^{\mathrm{E},*}$. The grey pinch lines in Figure 3.11 which are isolated in Figures 3.9 and 3.10 are connected by the line of bifurcation points. The solutions of the bifurcation lines can consequently be employed to find starting points for the pinch lines.

The continuation of higher-order bifurcations has not only the potential to find isolated solutions, but also to provide insight on good operating conditions. Saddle-node bifurcations represent limit points for the separations such as tangential pinch points. The effects of bifurcation points and possible conclusions for the separation is thoroughly discussed for extractive rectification (Brüggemann & Marquardt, 2004; Knapp & Doherty, 1994). Although this concept allows to find isolated solutions and provides insight into the separation, the continuation of the bifurcation, i.e., Eq. (3.12), proved to be difficult to solve reliably in an automated manner. Therefore, an alternative is suggested in the following which relies on an analogy to distillative separations.

For distillative separations, the existence of isolated pinch points, which are not connected with the product of one column section, is well-known (Bausa et al., 1998; Beneke et al., 2011; Felbab, 2012; Felbab et al., 2011; Skiborowski et al., 2016). Nevertheless, all pinch points can be found reliably, because initial points for the continuation are provided by the pure components and the azeotropes of an investigated mixture. For isothermal liquid-liquid separations, the critical points share the property of azeotropes, because the concentrations in one liquid phase are the same as in the other liquid phase. However, in contrast to distillative separations, only in ternary mixtures critical points are isolated points. In a multi-component mixture critical points can form a line, e.g., in a quaternary mixture (cf. Figure 3.2), or a multi-dimensional plane in a mixture with more than four components. In consequence, in contrast to distillation, critical points where the pinch line starts or ends are unknown *a priori*.

For distillative separations, some works focused on the inverse problem (Felbab, 2012; Skiborowski et al., 2016). They determined the location of azeotropes and hence the starting points for all pinch lines from one pinch line initially starting in a pure product. Accordingly, for isothermal liquid-liquid separations, the pinch line starting in the pure product, Eq. (3.13), identifies controlling critical points which can serve as starting points for all pinch lines. The controlling critical points can be defined as pinch points close to critical points

$$\sum_{j=1}^{C-2} (x_{\mathrm{P},j}^{\mathrm{E}} - x_{\mathrm{P},j}^{\mathrm{R}})^2 = \varepsilon, \tag{3.15}$$

where ε is a small constant (i.e., $\varepsilon = 10^{-4}$). In order to find the controlling critical points for different compositions of the first stage, the controlling critical points are tracked while the compositon of the first stage is varied according to Eq. 3.14. The model to track controlling critical points is in the following referred to as controlling critical points model (CCM). It combines Eqs. 3.14, 3.15, equilibrium and summation equations for the first stage and the pinch, Eqs. 3.2-3.4 for $n \in \{1, \mathrm{P}\}$, and the pinch equations, Eq. 3.7.

In Figure 3.12, continuation of CCM starts at a given product $\mathbf{x}_1^{\mathrm{E}}$ corresponding to the critical points A, B, and C for $\xi = 0$. When the composition of the first stage varies from $\mathbf{x}_1^{\mathrm{E}}$ to $\mathbf{x}_1^{\mathrm{E},*}$, which is indicated by the arrow, the controlling critical points move to A* and B*, or stay in C*, which is also indicated by arrows. For the new composition of the first stage, $x_1^{\mathrm{E},*}$, pinch lines are not connected. However, for each pinch line the corresponding critical points A*, B*, and C* are identified for the new composition of the first stage $\mathbf{x}_1^{\mathrm{E},*}$ by a continuation of CCM. These critical points A*, B*, and C* can therefore serve as initial solutions for the continuation of pinch points. This concept reliably finds all pinch

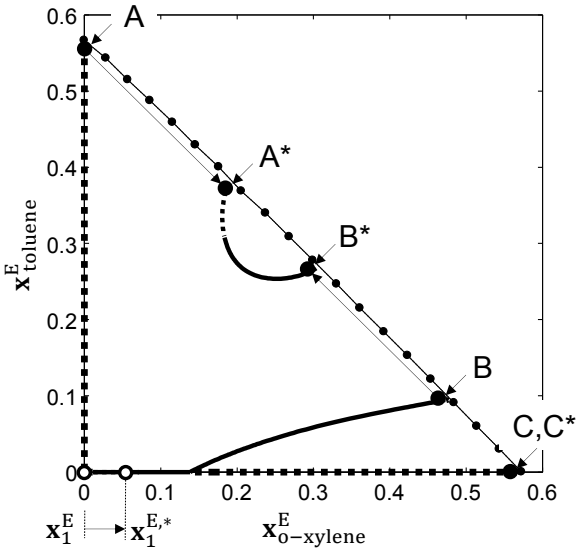

Figure 3.12.: Pinch lines for two compositions of the first stage, $\mathbf{x}_1^{\mathrm{E}}$ and $\mathbf{x}_1^{\mathrm{E},*}$. Pinch lines are isolated when the new composition of the first stage, $\mathbf{x}_1^{\mathrm{E},*}$, applies. Refer to Figure 3.5 for a description of the symbols.

solutions and proved to be numerically stable. Therefore, this concept is preferred to the continuation of bifurcation points and applied in the following studies.

3.2.3 Results of the basic shortcut model

The suggested procedure calculates all possible pinch points and then identifies the controlling pinch point from a set of possible solutions. Thus, the procedure solves the BSM reliably, if a solution exists. Infeasibility of the solution procedure can hence be related to an impossible separation, whereas in a conventional approach using local non-linear equation solver infeasibility could be caused by inaccurate initial guesses.

The implemented algorithm is summarized in Algorithm 1. The fully automated method is implemented in C/C++. In the presented case study, a solution is obtained within one

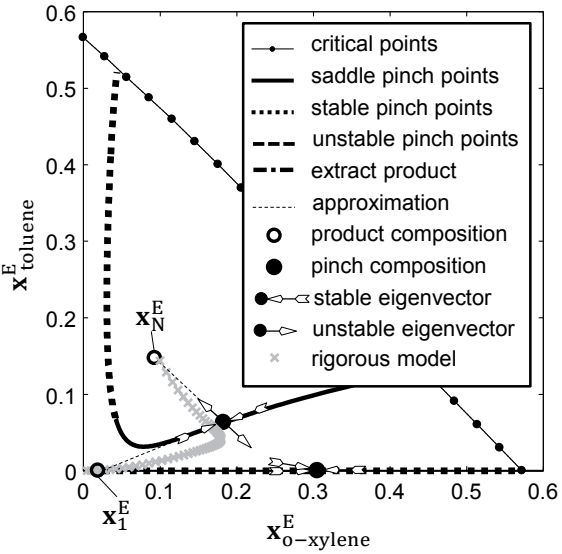

Figure 3.13.: Results of BSM. The result of a rigorous model (grey) with sixty stages is depicted for a comparison.

second on a standard Intel(R) Core(TM) i3-4150 3.5 GHz personal computer.

The results obtained for the shortcut model are summarized in Table 3.2. The method reliably determines product compositions, flow rates, and minimum solvent demand. For a comparison, the rigorous model with sixty stages is solved with the EXTRACT-module of AspenPlus®. Although the shortcut model relies on only three separation stages for the calculation of the minimum solvent demand, the deviation from the rigorous model is low, e.g., below 3 in terms of the solvent-to-feed ratio.

The shortcut and rigorous results are depicted in Figure 3.13 together with the pinch lines. The saddle pinch controls the separation and the directions of the stable and unstable eigenvector are used to approximate both parts of the stage-to-stage recurrence, from the first stage ($\mathbf{x}^E_1$) to the pinch, and from the pinch to the last stage ($\mathbf{x}^E_N$). The first and the last stage start or end close to the approximated first and last stage. Deviations between the shortcut and the rigorous results can be related to the curvature of the rigorous path of

Algorithm 1 Shortcut method

procedure SHORTCUT($L^{\mathrm{R}}_{\mathrm{N+1}}, \mathbf{x}^{\mathrm{E}}_{0}, \mathbf{x}^{\mathrm{R}}_{\mathrm{N+1}}, \sigma, T, p$)
  Set $\mathbf{x}^{\mathrm{E}}_{1}$, Eq. 3.13;
  Set *solutionFound* = FALSE;
  while *solutionFound* == FALSE **do**
    Solve RSM 1 with continuation;
    Solve RSM 2 with continuation;
    Combine solutions of RSM 1 and RSM 2;
    Find all solutions for RSM;
    Select solution with largest number of $\lambda < 1$;
    Calculate new $\mathbf{x}^{\mathrm{E},*}_{1}$;
    Solve BSM;
    if shortcut model is feasible **then**
      solutionFound = TRUE;
    else
      $\mathbf{x}^{\mathrm{E}}_{1} = \mathbf{x}^{\mathrm{E},*}_{1}$;
      Solve CCM with continuation;
    end if
  end while
end procedure

stage compositions.

3.2.4 Results of the improved shortcut model

Reduction of the approximation error is achieved by solving the ISM. Figure 3.14 depicts the solvent-to-feed ratio calculated with the ISM when M and O additional stages are gradually added to the approximations introduced by Eqs. (3.10) and (3.11). The improvement of the approximation was achieved in two phases: In the first phase, nine additional stages are added to the approximation representing the path from the pinch to the last stage ($M = 0$, $O = 9$), followed by a second phase, where twenty-six stages are added to the approximation representing the path from the first stage to the pinch ($M = 26$, $O = 9$). Both phases show an asymptotic behaviour because each additional stage reduces the approximation error by reducing the distance to the pinch. It should be remarked, that in this case study the deviation of the shortcut result from the final rigorous solution increases in the first phase, before it decreases in the second phase. Apparently, the approximation error caused by the approximation of the first part of the trajectory compensated for the even

Table 3.2.: Results determined with BSM and rigorous model with sixty stages. Results of the ISM agree with rigorous results. Specifications for the separation are summarized in Table 3.1.

component	$\mathbf{x}_1^R$	$\mathbf{x}_N^E$	flow ratio	
basic shortcut model				
o-xylene	0.080	0.090	L_0^E/L_{N+1}^R	1.72
toluene	0.000	0.150	L_1^R/L_{N+1}^R	0.35
n-heptane	0.920	0.030	L_N^E/L_{N+1}^R	2.73
propylene-carbonate	0.000	0.730		
rigorous and improved shortcut model				
o-xylene	0.021	0.100	L_0^E/L_{N+1}^R	1.77
toluene	0.000	0.143	L_1^R/L_{N+1}^R	0.33
n-heptane	0.979	0.033	L_N^E/L_{N+1}^R	2.44
propylene-carbonate	0.000	0.724		

larger approximation error caused by the second part of the trajectory. As a consequence, although in general each additional stage should reduce the approximation error, because the linear approximation by the eigenvalues is replaced by a rigorous stage-to-stage calculation, for an accurate solution both parts of the trajectory need to be refined in order to accomplish an accurate solution. The improvement in each phase could be stopped if a desired accuracy is achieved, or, in order to validate the result, when a separation stage is sufficiently close (here: distance < 0.05) to the pinch.

Figure 3.15 shows the improved result of the shortcut model with in total thirty-five additional stages ($O = 9$, $M = 26$). The results of the improved shortcut model agree with the rigorous results (cf. Figure 3.13 and Table 3.2). Nevertheless, the rigorous model requires a large number of stages to overcome the low driving force at the pinch, whereas the shortcut model with additional stages relies on the direction of the eigenvectors to approximate the behavior in the vicinity of the pinch. A sufficiently accurate representation of the rigorous results is already obtained when the results of ISM are close to saturation during each phase of the improvement in Figure 3.14. Thereby, in order to achieve an accurate result, nineteen stages can already be sufficient; nine stages to approximate the path from the pinch to the last stage, and ten for the path from first stage to the pinch.

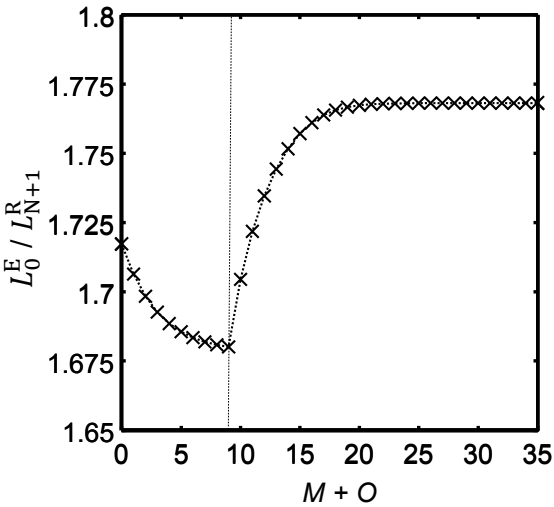

Figure 3.14.: Solvent-to-feed ratio subject to a step-by-step improvement using ISM. In a first phase, nine additional stages are added to the approximation form the pinch to the last stage ($M = 0$, $O = 9$); in a second phase, twenty-six additional stages are added to the approximation from the first stage to the pinch ($M = 26$, $O = 9$).

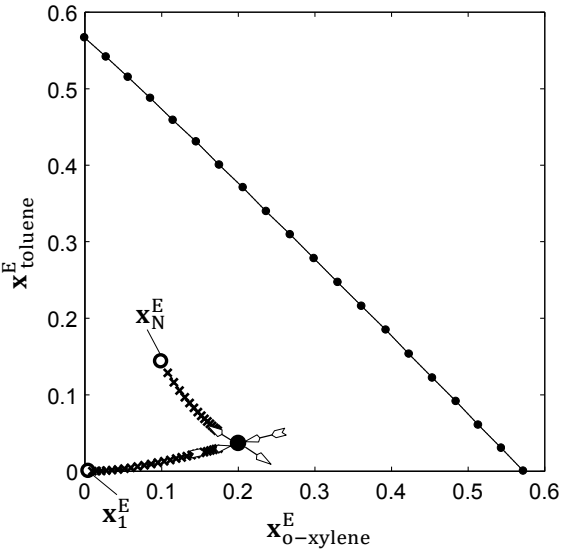

Figure 3.15.: Result of the ISM. Thirty-five additional separation stages improve the approximations.

3.3 Screening of solvents

The performance of the method is illustrated by a fully automated screening of solvents, which is only feasible because of the extremely reliable convergence of the BSM. Two examples are used for illustration: First, (I.) a ternary extraction of 2,3-butanediol from water, and second (II). a five-component extraction of fermentation products acetone, 1-butanol, and ethanol (ABE) from water. Specifications of the feed composition are adapted from literature (Krämer et al., 2011b; Xiu & Zeng, 2008) and are summarized in Table 3.3 for convenience.

Table 3.3.: Specifications for the screening of solvents. Isothermal extraction at 308 K is assumed for both examples.

case study	components	$\mathbf{x}^{\mathrm{R}}_{\mathrm{N+1}}$	$\mathbf{x}^{\mathrm{E}}_{0}$	σ
(I.)	2,3-butanediol	0.01	0	0
	water	0.99	0	-
	solvent	0	1	-
(II.)	acetone	0.003	0	-
	1-butanol	0.002	0	0
	ethanol	0.002	0	-
	water	0.993	0	-
	solvent	0	1	-

Possible solvent candidates are taken from the built-in COSMObase databank, which allows direct access to parameters for the NRTL model to describe the liquid-liquid equilibrium by activity coefficients. To ensure bio-compatibility of the solvents, only molecules containing carbon, hydrogen, and oxygen atoms are considered which leads to 3,868 possible solvent molecules (Scheffczyk et al., 2016b).

The extractive separation is then evaluated for all 3,868 solvent candidates. Calculation time is low. For each solvent, convergence only takes seconds, such that a total calculation time for all solvent candidates below one hour can be achieved. The full evaluation leads to the results shown in Figure 3.16 and Figure 3.17. Grey crosses mark the performance of each solvent candidate, represented by the concentration of the value components 2,3-butanediol ($x^{\mathrm{E}}_{\mathrm{N,\ 2,3\text{-}butanediol}}$) or, respectively, 1-butanol ($x^{\mathrm{E}}_{\mathrm{N,\ 1\text{-}butanol}}$) in the extract product and the minimum solvent demand ($L^{\mathrm{E}}_{0}/L^{\mathrm{R}}_{\mathrm{N+1}}$). For both examples, a typical asymptotic behavior can be observed such that low solvent to feed ratio results in high concentrations

of the value component but large solvent to feed ratios in low concentrations. In general, for subsequent downstream processes, favorable solvents will require low solvent to feed ratios but achieve large concentrations of the value components. The five top scoring solvents which result in separations with the lowest solvent-to-feed ratio are given in Table 3.4 and Table 3.5.

The sequential screening of large databases with the suggested shortcut method allows to select solvents based on process targets such as outlet compositions, flow rates, and minimum solvent demand. The method can be integrated into a flowsheet evaluation or complement existing solvent selection criteria (Papadopoulos & Linke, 2006; Pretel et al., 1994) such as viscosity, toxicity, or boiling temperature. Each of these thermodynamic quantities can have a strong influence on the final performance of a solvent and needs to be taken into consideration. Currently, the evaluation only relies on the NRTL activity coefficient model. Further operational constraints could, however, easily be integrated in an extension of the study. For example, availability of the solvent could play an important role if the solvent is produced or used somewhere else in the process. The use of such a solvent could sometimes be preferred over the use of an external solvent (Qi & Malone, 2011). For the separation of ABE, the utilization of 1-butanol as a solvent is a representative of this concept (cf. Table 3.5). The screening of solvents directly provides a benchmark of this and other interesting solvents compared to the top scoring candidates.

The shortcut method can also be used to benchmark well-known industrial solvents reported in literature (Bonet et al., 2015; Frank, 2008; Oudshoorn et al., 2009). Their performance is marked with black crosses for both examples in Figure 3.16 and Figure 3.17. The best performing five solvents are summarized in Table 3.4 and Table 3.5. Obviously, all the top scoring industrial solvent candidates are outperformed by solvents identified by the screening procedure. Oleyl-alcohol, which is a recommended solvent for the ABE extraction (Davison & Thompson, 1993; Krämer et al., 2011b; Qureshi et al., 1992), achieves a low solvent-to-feed ratio with moderate yield of 1-butanol. Many attractive solvents, including solvents reported in industrial practice, have the potential to outperform this established solvent, and selected candidates are given in Table 3.4 and Table 3.5.

In conclusion, the shortcut method presents a rapid screening tool to benchmark liquid-liquid extraction for the favorable operation point at minimum solvent demand. Arbitrary mixtures can be tackled, regardless the number of components or thermodynamic modeling.

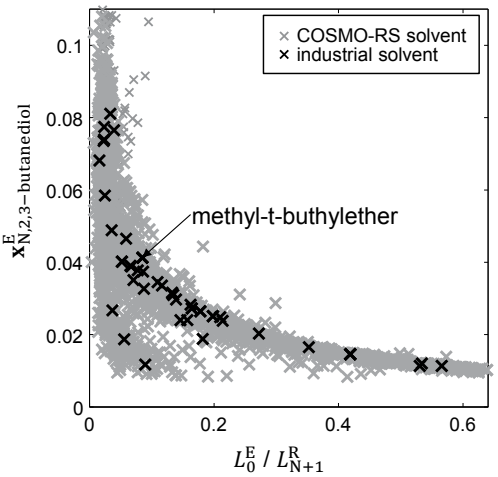

Figure 3.16.: Concentration of 2,3-butanediol subject to the minimum solvent to feed ratio for 3,868 solvent candidates.

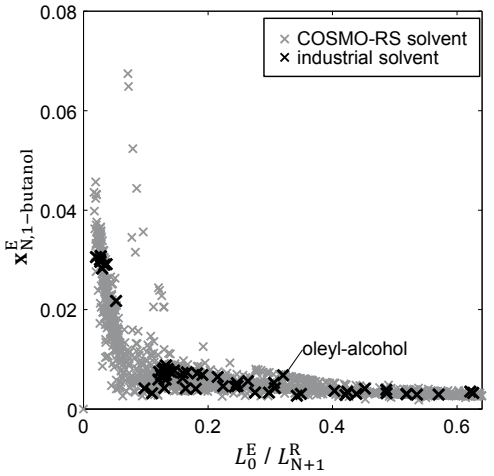

Figure 3.17.: Concentration of 1-butanol subject to the minimum solvent to feed ratio for 3,868 solvent candidates.

Table 3.4.: Selected results for the screening of solvents for a recovery of 2,3-butanediol. 3,868 solvents from the COSMObase databank are evaluated; among them are a number of industrial solvents, which have been reported in literature. Concentrations are given in the order 2,3-butanediol / water / solvent.

rank	solvent name	CAS	$\frac{L_0^E}{L_{N+1}^R}$	$\mathbf{x}_I^R$	$\mathbf{x}_N^E$
top scoring candidates					
1	2-ethylpiperidine	1484-80-6	0.003	0.000/1.000/1.000	0.040/0.947/0.947
2	59009-70-0-cation	n.a.	0.006	0.000/0.998/0.998	0.073/0.892/0.892
3	tri-n-butylamine-cation	n.a.	0.007	0.000/0.999/0.999	0.104/0.837/0.837
4	sucralose	56038-13-2	0.007	0.000/0.998/0.998	0.054/0.912/0.912
5	n,n-dipropyl-1-propanamine	102-69-2	0.009	0.000/1.000/1.000	0.059/0.887/0.887
industrial solvents					
56	3-chlorophenol	108-43-0	0.016	0.000/0.996/0.996	0.068/0.849/0.849
253	3-hydroxytoluene	n.a.	0.023	0.000/0.997/0.997	0.074/0.782/0.782
270	4-methylphenol	n.a.	0.023	0.000/0.997/0.997	0.074/0.774/0.774
275	2-methylphenol	95-48-7	0.024	0.000/0.997/0.997	0.077/0.759/0.759
308	phenol	108-95-2	0.025	0.000/0.990/0.990	0.058/0.846/0.846
reference solvent					
1179	methyl-t-butylether	1634-04-4	0.085	0.000/0.998/0.998	0.041/0.616/0.616

Table 3.5.: Selected results for the screening of solvents for a recovery of ABE. 3,868 solvents from the COSMObase databank are evaluated; among them are a number of industrial solvents, which have been reported in literature. Concentrations are given in the order acetone / 1-butanol / ethanol / water / solvent.

rank	solvent name	CAS	$\frac{L_0^E}{L_{N+1}^R}$	$\mathbf{x}_1^R$	$\mathbf{x}_N^E$
top scoring solvents					
1	3,5-diisopropylbenzenehydroperoxide	26762-93-6	0.02	0/0/0/1.000/0.000	0.065/0.044/0.044/0.481/0.366
2	1-naphthol	90-15-3	0.02	0/0/0/0.999/0.001	0.060/0.040/0.040/0.533/0.328
3	3-methylsalicylicacid	83-40-9	0.02	0/0/0/0.999/0.001	0.054/0.036/0.036/0.557/0.316
4	mono-tert-butylhydroquinone	1948-33-0	0.02	0/0/0/0.998/0.002	0.046/0.031/0.031/0.635/0.257
5	o-t-butylphenol	88-18-6	0.02	0/0/0/1.000/0.000	0.064/0.042/0.042/0.446/0.405
product used as a solvent					
447	1-butanol	71-36-3	0.13	0/0.009/0/0.991/-	0.010/0.341/0.007/0.583/-
industrial solvents					
43	3-hydroxytoluene	108-39-4	0.03	0/0/0/0.997/0.003	0.045/0.030/0.030/0.548/0.347
52	4-methylphenol	106-44-5	0.03	0/0/0/0.997/0.003	0.044/0.030/0.030/0.538/0.358
58	2-methylphenol	95-48-7	0.03	0/0/0/0.997/0.003	0.046/0.031/0.031/0.505/0.387
71	phenol	108-95-2	0.03	0/0/0/0.990/0.010	0.042/0.028/0.028/0.608/0.293
99	2,4-dimethylphenol	105-67-9	0.03	0/0/0/0.999/0.001	0.044/0.029/0.029/0.420/0.479
reference solvent					
	oleyl-alcohol	143-28-2	0.31	0/0/0/1.000/0.000	0.008/0.005/0.005/0.176/0.806

3.4 Conclusions

A pinch-based shortcut method for the design of isothermal extraction columns is presented. In contrast to existing pinch-based methods for extraction columns, the novel model is not limited to ternary mixtures. The suggested basic shortcut model relies on three stages only: the first stage, the last stage, and the pinch. Any desired accuracy of the shortcut model could then be achieved by an improved shortcut model, if additional stages are included. The subsequent step-by-step procedure leads to a model solution reliably and within seconds. No manual user-interaction is required. The full potential of the method is highlighted by a screening of more than 3,500 solvents for the extraction of 2,3-butanediol and acetone, 1-butanol, and ethanol from aqueous solution.

The screening based on the shortcut method differs from current established attempts, which only evaluate solvents by their thermodynamic properties such as the activity coefficient at infinite dilution. Instead, the shortcut method offers a thermodynamically sound criterion to assess the operation of the extraction column. The separation performance is fully captured at the operating point with minimum solvent demand. The assessment can also be extended to extraction columns integrated into complex flowsheets. For example, the extraction shortcut can be combined with a pinch-based shortcut method for distillation columns (Bausa et al., 1998) to screen a large number of solvents for their performance in hybrid extraction-distillation separation processes which is presented in the following Chapter.

Chapter 4

Pinch-based solvent screening for absorption and extraction processes

Selection of the solvent has a strong influence on the efficiency and economics of absorption processes. On the one hand, the solvent has to be tailored to the specific separation task while carefully considering competing and interacting process objectives. On the other hand, the large variety of possible molecular structures leads to countless solvent candidates which requires modern computing technology but poses a great challenge to the automated evaluation of such processes. In conclusion, process performance assessment in a robust and automated manner is ultimately required (Adjiman et al., 2014; Ng et al., 2015).

Accurate performance assessment is difficult to achieve in an automated manner. The performance is usually determined by using rigorous models where the separation units are described by a set of mass, equilibrium, and enthalpy (MESH) equations (Cremaschi, 2015) leading to a large-scale set of nonlinear equations. Optimization techniques need to be employed, not only to determine the optimal operating point, but also to identify the optimal flowsheet structure. Examples for structural alternatives are different number of separation stages, the existence and location of sidestreams, or the structure of heat-exchanger networks in heat-integrated separation sequences, which are often modeled by mixed integer non-linear programming (MINLP) problems. MINLP optimization problems are already difficult to solve for a single solvent and therefore a topic of current research (e.g., Bhattacharyya & Miller (2017); Hasan et al. (2012); Lee et al. (2016); Nuchitprasittichai & Cremaschi (2013)). The fully automated solution for a large number of solvent candidates is still not established.

As a consequence, according to the hierarchical technique of conceptual process design, promising solvent candidates are typically pre-selected prior to the detailed superstructure optimization with rigorous models (Douglas, 1988; Kossack et al., 2008; Marquardt et al., 2008). The methods applied for the pre-selection in the early phase of conceptual process design require not only the automated solution to evaluate a large number of solvent candidates, but also have to represent the separation columns and their interactions according to a flowsheet as accurately as possible. The automation combined with accurate performance assessment are decisive for the quality of the early performance assessment. Different methods for this design step are available, offering a diverse range of detail and quality.

Often, solvents are pre-selected based on heuristic rules such as physical solvent properties (e.g., solubility, solvent loss, phase distribution, e.g., Gmehling & Schedemann (2014); Pretel et al. (1994)) or simple performance correlations (e.g., the equation of Underwood (1949), used by Papadopoulos & Linke (2005, 2006)). These simple rules can be evaluated in a fully automated manner. Currently, the screening of solvents based on these rules is directly implemented in the software tool ICAS (integrated computer aided system, Eden et al. (2002); Gani et al. (1997); Kongpanna et al. (2016)) or could be calculated via COSMOtherm (Klamt et al., 2010). However, separation units or even flowsheets cannot be described only by one single heuristic rule alone. A combination of rules representing the combination of units by multiple objectives is required, and multiple competing objectives ultimately demand for multi-objective optimization (Papadopoulos & Linke, 2006). As the weights for the objectives are unknown, heuristic rules are likely to lead to wrong conclusions (Kossack et al., 2008).

The resulting complex superstructure optimization problem could be simplified by ignoring any structural choices and reducing the set of nonlinear model equations. Instead of identifying the optimal number of stages of the separation columns by superstructure optimization, a low and fixed number of separation stages can be assumed. For instance, in two recent works either a fixed number of stages are used to describe the absorption column and the flash stages for the recovery by desorption (Burger et al., 2015; Stavrou et al., 2014). The predefined number of stages reduces the design degrees of freedom and the low number of stages (≤ 10) leads to less nonlinear equations resulting in a less complex algebraic model. This way, all interactions of the flowsheet are covered and the performance of the solvent can be represented by the costs of the separation.

However, the assumption of a low number of separation stages favors investment over operating cost. Although for bulk processes usually operation at minimum operating cost is preferred, an insufficient number of stages can prevent the identification of solvents

accomplishing low operating cost, or, even worse, the separation can be infeasible if the number of stages is insufficient resulting in the exclusion of potentially cost-efficient solvent candidates. Selection of solvents based on such a simplification is therefore of limited value, because solvents are selected based on an improper objective.

Alternatively, solvents can be selected based on minimum operating cost which is a preferable selection criteria for bulk processes (Bauer & Stichlmair, 1996). Minimum operating cost is directly related to minimum energy demand of a process. As pointed out in previous sections, at minimum energy demand thermodynamic driving forces just vanish which is indicated by the occurrence of pinch points. Pinch points occur in any counter-current separation unit in case an infinite time for heat and mass transfer is assumed, which corresponds to an infinite number of stages in a separation column (Köhler et al., 1995) or an infinitely large area in a heat-exchanger (Klemeš & Kravanja, 2013). Thus, the minimum energy demand can be determined by only detecting the existence of pinch points, which allows for a simplified targeting instead of solving the complex rigorous models. The simple nature of pinch-based shortcut methods thereby reduces the computational effort and allows to employ problem specifically designed solution procedures to solve the pinch-based shortcut models reliably, in a fully automated manner, and without the need of manual intervention. These advantages have been highlighted multiple times throughout this thesis. Pinch-based shortcut methods are already available for heat exchanger networks (Linnhoff & Hindmarsh, 1983) and rectification columns (Bausa et al., 1998), and have been introduced for absorption columns in Chapter 2 and extraction columns in Chapter 3.

The value of pinch-based methods for an automated screening of solvents has already been demonstrated for hybrid extraction-rectification processes by Scheffczyk & Redepenning et al. (2016) using the methods introduced in this thesis. It has been shown that the estimates of pinch-based methods agree well with the results of rigorous models operating at minimum energy demand and argued that selection by minimum energy demand of the solvent recovery column is superior to conventional screening by heuristic rules. However, solvents are selected only based on the minimum energy demand of the solvent recovery column. The evaluation of additional units, heat integration, or optimization of the operating point is ignored.

This chapter illustrates how the pinch-based evaluation of complete hybrid absorption and extraction processes can be accomplished. Multiple separation columns as well as all additional devices such as compressors, pumps, and additional heat exchangers are considered. The pinch-based methods for heat integration, rectification, absorption, and extraction perfectly complement. All interactions of the flowsheet are covered, exploiting

the full potential of each solvent candidate, and allowing to summarize the performance of each solvent by minimum operating costs. Finally, fully automated evaluation of the flowsheet is established to determine the performance of thousands of solvent candidates by targeting minimum operating cost.

In the next section, methods and workflow to accomplish the large-scale screening of solvents are briefly discussed. The following section then illustrates the new selection of solvents by pinch-based methods for the removal of carbon-dioxide by a hybrid absorption-rectification process. Several thousands of solvents are screened and heat integration as well as optimization of the operating point is considered to tap the full potential of solvent candidates. Two additional case studies further illustrate the performance of the method; one case study investigates the absorption of dimethyl ether, and the other case study the extraction of aceton, 1-butanol, and ethanol from fermentation broth. Conclusions are finally given in the last section.

4.1 Methods

This work introduces methods for the fully automated evaluation of solvents based on minimum operating costs. The workflow is schematically illustrated in Figure 4.1: The workflow starts with a given process task which requires the screening of large number of solvents, and ends with a ranking of these solvents. In the first step, solvent candidates are identified from a database. In the second step, the full set of thermodynamic property parameters is determined which involves both pure component parameters for the solvents as well as non-ideal interactions with the investigated mixture. In the third step, the flowsheet is evaluated with pinch-based methods which finally provides a ranking of all solvents based on operating costs. The pinch-based process evaluation can be applied to any solvent and combined with any method for the generation of thermodynamic property parameters. In the following, a brief overview on existing methods for the identification of solvent candidates and generation of property data is given, and the methods used in this work are discussed.

4.1.1 Identification of solvent candidates

Candidate solvents can be found in large databases (e.g., DDB, COSMObase Gmehling & Schedemann (2014)) or determined by CAMD methods, where the optimal structure of the solvent molecule is designed subject to a performance target (e.g., Achenie et al. (2003), Austin et al. (2016), CoMT-CAMD by Bardow et al. (2010); Stavrou et al. (2014),

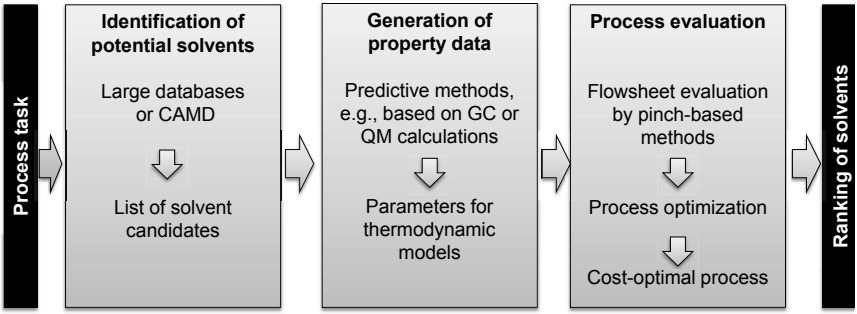

Figure 4.1.: Three-step workflow for the screening of solvents: (1) Identification of potential solvent candidates, (2) generation of thermodynamic property data, and (3) pinch-based process evaluation.

COSMO-CAMD by Scheffczyk et al. (2016a)). For the latter, the molecule can be an actual molecular structure (Scheffczyk et al., 2016a; Zhou et al., 2015), or a hypothetical, if a physically sound thermodynamic model (e.g., PC-SAFT) allows to identify a representative solvent molecule by reverse targeting (Bardow et al., 2010; Burger et al., 2015; Stavrou et al., 2014). Screening large databases can only find the optimal solvent, if this solvent is part of the database, whereas optimization of the solvent's molecular structure is more versatile, but increases the complexity of the overall design problem and in turn demands, compared to a sequential screening, simpler process models or tighter bounds for the optimization. Thus, both concepts might exclude unconventional solvent candidates, either because of lacking reliability of the computational methods or too small databases. Alternatively, hierarchical methods try to combine the advantages of both concepts to identify the optimal solvent (Burger et al., 2015).

In this work, solvent candidates are retrieved from the database COSMObase which is part of the commercially available software COSMOtherm. The structures as well as pre-calculated compound information are available for several thousand components.

4.1.2 Estimation of thermodynamic data

For any solvent selected from a database or determined by CAMD, thermodynamic model-parameters are required to describe pure component behavior and the interactions between

the solvent and the components of the mixture to be processed. While experimental data is of course preferred, it is often not available for a large set of solvent candidates in the early phase of conceptual process design. Therefore, predictive methods become more and more important because they provide immediate access to thermodynamic information. Currently, the most popular predictive methods are group contribution (GC) methods (Gmehling, 2009) (e.g., UNIFAC) or quantum-mechanical-based (QM) methods (Lehmann & Maranas, 2004; Struebing et al., 2013). GC methods are computationally cheap, but restricted to parameterized classes of components which have to be investigated experimentally. QM methods, in comparison, are unrestricted, but computationally demanding. Although predictive tools always involve some estimation error (Bureš et al., 1981), they are preferred in the early phase of conceptual design when many alternatives need to be compared. Nevertheless, for the final design, estimations always demand a validation by experiments which can be integrated in the solvent selection (Zhou et al., 2015) or accomplished by model-based experimental analysis (MEXA, Bonvin et al. (2016); Franceschini & Macchietto (2008); Marquardt (2005)).

The equations of the thermodynamic models can be functions of pressure, temperature, or composition. For all model equations, the thermodynamic properties are predicted by GC and QM methods for different sets of temperature, pressure, and composition and then fitted to the model equations. Both QM and GC methods are used in this work. In general, QM methods are preferred because they usually show low estimation error (Alevizou & Voutsas, 2014; Klamt, 1995). The thermodynamic model COSMO-RS (Eckert & Klamt, 2002; Klamt, 1995) is used to estimate activity coefficients, vapor pressure, heat of vaporization, Henry's coefficient, and the molar volume. The generation of model-parameters by using COSMO-RS has been described in a previous article by the authors (Scheffczyk et al., 2016b). Only for the calculation of heat capacities, the GC method of Benson & Buss (1958) is used which combines low computational time with good accuracy compared to other methods for the estimation of heat capacities (Poling et al., 2001). For GC calculations, the molecule needs to be decomposed into group fragments. The contribution of the individual group fragments is supported for 4,687 molecules in the COSMO*base* database, for which therefore the full set of thermodynamic model parameters, which are required for the process evaluation, can be determined.

4.1.3 Pinch-based methods for rectification columns

Shortcut methods for rectification columns are available for a long time and brief reviews can be found in the works of Lucia et al. (2008) or Krämer et al. (2011b). Graphical ap-

proaches such as McCabe-Thiele plots (McCabe & Thiele, 1925) or Petlyuk's methods (Petlyuk & Danilov, 2001; Petlyuk et al., 2008) are valuable to get insights into a separation, but cannot be used for an automated computer-aided evaluation. Likewise, laborious shortcut methods such as the boundary value method (BVM, Levy et al. (1985)) or the shortest stripping line (SSL, Amale & Lucia (2008)) can give good results, but require stage-to-stage calculations and have not been automated on a large scale. The model of Underwood (1949) has been used for a screening of solvents (Papadopoulos & Linke, 2006) but strongly simplifies thermodynamic behavior which can lead to inaccurate results.

Alternatively, good accuracy can be achieved if the rectification shortcut also builds on pinch points as a thermodynamic sound reference. In pinch points, the thermodynamic driving force vanishes which refers to minimum energy demand of a rectification column. Operation at minimum energy demand requires an infinite number of separation stages (Köhler et al., 1995; Lucia et al., 2008). The shortcut model, however, approximates the behavior between pinch points and the outlets of a column section. Levy et al. (1985) showed that for thermodynamically ideal mixtures (ideal liquid and gas phase, constant molar overflow), the path of a stage-to-stage calculation, represented by liquid or vapor compositions, is a straight line. Therefore, all existing pinch-based shortcut models share the assumption of a linear path of stage compositions. Some well-known models are the eigenvalue criterion (EC Poellmann et al. (1994)), the feed-angle method (FAM Krämer et al. (2011b)), the concept of moving triangles (Holland et al., 2004), and the rectification body method (RBM Bausa et al. (1998)). For thermodynamically ideal mixtures, when the assumption of a linear path of stage composition is valid, all methods lead to identical and accurate results. If the investigated mixture is thermodynamicially non-ideal, the models can also be applied and the deviation is usually small compared to the rigorous solution.

The simple nature of the pinch-based model fostered the development of problem specific solution procedures to solve a shortcut model reliably. Such a procedure is established by the RBM which is used in this work: A continuation algorithm is applied to calculate all existing pinch point solutions of the candidate separations from the pinch equation system (Bausa, 2001; Skiborowski et al., 2016). Then, possible paths along pinch points with an increasing entropy production are generated which allows to identify thermodynamicially consistent paths and thus feasible separations. The so-called rectification bodies summarize the manifold of possible paths and therefore represent an attainable region of one rectification column section. The size of rectification bodies increases, if more energy is applied in the reboiler or condenser, and decreases, if the employed energy is reduced. The minimum energy demand is identified, if two rectification bodies, one for each column

section, just touch.

Minimum energy demand can be calculated by the RBM without any simplification regarding thermodynamic modeling or number of components. Even the extension to heterogeneous rectification with decantation is possible (Bausa, 2001; Urdaneta et al., 2002). The calculation of pinch points with continuation methods is very efficient (Bausa, 2001; Skiborowski et al., 2016) as well as the check for intersection of the convex rectification bodies, which allows to determine the minimum energy demand within seconds in a fully automated manner. Examples are the automated screening of zeotropic rectification sequences (Harwardt et al., 2008) or the optimization of rectification processes for mixtures with distillation boundaries (Brüggemann & Marquardt, 2011b).

4.1.4 Pinch-based heat integration

Heat integration is an established concept to identify minimum external heating and cooling utility. A comprehensive review of different design procedures for the energy recovery is given by Klemeš & Kravanja (2013). Usually, the identification of the optimal heat-exchanger network requires the solution of a MILP (Papoulias & Grossmann, 1983) or MINLP (Duran & Grossmann, 1986) superstructure problem to identify the optimal heat-exchanger areas and temperature levels. Alternatively, if the heat-exchanger network exhibits a pinch, the actual network structure can be ignored and minimum heating and cooling requirements can be determined directly. To avoid (infinitely) large heat-exchangers, usually a minimum temperature difference (i.e., 10 K) is demanded between hot and cold streams. The results of the pinch analysis are usually visualized by the so-called grand composite curve (GCC) which shows the minimum heating and cooling requirements as a function of the temperature level. The relation between heating or cooling demand and temperature level finally allows to identify heating and cooling cost, which usually depend on the relevant temperature level.

4.1.5 Optimization of pinch-based processes

Operational and structural alternatives of separation processes often have a large impact on process performance. In conceptual process design, process optimization has therefore become an important tool to identify the best process configuration among competing alternatives. While both, the choice of the optimal operating point and of the optimal solvent contribute to the performance of the process, both aspects need to be included by an integrated design approach.

Existing methods for the screening of solvents which involve process evaluation rely on an equation-based representation of the flowsheet (c.f. Burger et al. (2015); Stavrou et al. (2014)). For the optimization of the operating point, this has the advantage that numerical algorithms can be applied directly. In comparison, pinch-based methods have the advantage that their performance assessment already allows conclusions on optimal operation of the separation columns at minimum solvent or energy demand. On the other hand, for pinch-based methods the direct application of numerical algorithms is more complicated. As pointed out, problem specific solution procedures are necessary to solve pinch-based shortcut models. As a consequence, only a few attempts have been made on the combination of pinch-based methods and flowsheet optimization.

Pinch-based methods for rectification columns have been combined with optimization algorithms to determine optimal recycle policies and operating points of flowsheets (Brüggemann & Marquardt, 2011b). Such an optimization reliably identifies optimal operation. However, the calculation time is long because of the shortcut methods, which are treated as a black-box for the optimization. Derivatives are estimated at each iteration which requires frequent calls of the shortcut solution procedure. Alternatively, an equation-based representation of the pinch-based models can be used and the time-consuming call of the solution procedure is avoided, if the relevant type of pinch (saddle, stable, unstable, saddle-node) to distinguish the different type of models is identified prior to the optimization, and if the relevant type of pinch does not change during optimization. The optimization using an equation-based representation of pinch-based shortcuts has been investigated for the design of heteroazeotropic rectification (Krämer et al., 2011b) and hybrid reaction-separation processes (Recker et al., 2015). However, neither the implementation for an automated set-up of relevant equations is available, nor appropriate measures which need to apply when the type of model changes during the optimization. In consequence, although this concept has the potential to significantly shorten the optimization time, in this study, the solution procedures are executed at each iteration of the optimization.

The optimization algorithm applied in this study is a derivative-free pattern-search technique (Audet & Dennis, 2002) form the Matlab Optimization Toolbox®. The algorithm does not require information on the derivatives, which makes it particularly suitable for black-box models where derivatives can be difficult to determine. There is no guarantee that this type of derivative-free optimization converges to a globally or even locally optimal solution, but in general a reliable optimization of the operating point is observed.

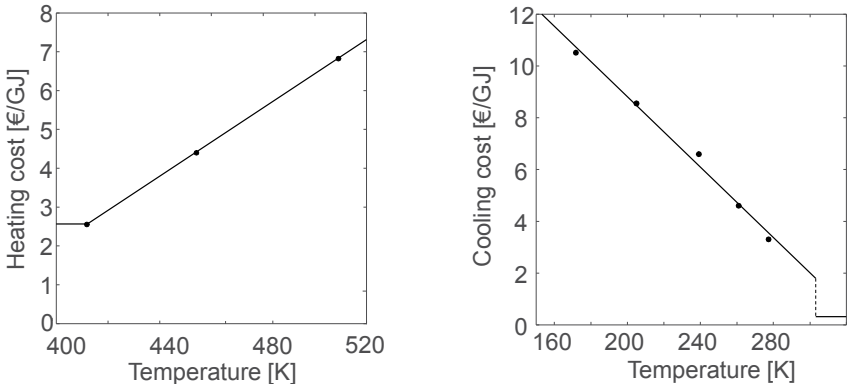

Figure 4.2.: Heating cost (left), cooling cost (right), and corresponding temperature level compared to literature data (Seider et al., 2010)

.

4.1.6 Flowsheet evaluation

The expenses for the separation are finally summarized to result in the minimum operating cost (*OC*). In this work, electricity cost (*EC*), solvent cost (*SC*) to compensate for solvent loss, minimum heating cost (*HC*) and minimum cooling cost (*CC*) are considered,

$$OC = HC + CC + EC + SC. \tag{4.1}$$

Electricity, required for pumps and compressors, is considered at a price of $11,1\,\frac{€}{GJ}$. For all solvents, a constant price of a high-value chemical is assumed as $4\,\frac{€}{kg}$ (Stavrou et al., 2014). The high price can be justified because solvent loss should always be avoided for environmental reasons or possible implications on downstream processes. The costs for heating and cooling usually depends on the required temperature level which is identified after applying the method of pinch-based heat-integration.

In order to cover the relation between cost for heating, cost for cooling, and necessary temperature level, simple linear correlations are assumed which are derived from literature data (Seider et al., 2010) according to Figure 4.2. For the heating cost of any unit d of the flowsheet, $\tilde{HC}_d$, a constant price is assumed below the temperature of 412 K, and above this temperature, a linear correlation with the required temperature level T_d. For the cooling cost of each unit d of the flowsheet, $\tilde{CC}_d$, a constant price is assumed above

the temperature of 303 K, and below this temperature, also a linear correlation with the required temperature level. Total heating and cooling cost, HC and CC, summarize the heating and cooling cost for each unit, $\tilde{HC}_d$ and $\tilde{CC}_d$,

$$HC = \sum_d \tilde{HC}_d = \\ = \begin{cases} \dot{Q}_d \cdot 2.564 \frac{€}{\mathrm{GJ}}, & T_d \leq 412\mathrm{K}, \\ \dot{Q}_d \cdot (0.044 \cdot T_d - 15.566) \frac{€}{\mathrm{GJ}}, & T_d > 412\mathrm{K}, \end{cases} \tag{4.2}$$

$$CC = \sum_d \tilde{CC}_d = \\ = \begin{cases} \dot{Q}_d \cdot 0.31 \frac{€}{\mathrm{GJ}}, & T_d \geq 303\mathrm{K}, \\ \dot{Q}_d \cdot (-0.068 \cdot T_d + 22.411) \frac{€}{\mathrm{GJ}}, & T_d < 303\mathrm{K}, \end{cases} \tag{4.3}$$

where Q_d denotes heating and cooling requirement at the specific temperature level T_d.

While conventional flowsheet evaluation using rigorous models is difficult, using pinch-based flowsheet evaluation three difficulties can be effectively avoided: These are, first, the complexity of the models in general, second, dependencies between separation units caused by recycles which require iterative calculations, and third, the unknown structure of a heat-exchanger network. A discussion on these three advantages is given in the following.

The models for the separation columns, i.e., extraction, absorption and rectification columns, require less equations due to the employed approximation. Also, these models are then solved by problem specific solution procedures which ultimately allows to solve underlying models reliably and in a fully automated manner.

Flowsheets of hybrid absorption-rectification processes usually show recycles where solvent is recycled from the solvent recovery column to the absorption column. Recycles complicate the flowsheet evaluation because they cause dependencies between units and usually require an iterative solution. Alternatively, pinch-based methods assume an infinite number of stages in which case trace impurities are always fully removed, i.e., pure solvent is separated at the solvent recovery column. As a consequence, prior to the evaluation of the solvent recovery column, the composition of the solvent recycle is known and iterations are not required.

The separation columns are combined in a flowsheet with all other necessary units such as compressors, pumps, vents, or additional heat-exchangers to allow for different oper-

ating points in the separation columns (cf. Figure 4.3). All process streams and states are determined. Then, in a following step, the pinch-based heat integration determines minimum heating and cooling requirements for the flowsheet. No knowledge of the actual heat-exchanger network is required and this step doesn't need to be carried out simultaneously with the flowsheet evaluation.

In conclusion, the simple nature of pinch-based methods allows to evaluate flowsheets quickly, and problem specific solution procedures, which are available for the separation columns and heat integration, allow for the reliable automation. Finally, solvents can be compared based on minimum operating cost, which is a favorable selection criterion for bulk chemical processes.

4.2 Illustrating case study 1: Carbon dioxide absorption process

Carbon dioxide (CO_2) is a greenhouse gas which can be separated by physical absorption. A prominent physical absorption process is the Rectisol® process which uses methanol as a solvent for the acid gas removal of CO_2 from syngas produced by coal gasification (Gatti et al., 2014; Sharma et al., 2016). The feed-gas in this work is assumed to be composed of three components hydrogen (H_2), carbon-monoxide (CO), and carbon dioxide (CO_2). The mole fractions of the feed gas stream as well as the temperature T_{feed} and the pressure p_{feed} are summarized in Table 4.1 and are adapted from a physical absorption process from literature, which uses methanol as a solvent (Gatti et al., 2014).

The quaternary mixture is described by equilibrium-based models. Some idealized assumptions are used to describe the thermodynamic equilibrium. The gaseous phase is assumed to be ideal while the non-idealities of the liquid phase are described by the NRTL model for the binary pair of CO_2 and the solvent molecule. The vapor pressure for hydrogen is described by Henry's law and for the other components by Antoine's extended equation, which extrapolates beyond the critical point. Pure component parameters for the feed components, H_2, CO, and CO_2, are taken from the AspenPlus® database and for the solvent molecules pure component parameters and binary interaction parameters are estimated with GC or QM methods as described in the previous section.

The flowsheet evaluated in this case study is shown in Figure 4.3. The major unit operations are the absorption column, the rectification column for the solvent recovery, and a flash to recover parts of the remaining solvent component from the cleaned gas. The absorption and rectification columns assume an infinite number of stages and are described by pinch-based methods, thus, CO_2 is fully absorbed from the cleaned gas leaving the ab-

sorption unit, no solvent (S) is found in the gaseous product leaving the rectification unit, and pure solvent is recycled to the absorption column. The solvent make-up stream consists of pure solvent which is fed at ambient pressure and temperature. Additional pumps, compressors, and heat-exchangers are used to set different pressures and temperatures in the separation units. For the compressors, a polytropic and adiabatic compression model is used (Smith, 2016). The product gas is compressed to 11 MPa and cooled to 313 K. The specifications for the feed stream, product stream, solvent make-up stream, and equipment are summarized in Table 4.1.

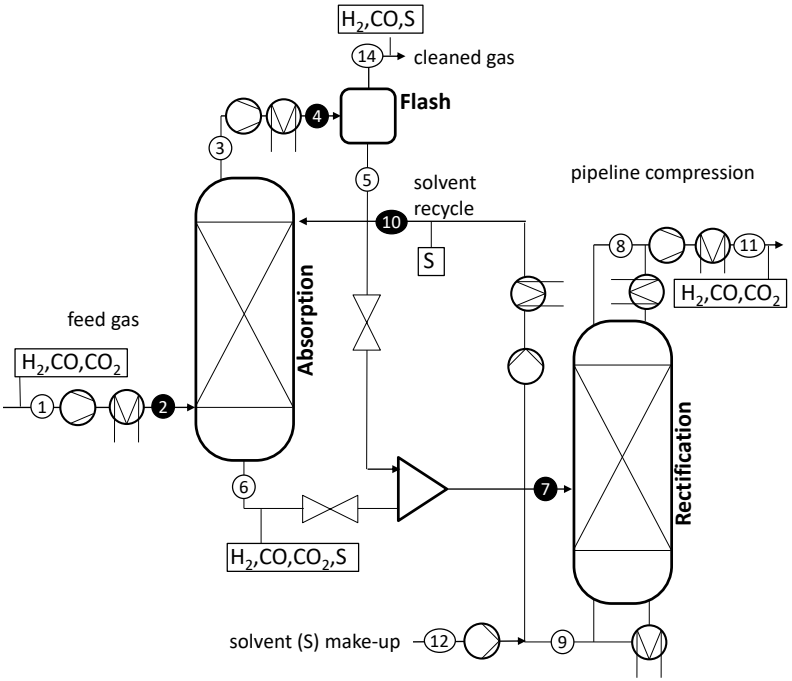

Figure 4.3.: Flowsheet for the physical absorption of CO_2.

Table 4.1.: Specifications for an absorption process for the physical absorption of CO_2. The operating points marked by an asterisk are subject to optimization.

stream specifications		
feed composition	x_{H_2}	40 mol-%
	x_{CO}	23 mol-%
	x_{CO_2}	37 mol-%
feed gas temperature	T_{feed}	303 K
feed gas pressure	p_{feed}	3 MPa
product gas temperature	$T_{product}$	313 K
product gas pressure	$p_{product}$	11 MPa
solvent make-up temperature	$T_{make\text{-}up}$	303 K
solvent make-up pressure	$p_{make\text{-}up}$	1 MPa
absorption column pressure	p_2^*, p_{10}^*	6 MPa
rectification column pressure	p_7^*	1 MPa
flash pressure	p_4^*	6 MPa
absorption feed temperature	T_2^*	303 K
solvent recycle temperature	T_{10}^*	243
cleaned gas temperature difference	$(T_4 - T_3)^*$	-10 K
equipment specifications		
compressor efficiency	$\eta_{comp.}$	0.82
pump efficiency	$\eta_{comp.}$	1
min. heat integration temp. difference	ΔT	10 K

4.2.1 Screening of solvents for a specified operating point

The flowsheet is evaluated for the operating point summarized in Table 4.1, which has been adapted from a case study from literature for the physical absorption of CO_2 (Gatti et al., 2014). The absorption column operates adiabatically and isobarically at 6 MPa, and the rectification column at 1 MPa. The feed gas enters the column at 303 K and the solvent stream at 243 K. The temperature of the cleaned gas is reduced by 10 K and a solvent-rich liquid is recycled to the solvent recovery column. The complete flowsheet evaluation for one solvent takes five seconds on average. The full evaluation of all solvents is parallelized on multiple cores and results can be available within a few hours.

Results for this operating point are summarized in Figure 4.4. In the upper left part of the figure (A), for the top scoring solvent candidates total operating cost are plotted over

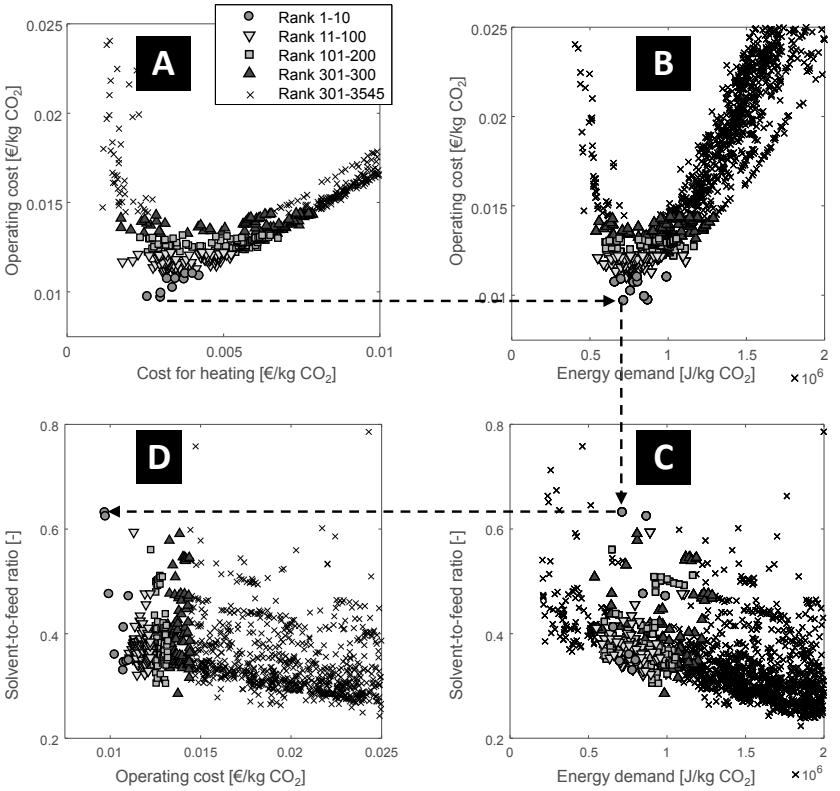

Figure 4.4.: Results for specified operating point. Each symbol represents the complete flowsheet evaluation for one solvent candidate. Different selection criteria are compared from A to D. The best candidate regarding operating cost is marked by a dashed line. According to this dashed line, alternative solvent candidates can be connected in each figure.

the respective cost for heating. Each symbol represents the complete flowsheet evaluation for one solvent candidate. Different symbols are used to emphasize the rank order. Circles show the performance of the best ten candidates, then, downside pointing triangles candidates show the best 100, squares the best 200, and upwards pointing triangles the best 300 candidates. The performance of the remaining 3,244 solvents are marked by crosses. In this part of the figure (A), the general shape of all symbols resembles a parabola where symbols forming the peak represent solvents with the lowest operating cost.

Recently, a new pinch-based screening of solvents has been introduced for hybrid extraction-rectification processes (Scheffczyk et al., 2016b), where solvents are selected based on the minimum energy demand of the solvent recovery column. Alternatively, this work considers not only the performance of the separation columns, but also pumps, compressors, additional heat-exchangers, and heat integration, allowing the selection of solvents based on operating cost. A comparison of different selection criteria, solvent-to-feed ratio of the absorption column, energy demand of the solvent recovery column, and total operating cost is provided in parts B, C, and D of Figure 4.4.

The upper right figure (B) shows operating cost compared to the energy demand of the solvent recovery column. No simple correlation between operating cost and energy demand of the solvent recovery column can be observed. Therefore, the selection solely based on the energy demand of the solvent recovery column cannot identify solvents with low operating cost. The lower left figure (D) shows the performance of the absorption unit by comparing operating cost to the solvent-to-feed ratio for this unit. Also, the selection solely based on solvent-to-feed ratio cannot identify the best candidates. In fact, some of best candidates, one of them is marked by the dashed line, can require a high solvent-to-feed ratio. The lower right figure (C) compares the two performance targets energy demand of the solvent recovery column and solvent-to-feed ratio of the absorption column. An inversely proportional behavior can be observed for many solvents. The best 300 solvent candidates are located in the center of this figure. Thus, good candidates show a compromise between the performance of these two units. The comparison shows clearly that solvents with low operating cost cannot be identified by the performance of one separation unit alone. Energy for additional heat-exchanger as well as costs for solvent loss can have an important influence, which can only be holistically determined by evaluating the actual flowsheet and summarizing the performance by an appropriate performance metric such as minimum operating cost.

A list of solvent candidates with the lowest operating cost is provided in Table 4.2. Interestingly, on the second position, the industrially favored solvent methanol for the physical absorption of CO_2 is found. On the one hand, when several thousand solvents are eval-

Table 4.2.: Best performing sovlent candidates, their operating cost (OC), and concentration of the product gas, y_{11,CO_2}, for the specified operating point by Table 4.1.

rank	solvent name	CAS	OC in €/t CO_2	y_{11,CO_2}
1	2-propynal	624-67-9	9.70	0.92
2	methanol	67-56-1	9.75	0.90
3	ethanol	64-17-5	9.93	0.92
4	3,4-hexanedione	4437-51-8	10.25	0.95
5	2,6-octadiene	4974-27-0	10.73	0.95
6	3-methoxy-propyne	627-41-8	10.75	0.95
7	5,5-dimethyl-1-hexene	7116-86-1	10.75	0.95
8	1,5-hexadiyne	628-16-0	10.91	0.96
9	2-propanol	67-63-0	11.03	0.92
10	hexanal	66-25-1	11.03	0.95

uated, one would expect to identify a better solvent candidate for the absorption of CO_2. On the other hand, if methanol is in fact a good choice for the physical absorption of CO_2, which could be concluded from the fact that methanol is still the reference physical solvent despite many research efforts, then this is a strong validation for the suggested solvent selection. Furthermore, this ranking relies on an operating point derived from an optimized physical absorption process which already uses methanol as a solvent (Gatti et al., 2014). This operating point therefore favors the solvent methanol and similar alcohols such as ethanol on third position, whereas for other solvents this operating point is not optimal. In consequence, an optimization of the operating point has the potential to improve the ranking.

4.2.2 Screening of solvents for an optimized operating point

Optimization of the operating point allows to compare solvents based on their full potential. Variables for optimization are the pressures of the absorption column, of the rectification column, and of the flash, as well as the temperatures of the feed stream to the absorption column, of the solvent recycle stream. The corresponding specifications are marked by an asterisk in Table 4.1 and the corresponding stream numbers are 2, 4, 7, and 10; they are highlighted by filled black circles in Figure 4.3. The optimization is performed with a local pattern-search technique from the Matlab Optimization Toolbox. One optimization run can take several minutes. Therefore, optimization is limited to the best

performing 300 solvent candidates identified in the previous step, which could easily be extended if necessary.

In Figure 4.5, the symbols filled with white represent the performance of solvents with optimized flowsheets. For comparison, the greyish symbols show the results before optimization (b.o.) and the shape refers to the corresponding rank before the optimization. This allows to observe changes of the ranking due to the optimization. For many solvents the optimization causes a significant variation of the ranking. Consequently, the reliable selection of a suitable solvent is not possible, if the optimal operating point is not considered.

For instance, the best solvents before optimization, which are marked as circles, also perform well after optimization. Although there is of course no guarantee that other solvent candidates could show stronger sensitivity towards the variation of the operating point, this justifies the limitation of the optimization to 300 candidates when a reasonable operating point is selected for the preliminary screening. The best candidate before optimization (cf., Table 4.2) results in operating cost about 9.7 €/t CO_2, while the best candidate after optimization results in 8.4 €/t CO_2. Optimization therefore achieves a reduction by 13 % for the best candidate.

Table 4.3 summarizes top scoring solvents after optimization (a. o.) and their optimized operating point. The process relying on the solvent methanol shows only small improvements after the optimization. While ranking second before optimization, methanol is outperformed after optimization (a. o.) by 82 solvents based on operating cost.

Beside operating cost, there are other constraints which need to be considered when selecting a solvent. Examples are availability, toxicity, or the risk of explosion. If models of sufficient quality are available, they could be integrated in our procedure, but often these constraints can only be captured with significant additional effort. Therefore, promising candidates still need to be selected from the list based on experience and expert knowledge. An interesting candidate, which can be found at position 9 in the ranking, is butanone (also known as 2-buantone or methyl-ethyl-ketone, MEK). A detailed discussion of the optimized flowsheet for the solvent candidate 2-butanone is provided next.

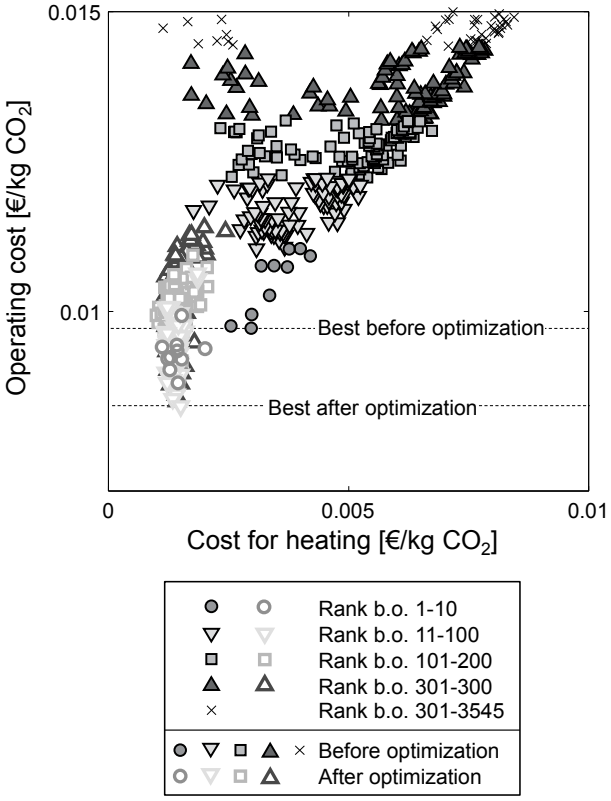

Figure 4.5.: Optimized operating cost subject to cost for heating. Unfilled symbols represent solvents after process optimization, and for comparison filled symbols solvents before optimization (b. o.).

Table 4.3.: Solvents for the absorption of CO_2 according to the flowsheet in Figure 4.3 for an optimized operating point.

						operating point					
rank a.o.	rank b.o.	solvent name	CAS	OC [€/t CO_2]	y_{1,CO_2} [-]	p_2 [MPa]	T_2 [K]	T_{10} [K]	p_7 [MPa]	p_4 [MPa]	$T_3 - T_4$ [K]
top scoring candidates											
1	85	cis-crotonaldehyde	15798-64-8	8.42	0.96	3.7	303	255	0.45	3.7	-48
2	242	vinylformate	692-45-5	8.50	0.95	4.9	305	244	0.75	4.9	-50
3	53	valeraldehyde	110-62-3	8.54	0.95	5.2	304	252	0.61	5.2	-50
4	278	trans-2-hexene	4050-45-7	8.60	0.94	5.4	307	243	0.80	5.4	-50
5	50	3-ethyl-1-pentene	4038-04-4	8.62	0.93	6.0	307	251	0.83	6.0	-49
Promising candidates											
9	252	butanone	78-93-3	8.78	0.96	4.2	288	251	0.42	4.2	-49
17	192	methylisobutylether	625-44-5	8.88	0.94	5.4	306	249	0.63	5.4	-50
25	273	methyl-t-butylether	1634-04-4	8.96	0.95	4.4	303	243	0.53	4.4	-50
27	182	ethylpropylether	628-32-0	9.00	0.94	5.1	304	248	0.52	5.1	-49
35	11	diisopropylether	108-20-3	9.10	0.94	6.0	304	267	0.45	6.0	-49
Reference solvent											
83	2	methanol	67-56-1	9.37	0.93	6.0	303	243	0.80	7.7	-7

4.2.3 Exemplary results for the solvent 2-butanone

2-butanone is a well-known industrial solvent. It is currently synthesized from fossil C4-raffinates (Hoell et al., 2000), but could also be produced competitively from biomass, which has recently been investigated in a conceptual process design study (Penner et al., 2017).

Figure 4.6 shows the flowsheet for the optimized operating point with details on the streams and energy demand for heat-exchangers, compressors, and pumps. Compared to the given operating point in Table 4.1, the absorption column operates at a lower pressure. This reduces electricity cost for the feed gas compression, but increases solvent loss caused by a higher temperature in the absorption column. The temperature of the solvent has increased which reduces cooling cost. The main driver in terms of energy demand is the heating required for the solvent recovery column. The lower pressure decreases the boiling temperature and thereby reduces the cost for heating. The process already achieves a high concentration of CO_2 in the product gas with about 96 mol-%.

For each flowsheet, pinch-based heat integration is considered which allows to draw the grand composite curve in Figure 4.7. For the averaged temperature difference between hot and cold streams, a temperature difference of $\Delta T_{\min} = 10\,\mathrm{K}$ is assumed. A comparison of the heating and cooling demand with and without heat-integration is given in Figure 4.8. Heat integration allows to reduce the total heating requirement by 12 % and the cooling demand by 6 %, therefore leading to a total minimum heating demand about 0.5 MJ/kg CO_2 and total minimum cooling demand about 1.05 MJ/kg CO_2.

Total operating cost for the solvent butanone are 8.78 €/t CO_2. Figure 4.9 summarizes the total cost distribution. In total, 15 % of the total operating cost are used for heating, 33 % for cooling, 49 % for electricity, and 3% to compensate for solvent loss. Compared to an optimized flowsheet using the reference solvent methanol, a reduction in operating cost of about 7 % can be achieved, suggesting butanone as a promising solvent alternative for the physical absorption of CO_2.

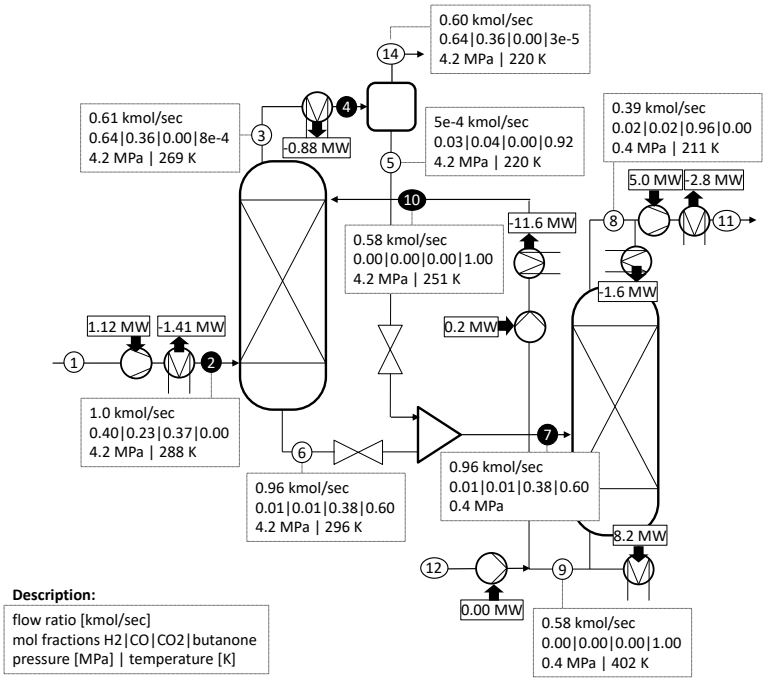

Figure 4.6.: Flowsheet for 2-butanone with optimized operating point.

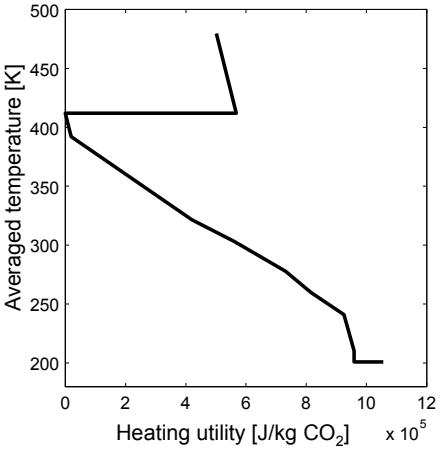

Figure 4.7.: Grand composite curve for the optimized absorption process using butanone as a solvent.

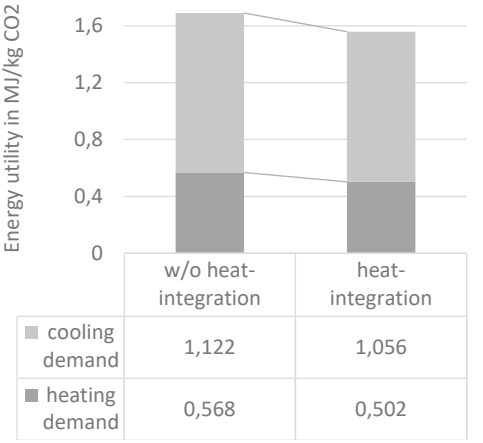

Figure 4.8.: Comparison of total energy demand for heating and cooling with and without heat-integration.

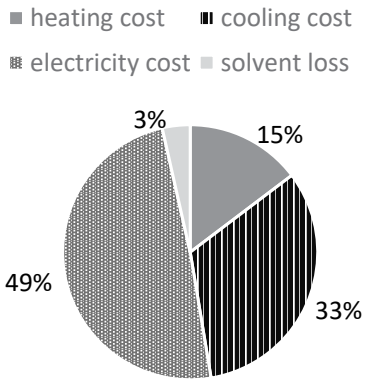

Figure 4.9.: Total cost distribution for optimized absorption process using butanone as a solvent. Total operating cost are 8.78 €/t CO_2.

4.3 Case study 2: Dimethyl ether absorption process

Dimethyl ether (DME) is an emerging alternative fuel. It can be produced from biomass in processes similar to methanol, shows low emissions, and can mostly rely on given infrastructure to distribute the fuel (Clausen et al., 2010). However, in order to be competitive with conventional fossil-based fuel alternatives, the separation needs to be energy-efficient. Currently, DME is separated by a sequence of distillation units. Alternatively, a physical absorption process could be used to separate DME from light gases. This demands for the identification of an optimal solvent to design or benchmark an alternative absorption process.

Table 4.4.: Specification of feed stream, stream number 0.

H_2	CO	CO_2	DME	MeOH	H_2O	p	vapor
mol-%						MPa	fraction
56	1	18	6	2	17	3	1

In direct DME production from syngas, the mixture to be processed mainly contains DME, methanol (MeOH), water (H_2O), and light gases hydrogen (H_2), carbon-monoxide (CO), and carbon dioxide (CO_2). Table 4.4 summarizes the composition and state of the mixture, which is taken from literature (Bongartz et al., 2016; Otto, 2015). The gaseous phase is assumed to be ideal and non-idealities of the liquid phase are described by the NRTL model for the binary pairs water and methanol, water and DME, methanol and DME, as well as DME and the solvent. The vapor pressure is described by Antoine's extended equation, and overcritical hydrogen is described by Henry's law. Pure component and binary interaction parameters for all feed components are taken from the AspenPlus® database and, for the solvent molecule, are estimated with GC or QM methods. The thermodynamic model equations are summarized in Appendix B.

The mixture needs to be separated into four products: Methanol, the light gases which can be partially recycled to the reactor, water, and the value product DME. The separation can be performed by simple rectification columns which is introduced as a benchmark. For the separation of the feed mixture from Table 4.4 into the four products, three rectification columns are required which can be ordered by the five different configurations depicted in Figure 4.10. In studies published in literature different rectification sequences are applied, for example, rectification sequence 3 (Clausen et al., 2010), rectification sequence 4 (Otto, 2015), and rectification sequence 5 (Zhang et al., 2015). For the selection of one configuration over the other, both economic and operational reasons are possible. For instance,

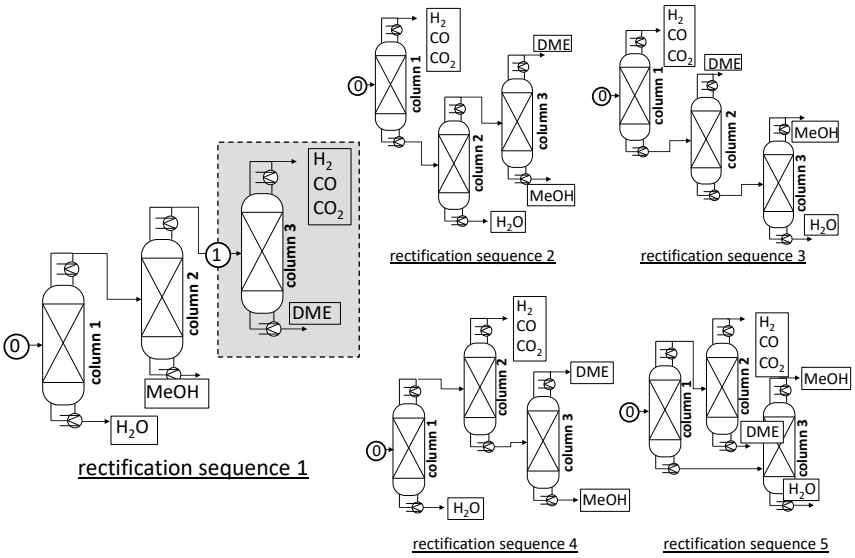

Figure 4.10.: Five alternatives to separate DME by simple rectification. The separation of DME from light gases, marked as a grey box, can be replaced by a physical absorption process.

in order to meet high product requirements for DME (International Organization for Standardization, 2015), separation of DME at the top of a column with rectification sequence 3 or rectification sequence 4 could be preferred. However, regarding operational costs, no systematic comparison of all alternative sequences has been performed, yet.

Pinch-based methods have proven to be highly suitable to quickly compare alternatives. For the separation of zeotropic mixtures by rectification, a systematic generation of alternatives and their evaluation is available (Harwardt et al., 2008). If isobaric pressure at 3 MPa is assumed for all rectification columns, the resulting OCs for each rectification column and total OC for each sequence are summarized in Table 4.5. With regard to operating costs, rectification sequence 1, which is currently not applied in any of the studies published in literature, performs best. The most expensive separation column of this sequence is column 3, demanding operating costs of 7.3 €/t DME. In Figure 4.10, this column, where light gases are separated from the value product DME, is highlighted in grey. The separation of DME from light gases can be replaced by a physical absorp-

Table 4.5.: Operating costs (OC) for five rectification sequences in Figure 4.10.

sequence	1	2	3	4	5
OC, column 1 [€/t DME]	6.4	41.3	41.3	6.4	22.8
OC, column 2 [€/t DME]	4.5	8.5	4.4	13.3	6.1
OC, column 3 [€/t DME]	**7.3**	12.5	6.1	12.5	7.3
total OC [€/t DME]	18.1	62.3	51.9	32.2	36.3

tion process which is investigated in literature for the solvents methanol and water (Zhang et al., 2015). While processes with these conventional solvents are inferior to rectification sequences, the large screening of solvents can identify, if an absorption process could be an alternative to conventional rectification, and if this is the case, which solvents would be the most promising.

The flowsheet which is used for the physical absorption of DME is analogous to the flowsheet shown in Figure 4.3. The composition and state of the feed stream, marked as stream number 1, can be calculated from rectification sequence 1 in Figure 4.10 where the third rectification column of the sequence is replaced by the physical absorption process. The feed enters the absorption process at boiling temperature at a pressure of 3 MPa, which is the pressure of the previous reaction and rectification columns (Clausen et al., 2010). The cleaned gas (stream 14 in Figure 4.3) is composed of light gases H_2, CO, and CO_2, and small amounts of solvent. Solvent is fully separated from the distillate of the rectification column (stream 8), which is composed of concentrated DME and small amounts of light gases. Pipline cooling or pipeline compression is ignored ($p_8 = p_{11}$, $T_8 = T_{11}$) for this case study. Specifications for the separation are summarized in Table 4.6. The absorption column operates at 3 MPa, the solvent recovery column is assumed to operate at atmospheric pressure at 0.1 MPa, and the solvent recycle (stream 10) is cooled to 303 K, which is the lowest temperature possible before costs for cooling increase according to Figure 4.2 The flash for the solvent recovery operates at identical pressure as the absorption column, and cleaned gas is cooled by 20 K which condensates parts of the solvent.

Figure 4.11 shows the operating costs for the absorption of DME subject to the costs for heating. The best 300 candidates are highlighted by circles, triangles, and squares. For the best candidates, low costs for heating also lead to low operating costs. The performance of ten top scoring candidates and the performance of the reference solvent methanol are summarized in Table 4.7. Methanol, a good choice for absorption of CO_2 and also already investigated for the absorption of DME, is obviously outperformed by a large number of

Table 4.6.: Specifications for a process for the physical absorption of DME.

stream specifications		
feed composition	x_{1,H_2}	40 mol-%
	$x_{1,CO}$	23 mol-%
	x_{1,CO_2}	37 mol-%
	$x_{1,DME}$	37 mol-%
feed temperature	T_1	276 K
feed pressure	p_1	3 MPa
pipeline gas temperature	$T_{pipeline}$	$T_{11} = T_8$
pipeline gas pressure	$p_{pipeline}$	$p_{11} = p_8$
solvent make-up temperature	$T_{make\text{-}up}$	303 K
solvent make-up pressure	$p_{make\text{-}up}$	0.1 MPa
absorption column pressure	p_2, p_{10}	3 MPa
rectification column pressure	p_7	0.1 MPa
flash pressure	p_4	3 MPa
feed gas temperature	T_2	276 K
lean solvent temperature	T_{10}	303
cleaned gas temperature difference	$T_4 - T_3$	-20 K
equipment specifications		
compressor efficiency	$\eta_{comp.}$	0.82
pump efficiency	$\eta_{comp.}$	1
min. heat integration temp. difference	ΔT	10 K

alternative candidates.

Optimization of the operating point allows to compare solvent candidates according to their optimal operational range. The 300 top scoring candidates for the specified operating point are optimized and results are depicted in Figure 4.12. Empty symbols represent optimized candidates and filled symbols are shown for comparison. A list of the five top scoring and manually selected solvent candidates is summarized in Table 4.8. All five top scoring compounds are phenolic, while the selected compounds are alcohols. It can be observed that structurally similar molecules lead to similar performance. The optimized operating point shows only small variations regarding the pressure of the absorption column and pressure of the flash, whereas the pressure of the solvent recovery column tends to lower pressures. The temperature of the solvent stream is larger for the top scoring

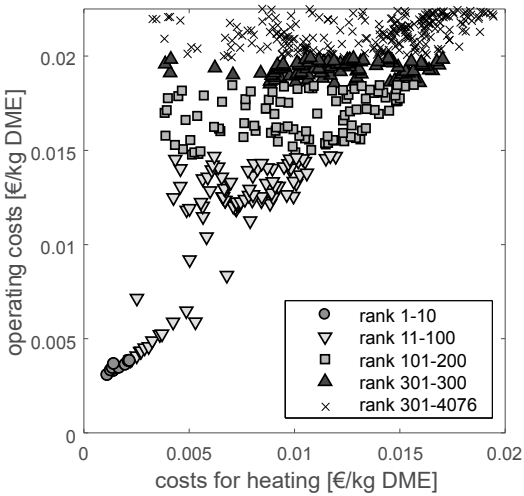

Figure 4.11.: Operating costs for specified operating point.

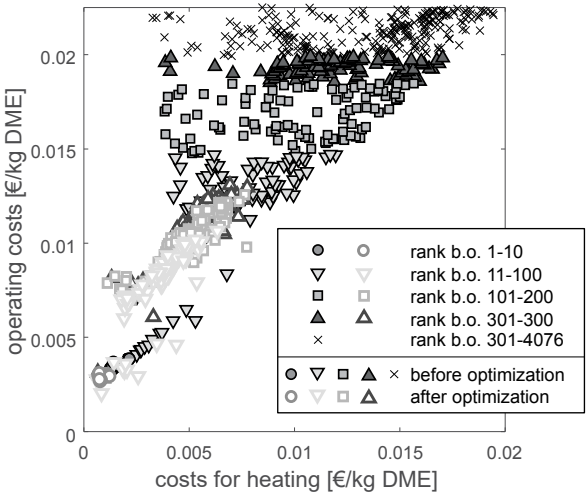

Figure 4.12.: Operating costs for optimized operating point. Filled symbols represent solutions before optimization (b.o.), empty markers after optimization.

Table 4.7.: Top scoring candidates and reference solvent the absorption of DME for the specified operating point in Table 4.6.

rank	solvent name	CAS	OC in €/t DME	$y_{1,\mathrm{DME}}$
top scoring candidates				
1	2,5-dimethylphenol	95-87-4	3.06	0.88
2	abhexone	n.a.	3.28	0.88
3	3-hydroxytoluene	108-39-4	3.32	0.89
4	o-propylphenol	644-35-9	3.44	0.87
5	2,3-dimethylphenol	526-75-0	3.44	0.88
6	4-ethylphenol	123-07-9	3.45	0.88
7	p-vinylphenol	2628-17-3	3.62	0.89
8	2-ethylphenol	90-00-6	3.65	0.87
9	4-(1-methylethyl)-phenol	99-89-8	3.82	0.87
10	4-(2-propenyl)phenol	501-92-8	3.82	0.88
reference solvent				
1161	methanol	67-56-1	36.00	0.93

candidates and smaller for the selected candidates compared to the specified solvent temperature. Next, for the selected solvent 2-pentanol, the optimized flowsheet is discussed in detail.

Table 4.8.: Top scoring phyiscal solvents for the absorption of DME from syngas for the operating point specified in Table 4.6.

						operating point					
rank a.o.	rank b.o.	solvent name	CAS	OC [€/t DME]	$y_{1,DME}$ [-]	p_A [MPa]	T_F [K]	T_S [K]	$p_{D,1}$ [MPa]	p_F [MPa]	ΔT_F [K]
top scoring candidates											
1	19	2-isopropyl-6-methylpyrocatechol	490-06-2	2.03	0.96	3	281	303	0.03	3	-4
2	9	4-(1-methylethyl)-phenol	99-89-8	2.65	0.95	3	280	320	0.04	3	-8
3	11	4-propylphenol	645-56-7	2.67	0.95	3	280	311	0.03	3	-5
4	7	p-vinylphenol	2628-17-3	2.71	0.96	3	288	304	0.05	3	-18
5	13	p-isopropenylphenol	4286-23-1	2.73	0.96	3	286	327	0.03	3	-14
selected candidates											
33	80	2-pentanol	6032-29-7	7.01	0.78	3	296	248	0.04	3	-24
34	109	2-methyl-1-butanol	137-32-6	7.04	0.77	3	294	265	0.04	3	-23
37	151	1-butanol	71-36-3	7.10	0.77	3	294	252	0.08	3	-24
50	30	isopentanol	123-51-3	7.55	0.77	3	284	241	0.10	3	-9
53	236	3-methyl-2-butanol	598-75-4	7.76	0.76	3	280	256	0.10	3	-30

2-pentanol (PEN) is used as an industrial solvent or intermediate chemical. It is non-toxic, non-corrosive, and has a low viscosity, which makes it interesting for a physical absorption process. The optimized flowsheet for the solvent 2-pentanol is depicted in Figure 4.13. Compared to the preliminary specified operating point, the solvent recovery column operates at lower pressure and the solvent recycle is cooled to lower temperatures. Solvent loss is low and in the product gas a concentration of 78 mol-% can be achieved. Table 4.9 summarizes energy utility and costs for the separation. Heat integration allows to reduce the total heating demand by 21 % and total cooling demand by 12 %, leading to total operating costs of 7.15 €/t DME.

Compared to the total operating costs of a conventional separation by a simple rectification column of 7.3 €/t DME (cf. Table 4.5), the separation by a physical absorption process is competitive. However, separation by simple rectification requires not only a lower number of devices, but also achieves a higher product concentration. For instance, when using the promising solvent 2-pentanol, a purity of only 80 mo-l% is achieved, whereas simple rectification can achieve almost pure DME, which meets the high purity requirements for the use of DME as a fuel (International Organization for Standardization, 2015).. Although there is still room for improvement in the absorption process, for example through process intensification measures such as multi-feed columns or intercooling (see, e.g., Lee et al. (2016)), when investment costs are included in a subsequent step of conceptual process design, the absorption process will hardly be competitive. Finally, the screening could identify promising solvent candidates for this separation task and allowed quick conclusions on the potential of an absorption process compared to alternative separation concepts.

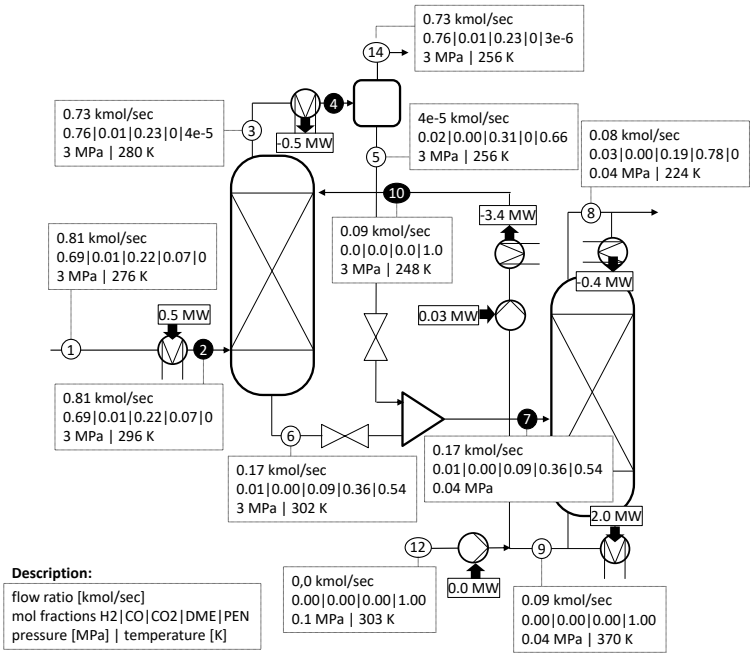

Figure 4.13.: Flowsheet for the absorption of DME with the solvent candidate 2-pentanol (PEN).

Table 4.9.: Summary of energy utility and costs for optimized absorption process using 2-pentanol as a solvent.

energy utility	
total heating demand	0.90 MJ/kg DME
total cooling demand	1.58 MJ/kg DME
heat integrated heating demand	0.71 MJ/kg DME
heat integrated cooling demand	1.39 MJ/kg DME
costs	
heating costs	1.82 €/t DME
cooling costs	4.91 €/t DME
electricity costs	0.12 €/t DME
solvent loss	0.29 €/t DME
total operating costs	7.15 €/t DME

4.4 Case study 3: Acetone-butanol-ethanol extraction process

1-Butanol can serve as an alternative fuel candidate and platform chemical which can be produced from biomass feedstock via acetone-butanol-ethanol (ABE) fermentation (Qureshi & Ezeji, 2008). The economic production is, however, difficult, because the low productivity of the batch fermentation leads to a strongly diluted aqueous mixture. Due to the lower boiling point of water compared to butanol, water needs to be evaporated. Futhermore, simple rectification cannot be applied due to the azeotope which separates butanol and water. Therefore, creative separation concepts are demanded to break the azeotrope and to avoid the inefficient evaporation of water.

The cost of the downstream process can be reduced by combining the strength of different separation techniques by a hybrid separation process. For the separation of butanol, prominent examples are extraction-rectification processes (Ishii et al. (1985); Liu et al. (2004)), pervaporation processes (Groot et al., 1984), gas stripping processes (Groot et al., 1989), or adsorption processes (Qureshi & Ezeji, 2008). A critical discussion and review of different separation alternatives can be found in the works of Groot et al. (1992) and Qureshi et al. (2005). Among these hybrid separation alternatives, the hybrid extraction-rectification process is particularly interesting because value components of the diluted aqueous system can be concentrated in the solvent, and, when using an appropriate solvent, ultimately less water needs to be evaporated. In consequence, efficiency of the separation concept is strongly determined by the choice of the right solvent. Extensive solvent screenings for the extractive separation of butanol have been performed by various authors (Groot et al., 1990; Ishii et al., 1985; Krämer et al., 2011a; Oudshoorn et al., 2009; Roffler et al., 1987a,b). However, all of these screenings only rely their selection on physical solvent properties, i.e., the activity coefficient at infinite dilution, solvent loss, toxicity, or combination of these physical properties. Alternatively, the novel pinch-based shortcut method for extraction columns allows to rank solvents by the operating costs of the hybrid extraction-rectification process.

Table 4.10 summarizes the specifications for the separation. The feed stream is assumed to contain four components acetone (A), butanol (B), ethanol (E), and water (H_2O). The mixture is described by equilibrium-based models. The non-ideality of the liquid phase is described by the NRTL activity coefficient model and an ideal gas phase is assumed. Pure component parameters are taken from the built-in AspenPlus® database and for the solvent molecule pure component parameters and binary interaction parameters are estimated with GC or QM methods.

In Figure 4.14, the flowsheet for the investigated hybrid extraction-rectification process

Table 4.10.: Specifications for the isothermal extraction of aceton, butanol, and ethanol from the aqueous feed.

stream specifications		
fermentation feed composition	$x_{0,\mathrm{A}}$	0,3 mol-%
	$x_{0,\mathrm{B}}$	0,2 mol-%
	$x_{0,\mathrm{E}}$	0,2 mol-%
	$x_{0,\mathrm{H_2O}}$	99,3 mol-%
fermentation feed temperature	T_0	303 K
fermentation feed pressure	p_0	0.1 MPa
downstream temperature	T_8	303 K
downstream pressure	p_8	0.1 MPa
solvent make-up temperature	T_6	303 K
solvent make-up pressure	p_6	0.1 MPa
extraction temperature	T_1, T_4	303
feed state to rectification	v-frac.$_2$	0
equipment specifications		
pump efficiency	η_{pump}	1
min. heat integration temp. difference	ΔT	10 K

is illustrated. The major separation devices are the extraction column and the rectification column. The liquid feed stream from fermentation (0) entering the hybrid process has ambient pressure and temperature (p_0, T_0), as well as the stream leaving the hybrid process to fermentation or waste treatment (p_5, T_5), and the stream leaving the process to further downstream processing (p_8, T_8). The solvent (S) is used to fully separate value components acetone, butanol, and ethanol from water in the extraction column. The solvent-rich extract stream (2) is then heated up to boiling conditions (vapor fraction / v-frac. = 0) and separated in a rectification column. The distillate product (8) only contains acetone, butanol, ethanol and water, which continue to further downstream processing. At the bottom product, a stream containing only solvent and water is fully separated and recycled to the extraction column (4). Small losses of solvent always occur in the raffinate stream (5) of the extraction column, and continuous production therefore demands a small solvent make-up stream (6). If the solvent is compatible with the fermentation organism, the raffinate can be recycled to the fermentation. Alternatively, the raffinate requires waste water treatment or advanced back-extraction using a bio-compatible solvent which has recently been investigated for ABE extraction (Kurkijärvi et al., 2014).

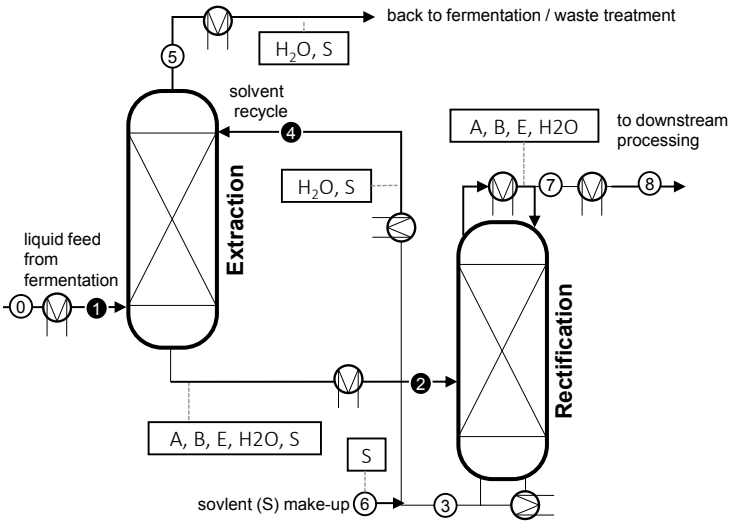

Figure 4.14.: Flowseet for the hybrid extraction-rectification process for the separation of acetone (A), butanol (B), ethanol (E) from water (H2O) by using a suitable solvent (S).

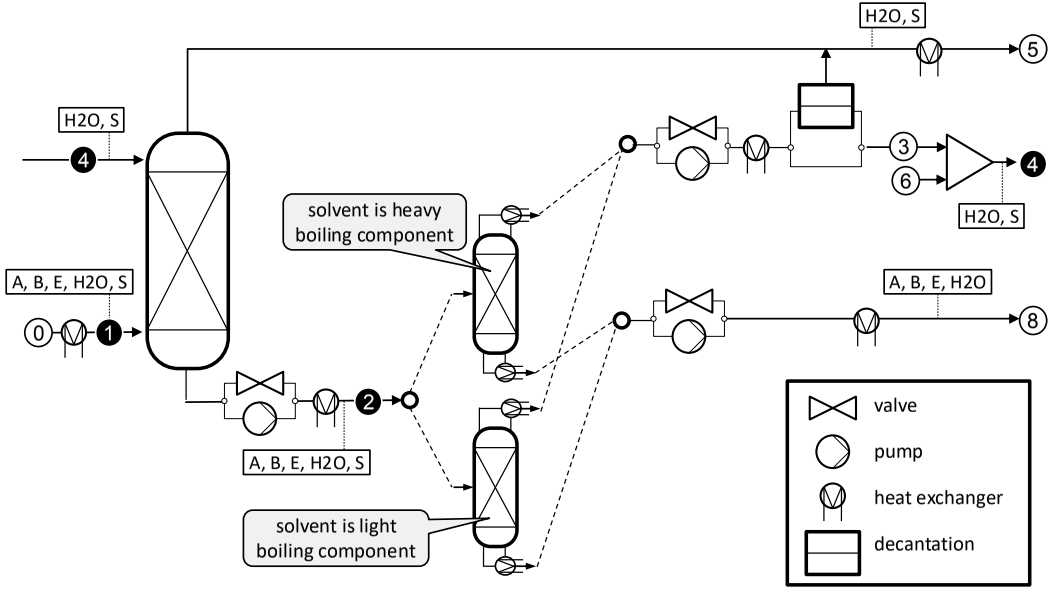

Figure 4.15.: Variants considered in this work. Stream numbers correspond to numbers of the simplified version of this flowsheet in Figure 4.14.

Depending on the desired operating point, pumps, valves, and additional heat-exchanger are necessary. Furthermore, the boiling point of the solvent as well as the existence of azeotropes determines the type of split in the rectification column. The alternatives which arise from the different operating conditions and type of splits lead to a superstructure which is shown in Figure 4.15. The extraction column always operates at ambient pressure, while pumps and valves allow for elevated or decreased pressure in the rectification column. The model assumes that heat exchanger can supply heating or cooling utility, depending on the desired temperature level in the extraction column.

For the split in the rectification column, restrictions arise from different boiling temperatures and existence of azeotropes. In this evaluation, the complete separation of solvent and value products acetone, butanol, and ethanol by one singe rectification column is demanded. Therefore, mixtures which would require an additional column, for example, due to a ternary azeotrope, are discarded. The type of split is distinguished by the boiling temperature of the solvent. When the solvent is the light boiling component, then it is separated as a pure component at the top of the column. Alternatively, when the solvent is the heavy boiling component, it is separated at the bottom of the column, which is the most common type of split. Of all investigated solvents, 78 % are heavy boilers, 21 % are medium boilers and therefore discarded, and less than 1 % are light boilers.

Figure 4.16 illustrates schematically a possible split for a heavy boiling solvent. The value components acetone, butanol, and ethanol are summarized for a better readability at the top of the ternary diagram. The mixture contains at least two azeotropes, one azeotrope containing ethanol and water, and one azeotrope containing butanol and water. Further azeotropes can occur depending on the choice of the solvent. Often, a heteroazeotrope between water and solvent can be observed. The solvent-rich extract, which is fed to the rectification column (2), is located on the miscibility gap and contains acetone, butanol and ethanol, together with fractions of solvent and water. For the desired split, solvent needs to be fully separated from the value components acetone, butanol, and ethanol. Furthermore, a preferably high concentration of these value components is desired. Therefore, the distillate product is located on the separation boundary caused by the butanol-water azeotrope, because this represents the highest concentration which can be accomplished by a simple rectification column. This concentration which is defined by the separation boundary is estimated according to the method of Rooks et al. (1998) (cf. Chapter 1.2). Based on the composition of the distillate product and the feed composition, the composition of the solvent-rich bottom product can be calculated. As the bottom product can contain fractions of water and thus could be located within the miscibility gap, decantation is considered in the superstructure in Figure 4.15. The water-rich stream

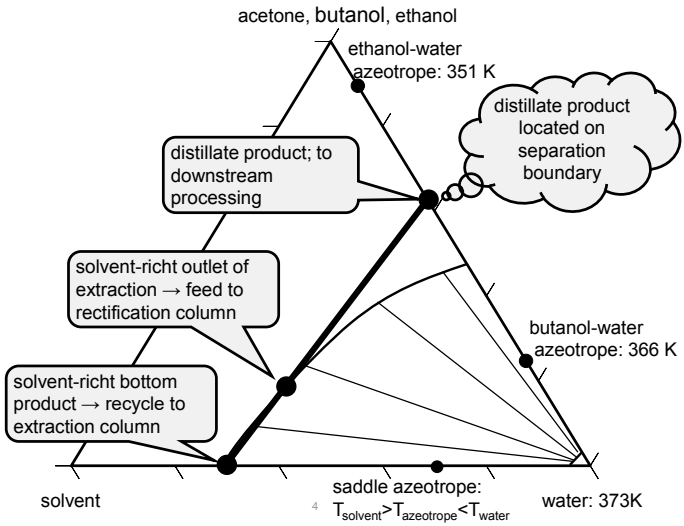

Figure 4.16.: Feasible split for the rectification column. The distillate product is located on the separation boundary caused by the butanol-water azeotrope.

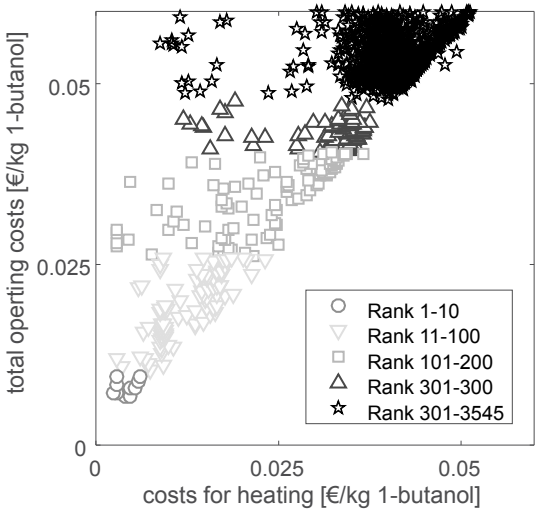

Figure 4.17.: Optimized operating costs and costs for heating.

is recycled to the raffinate stream (8) of the extraction column, and the solvent-rich stream (4) is recycled to the extraction column (4).

The operating conditions for this separation are described by two variables only, the temperature of the extraction column and the pressure of the rectification column. To obtain good initial values for the optimization, a preliminary screening is performed for a total number of 35 operating conditions, represented by a combination of five different temperature levels (288 K, 303 K, 328 K, 348 K) and seven different pressure levels (0.0005 MPa, 0.01 MPa, 0.05 MPa, 0.1 MPa, 0.5 MPa, 1 MPa, 3 MPa). The best performing 300 candidates are then optimized by the local pattern-search technique. In Figure 4.17, optimized operating costs are shown over the corresponding cost for heating. Layers of open circles, downwards pointing triangles, squares, and upwards pointing triangles show the best 300 candidates, while the remaining solvent candidates are marked by open stars.

Figure 4.18 and Figure 4.19 compare alternative criteria for the selection of solvents. Figure 4.18 compares solvent to feed ratio of the extraction column and the energy demand of the solvent recovery column. In general, there is an indication that low solvent to feed

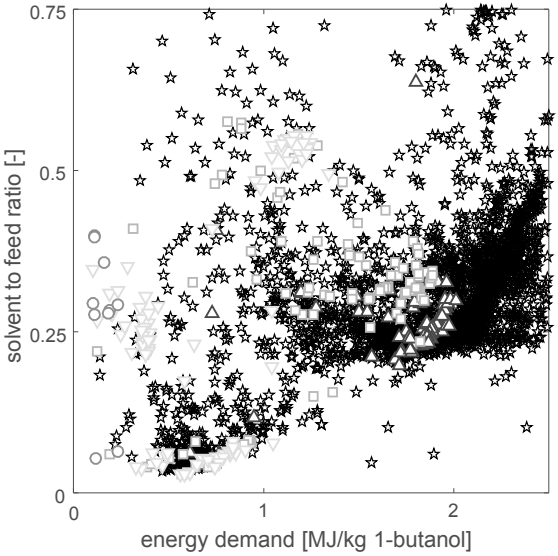

Figure 4.18.: Comparison between solvent demand of the extraction column and energy demand for the rectification column.

ratio results in low energy demand of the solvent recovery column. This contradicts the observation for absorption processes in Figure 4.4. For extraction processes, low solvent to feed ratio leads to low energy demand in the solvent recovery column, because less solvent needs to be evaporated. However, the comparison between operating costs and energy demand of the solvent recovery in Figure 4.19 shows that top scoring candidates are difficult to determine by evaluating only the energy demand of the solvent recovery column. Top scoring candidates show both low operating costs as well as low energy demand in the solvent recovery column. However, there are many solvents which require low energy demand but can involve high operating costs. Therefore, selection of solvents should involve comprehensive process evaluation based on operating costs, which can be established by pinch-based methods.

Table 4.11 summarizes the performance and optimized operating point for the top scoring solvent candidates and some manually selected candidates. For most solvents, low pressures in the solvent recovery column is preferred which reduces the temperature in the rectification column and thereby the costs for heating. For the extraction column, some

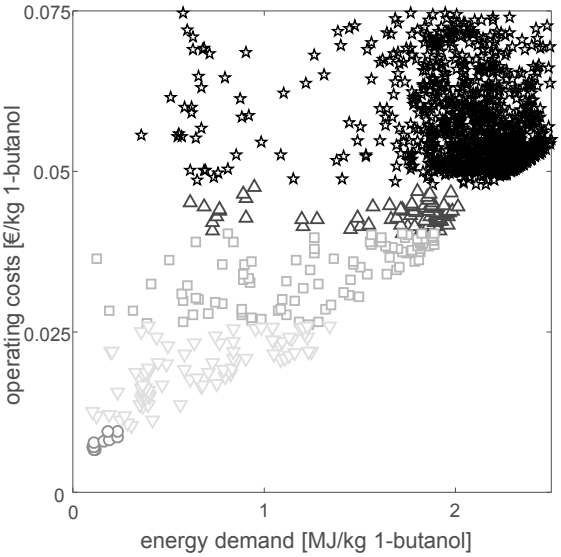

Figure 4.19.: Comparison between solvent demand of the extraction column and energy demand for the rectification column.

solvents show higher temperatures than ambient temperature, because this avoids cooling of the solvent recycle stream and subsequent heating of the extract stream. The top scoring solvent candidate is solid at ambient pressure and temperature, insoluble in water, and, therefore impossible to apply in an actual process. In consequence, promising solvents need to be selected manually based on the ranking, while also considering other constrains such as toxicity, availability, or risk of explosion.

Two promising solvent candidates which have recently been compared in a conceptual design study are oleyl alcohol and 1,3,5-trimethylbenzene (TMB, alternatively referred to as mesitylene) (Krämer et al., 2011a). The solvent 1,3,5-trimethylbenzene was identified from a solvent screening with the ICAS software[1] (Eden et al., 2002; Gani, 2004; Gani et al., 1997, 2005; Kongpanna et al., 2016), which only evaluates heuristics such as solubility of the value component in the solvent and predicting the interactions using group contribution methods. The following process simulation for both alternatives then showed

[1] Integrated Computer Aided System: www.capec.kt.dtu.dk/Software/ICAS-and-its-Tools

Table 4.11.: Ranking of solvents for the separation of ABE by an extraction process for an optimized operating pont.

rank a.o.	solvent name	CAS	OC [€/kg B]	$x^{D}_{1\text{-butanol}}$	p [MPa]	T [K]
top scoring candidates						
1	magnolol	528-43-8	0.007	0.15	0.050	302
selected candidates						
127	1,3,5-trimethylbenzene	108-67-8	0.030	0.18	0.050	288
202	dodecanol	112-53-8	0.040	0.15	0.094	369
1565	1-octanol	111-87-5	0.078	0.15	0.100	358
1649	n-hexylacetate	142-92-7	0.085	0.15	0.050	358
1653	2-ethyl-1-hexanol	104-76-7	0.085	0.15	0.100	328
1997	oleyl alcohol	143-28-2	0.123	0.15	0.050	328

Table 4.12.: Summary of energy utility and costs for the extraction process using trimethylbenzene as a solvent.

energy utility	
total heating demand	23 MJ/kg B
total cooling demand	23 MJ/kg B
heat integrated heating demand	5.2 MJ/kg B
heat integrated cooling demand	5.3 MJ/kg B
costs	
heating costs	0.015€/kg B
cooling costs	0.013€/kg B
electricity costs	$5.94 * 10^{-5}$€/kg B
solvent loss	0.002€/kg B
total operating costs	0.030€/kg B

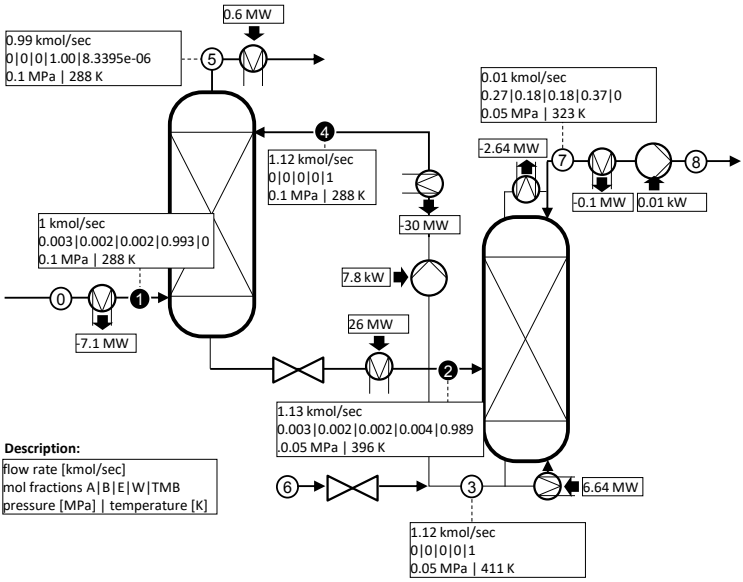

Figure 4.20.: Flowsheet for the extraction of acetone (A), butanol (B), and ethanol (E) with the solvent 1,3,5-trimethylbenzene (TMB).

significant better performance for TMB than for the solvent oleyl alcohol. This screening validates the promising performance of the candidate TMB. The optimized flowsheet is discussed in detail in the following.

The detailed flowsheet for the solvent trimethylbenzene is shown in Figure 4.20. The extraction column operates at low temperature of 288 K and the rectification column below ambient pressure at 0.05 MPa. At the distillate product of the rectificaiton column, a concentration of butanol of 18 mol-% is achieved. At the bottom, pure solvent is recycled to the extraction column. The results for this flowsheet are summarized in Table 4.12. For this solvent, electricity costs and costs for solvent loss are low compared to costs for heating and cooling, leading to total operating costs of 0.030€/kg butanol. Heat integration allows to reduce total heating and cooling demand by 77 %. This agrees well with the simulation study for the solvents trimethylbenzene and oleyl alcohol using rigorous models (Krämer et al., 2011a), where it was only through the implementation of heat-integration

that the remarkably good performance could be achieved for the solvent trimethylbenzene. The novel pinch-based screening directly covers heat-integration. Opportunities for heat-integration are the cooling of the solvent recycle to the extraction column, which can be used to heat the feed to the rectification column. This and all other opportunities for heat-integration are directly captured in each flowsheet which is evaluated for each solvent candidate.

The presented screening of solvents for ABE extraction validates the good performance of trimethylbenzene compared to oleyl alcohol. The pinch-based screening thereby identifies the economic potential of all investigated solvent candidates directly. All interactions of the flowsheet are covered including the potential for heat-integration. For future processes, when no pre-knowledge or experience is available, the pinch-based screening gives a good guarantee that complicated flowsheet interactions are fully covered, and that promising solvent candidates are reliably identified.

4.5 Conclusions

Solvent selection is successfully accomplished by pinch-based shortcut methods. Novel shortcut methods for absorption and extraction columns suggested in previous chapters thereby perfectly complement existing pinch-based methods for rectification columns or heat integration. Ultimately, the pinch-based methods allow evaluation of the performance of absorption, extraction and rectification columns combined in a flowsheet with all additional devices such as compressors, pumps, and heat exchangers. The knowledge of all process states allows consideration of heat integration and optimization of the operating point. Therefore, solvents are compared according to their full potential. Three case studies illustrate the performance for absorption and extraction processes. Novel solvents leading to energy efficient processes are identified, and their performance can directly be compared to conventional solvents or alternative separation techniques such as simple rectification.

For future investigations, the pinch-based methods can be combined with any method for the generation of thermodynamic properties. Both, more complex thermodynamic models as well as solvent design methods, where the structure of an actual solvent molecule is varied, could be considered directly. Furthermore, in extensions of this study, operational constrains such as toxicity, risk for explosion, or viscosity, which are difficult to predict but are decisive for the actual application, need to be included.

Finally, the pinch-based solvent screening offers an efficient tool for the comparison of

arbitrary solvents and process configurations. The screening allows to tackle a vast number of solvents, and to select solvents based on process performance, targeting minimum operating costs.

Chapter 5

Software

The previous chapters of this thesis illustrate both theory and application of pinch-based shortcut methods. The simple nature of pinch-based shortcut methods allows to develop tailored solution procedures to solve the pinch-based models without any *a priori* knowledge or the need of trial and error calculations. No simplifications are made concerning the number of components, type of mixture, or thermodynamic modeling, which opens a wide range of potential applications such as the fully automated screening of solvents for absorption or extraction processes.

The implementations, which are described in this thesis, could build on works of former colleagues, i.e., Bausa (2001), Brüggemann (2005), Wallert (2008), Pérez (2005), Kossack (2010), and Skiborowski (2015) as a part of their doctoral study projects. In general, software development always played an important role in the research group at AVT–Process Systems Engineering, RWTH Aachen University. To shorten the time of transfer for research prototypes into industrial application, the research group cooperated with the not-for-profit organization AixCAPE®[1]. Together with AixCAPE®, there have already been some attempts to integrate shortcut methods in commercial software packages prior to this thesis. Most of them focused on the RBM for simple rectification columns. In 2005, an interface which is compatible to the CAPE-OPEN standard, was developed (Brüggemann, 2005) and could be accessed from AspenPlus. In 2009, the stand-alone flowsheet simulator InSynTo (integrated synthesis toolbox) was intended to provide flowsheet capabilities for shortcut methods. However, AixCAPE has not continued service and development of these products.

[1] www.aixcape.org

Among other reasons, which might have led to this decision, this thesis revealed numerous programming bugs such as infinite loops as well as memory leaks in existing prototypes. This could be identified, because the screening of solvents as part of this thesis has exceptional requirements due to the automated solution of the shortcut methods. This shortcoming prior to this thesis probably prevented the robust integration of the prototypes into other software tools. When implementing the software framework for the automated screening of solvents as part of this thesis, many programming bugs in the existing prototypes could be identified and fixed. Therefore, besides an efficient tool for the automated screening of solvents, the case studies investigated in this thesis indicate the reliability of existing and novel software prototypes, which has been accomplished in this way.

The novel methods implemented as part of this thesis as well as existing methods are available as source codes under the general public licence (GPL) agreement on the web site of AVT–Process Systems Engineering[1]. For the experienced user, a set of specialized interfaces is available which provides full access to all functionalities. Figure 5.1 illustrates the organization of the software prototypes. In keeping with the philosophy behind the original package, the routines are implemented using ANSI-C in order to guarantee maximum portability, expandability, as well as numerical efficiency. New interfaces, new prototypes, and new frontends added as part of this work are highlighted.

The prototypes *separation analysis*, *rectification shortcut*, *extraction shortcut*, and *absorption shortcut* are the main features of the software package. The *separation analysis* module provides different flash algorithms for the calculation of the vapor-liquid equilibrium (VLE), vapor-liquid-liquid equilibrium (VLLE), or liquid-liquid equilibrium (LLE) of mixtures, access to property parameters, e.g., the density, vapor pressure, or the activity coefficients, and summarizes feasibility tests for simple distillation columns by the pitchfork distillation boundary (PDB) (Brüggemann & Marquardt, 2011a), stage-to-stage calculations, or linear separation regions (Rooks et al., 1998). The *rectification shortcut* module summarizes shortcut methods for simple distillation columns (Bausa et al., 1998), distillation columns with sidestreams (von Watzdorf et al., 1999), heterogeneous distillation columns (Urdaneta et al., 2002), and multi-feed distillation columns (Brüggemann & Marquardt, 2004). The *absorption shortcut* module (Redepenning & Marquardt, 2016) and *extraction shortcut* module (Redepenning et al., 2016) are the major contributions of this work. The theory behind the methods and the implemented solution procedures are discussed in Chapters 2 and 3.

[1] www.avt.rwth-aachen.de/softwareCollection

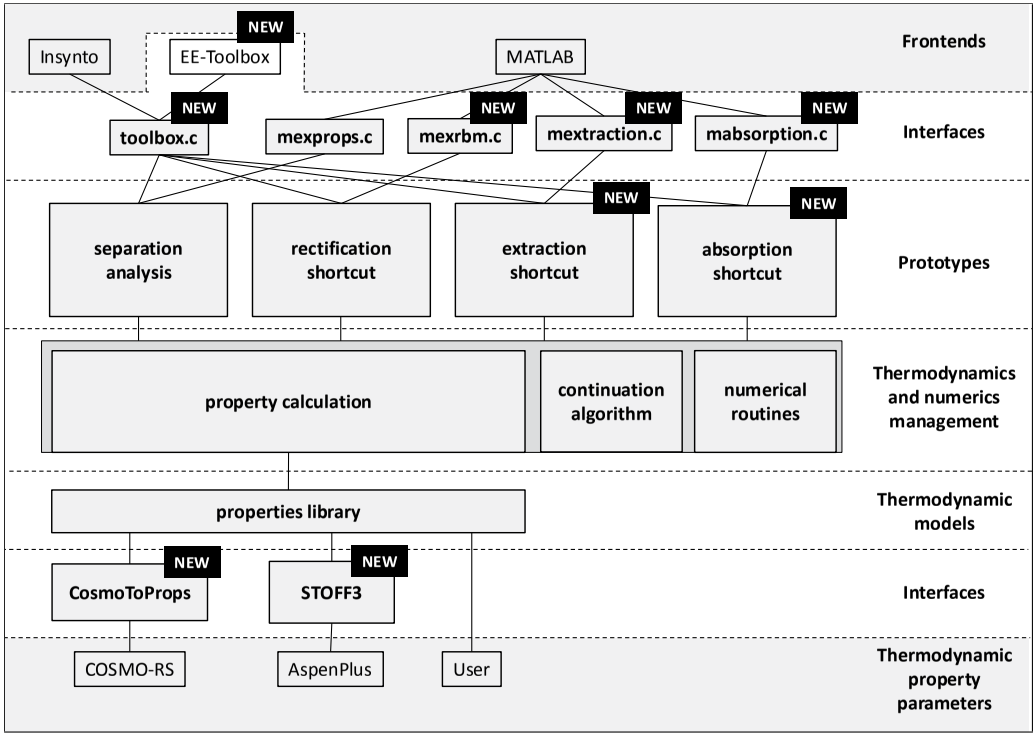

Figure 5.1.: Structure of the software package. The new features developed as part of this thesis extending the original package are labeled.

All prototypes can be applied with rigorous thermodynamic models. In consequence, the *property calculation* module located on the thermodynamics and numeric management level is a basis of the package accessed by all shortcut prototypes. The *property calculation* module provides the VLE, VLLE, and LLE flash calculations and therefore requires close communication with the *numerical routines* module and *continuation algorithm* module. The numerical routines provide standard numerical procedures, e.g., the decomposition into eigenvectors and eigenvalues or a simple Newton solver for non-linear systems of equations. Most routines are adapted from the numerical recipes (Press, 2007) and have been extended and improved in some cases. For the Open-Source publication, the routines have been re-implemented or replaced but still meet identical requirements. The *continuation algorithm* module provides a generalized predictor-corrector continuation solver which uses the arc-length concept (Jiménez-Islas et al., 2013) and different routines to allow for the stack management. Some widespread thermodynamic models are supported, e.g., Antoine's extended equation, the NRTL model or the UNIQUAC model to describe activity coefficients, as well as equation of states such as the Peng-Robinson equation. The thermodynamic model equations are implemented in the *property library* module. The implemented model equations are identical to the models used by the commercial property package PropertiesPlus[1]. Therefore, the property parameters provided by the AspenPlus®databank are fully compatible and can directly be applied.

Thermodynamically valid description of a mixture is crucial for the sound computer-aided evaluation. Therefore, access to valid property parameters is mandatory. Usually, parameters are obtained from literature and can directly be provided as text files written in a standardized syntax which is often referred to as a so-called '.dat-file'. In order to extract property parameters from AspenPlus®, a new software tool is developed as part of this thesis. In AspenPlus®, parameters are documented in report files (*.rep). In order to access the documented property parameters, the stand-alone software tool *Stoff3* is developed as a part of this thesis. *Stoff3* is a re-implementation of the old software tool *Stoff2* (Bausa, 2001), which was coded in VisualBasic and only poorly extendable. The new *Stoff3* is implemented in C# and allows better maintenance, supports more thermodynamic models, and can handle systems with more than six components. A new alternative to access thermodynamic properties is provided by the new package *CosmoToProps*. *CosmoToProps* summarizes MATLAB®[2] source files which call COSMO-RS[3] to estimate thermodynamic properties by quantum-mechanical calculations and provide the parameters for the *properties library* module.

[1] Aspen Technology Inc., http://www.aspentech.com
[2] The Math Works Inc., http://www.mathworks.com
[3] www.cosmologic.de

The prototypes can be accessed from different software platforms. The MATLAB®external functions (.mex) *mexprops.mex*, *mexrbm.mex*, *mextraction.mex*, and *mabsorption.mex* dock the prototypes to the commercial software package MATLAB®. MATLAB®allows convenient handling and storage of data and provides access to different toolboxes, e.g., the ParallelComputingToolbox™, which is perfectly suited to parallellize the screening of process alternatives, or the optimization toolbox TOMLAB[1], which provides several state-of-the art optimization algorithms, e.g., SNOPT, for large-scale flowsheet optimization. Originally, the software interface *toolbox.c*, which provides access to all software prototypes, was intended for an integration in the software tool InSynTo. InSynTo, which was developed between 2009 and 2010 by AixCAPE e.V.[2], is a GUI with simple flowsheet functionality. However, so far only a limited number of prototypes are implemented in the interface *toolbox.c*. Also, the InSynTo project phase ended before this thesis started. Without methods for extraction or absorption columns available in those days, the evaluation was limited to rectification processes. Therefore, as a part of this thesis, the software interface *toolbox.c* was extended to include the new prototypes developed as part of this thesis and close collaboration with AixCAPE e.V. guarantees easy integration into InSynTo or any followup project.

Alternatively, the prototypes implemented in *toolbox.c* can be accessed from the in-house development energy-efficiency (EE) toolbox. The EE-toolbox was developed as part of the research project Energy-Efficiency Management funded by the German Ministry of Research and Education (BMBF). The pinch-based methods allow to determine directly the operation at minimum energy or solvent demand, a central reference for the analysis of process by Energy Management Systems (EnMS). As part of the project, the Energy-Efficiency (EE) Toolbox was developed in close collaboration with Bayer Technology Services to improve the calculation of the minimum energy demand as the central reference of their EnMS STRUCTese® (Drumm et al. (2013), cf. Chapter 1).

Figure 5.2 shows a screenshot of the new EE-Toolbox. The EE-Toolbox provides methods for both the analysis of an existing process and the synthesis of new energy efficient processes. The following methods are available:

- Visualization of mixtures for the thermodynamic analysis by residue curves
- The rectification body method for simple rectification columns (Bausa et al., 1998).
- The rectification body method for heterogeneous rectification columns (Bausa, 2001).

[1]The TOMLAB Optimization Environment: www.tomopt.com
[2]AixCAPE e.V.: www.aixcape.org

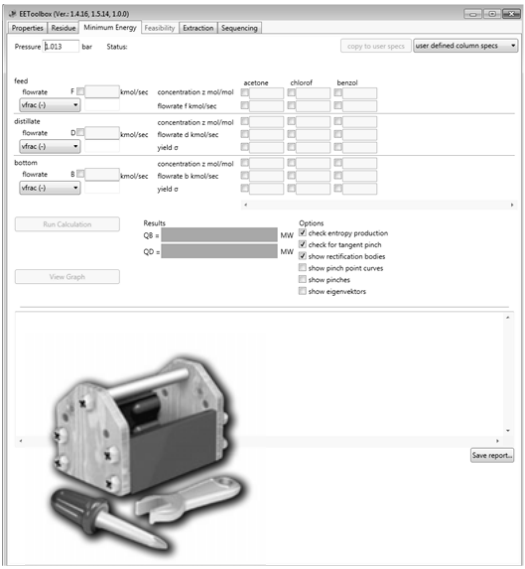

Figure 5.2.: Illustration of EE-Toolbox features. EE-Toolbox supports graphical visualization, generation of separation alternatives, and minimum energy calculation by pinch-based shortcut methods

- The rectification body method for rectification columns with sidestreams (von Watzdorf et al., 1999).
- The algorithmic detection of separation boundaries for rectification columns represented by a pitchfork distillation boundary (Brüggemann & Marquardt, 2011a).
- The automatic generation of zeotropic column sequences and calculation of minimum energy demand of each sequence by the rectification body method (Harwardt et al., 2008).
- The pinch-based shortcut methods for extraction columns (Redepenning et al., 2016).
- The pinch-based shortcut method for absorption columns (Redepenning & Marquardt, 2016).

Chapter 6

Recommendations for further research

Next research steps should obviously review existing pinch-based methods and provide an update with the new findings of this thesis. For instance, while the model of the RBM detects tangential pinch-points by heuristic rules and needs feasibility tests in case of azeotropic mixtures with separation boundaries (cf. Chapter 1.2), such simplifications are obsolete with the novel pinch-based model. Furthermore, the improvement of the basic shortcut model by adding additional stages allows to reduce the approximation error to any desired accuracy, which effectively solves the problem of approximation error when using a shortcut method. The new model can be readily extended to complex rectification configurations or integrated reaction-separation concepts.

Three recommendations for further research are discussed in detail in the following: Currently, the suggested solution procedures are important to accomplish the automation and therefore a key feature of the shortcut methods. However, the solution procedures are expensive to implement, to debug, and to main, and small changes to the separation devices, such as sidestreams or reactions, can require an extensive redesign. Therefore, alternative solution procedures based on global optimization techniques are discussed. Rigorous models for separation columns are important for conceptual design, but still difficult to solve in an automated manner. Alternatively, the pinch-based shortcut methods suggested in this work can allow for robust optimization-based design of rigorous models. Finally, actual separations are usually controlled by transport limitations. While the general pinch-based model employs no simplification regarding thermodynamic modeling, non-equilibrium modeling can be integrated into the shortcut method and allow for robust design of non-equilibrium separations.

6.1 Solving shortcut models by global optimization techniques

The challenge of solving the algebraically complex rigorous models of separation columns is touched multiple times throughout this thesis. The rigorous models, where each stage of the column is covered by MESH equations, are more difficult to solve than the pinch-based shortcut approaches, where MESH equations for only three stages need to be evaluated, i.e., for the first, the last, and the pinch stage (cf. Figure 1.5).

The simple nature of pinch-based shortcut models allowed to develop tailored solution procedures. The solution procedures suggested for absorption, extraction, and distillation then determine a solution reliably, which is exploited for the fully automated screening of solvents in Chapter 4. These solution procedures fulfill their purpose perfectly, however, and this is one major disadvantage, small variation of the separation device or the separation task often demand major revision of the solution procedure or even an entirely new solution procedure. For instance, for the pinch-based design of rectification columns the concept of the RBM presents the groundwork for simple columns (Bausa et al., 1998). Extensions to complex columns (von Watzdorf et al., 1999), batch distillation (Espinosa et al., 2005), reactive distillation (Lee et al., 2003), or extractive distillation (Brüggemann & Marquardt, 2004) required individual procedures for each device. Also, the pinch-based shortcut for adiabatic (absorption) and isothermal (extraction) counter-current columns are very similar regarding the model. Nevertheless, for each device, an individual solution procedure is necessary.

A general solution concept could be rewarding to allow for a simple extension to other devices, column configurations, or hybrid reaction-separation concepts. General-purpose numerical algorithms can provide such a general solution concept. Local algorithms are generally fast, but require initialization which includes the identification of the controlling model referring to a stable, unstable, saddle, or tangential pinch prior to the separation. Therefore, there is a need for appropriate model formulations to switch between models referring to different types of pinch points, as well as global search for solutions to distinguish between different types of models.

Global optimization techniques provide a global search for solutions. Given a representative problem formulation, global algorithms allow for the reliable calculation of a solution without any knowledge of an initial solution. However, calculation time is high compared to local algorithms, which is why complex rigorous models are still not solved by global optimization techniques. Yet, the simplicity of pinch-based shortcut models could allow for such an advanced solution strategy.

The potential of global optimization techniques is investigated in the following

Table 6.1.: Specifications and results for the illustrating case study. Specifications are bold. Isothermal extraction at 35°C is assumed.

component	$\mathbf{x}^{\mathrm{R}}_{\mathrm{N+1}}$	$\mathbf{x}^{\mathrm{E}}_{0}$	$\mathbf{x}^{\mathrm{R}}_{1}$	$\mathbf{x}^{\mathrm{E}}_{\mathrm{N}}$	flow ratio	
itaconic acid	**0.1**	**0**	**0**	0.049	$L^{\mathrm{E}}_{0}/L^{\mathrm{R}}_{\mathrm{N+1}}$	0.08
water	**0.9**	**0**	0.992	0.573	$L^{\mathrm{R}}_{1}/L^{\mathrm{R}}_{\mathrm{N+1}}$	0.88
3-MTHF	**0.0**	1	0.008	0.378	$L^{\mathrm{E}}_{\mathrm{N}}/L^{\mathrm{R}}_{\mathrm{N+1}}$	0.20

for the ternary extraction of itaconic acid from aqueous solution with the solvent 3-methyltetrahydrofuran (3-MTHF). The mixture is highly interesting as part of the research project Tailor Made Fuels from Biomass (TMFB), where 3-MTHF is identified as a promising fuel candidate (Geilen et al., 2010; Voll & Marquardt, 2012). 3-MTHF can be efficiently produced by fermentation via itaconic acid (Geiser et al., 2016; Klement & Buchs, 2013). If the product 3-MTHF could also be used as a solvent for the extraction of itaconic acid from the aqueous fermentation both, additional purification devices are avoided leading to reduced separation costs and improved competitiveness of the new fuel candidate. Feed composition, temperature, and pressure for the extraction are summarized in Table 6.1. The equilibrium is described by the NRTL activity coefficient model and parameters are taken from the AspenPlus® database.

In Chapter 3, pinch-based shortcut methods for ternary extraction are reviewed. For ternary mixtures, the observation of the pinch is sufficient to identify operation at minimum solvent demand (Minotti et al., 1996). Thereby, maximization of the solvent flowrate, L_0, subject to the existence of the pinch within the column section identifies operation at minimum solvent flowrate, when the pinch just vanishes. The identification of minimum solvent operation can be formulated as an optimization problem (Krämer, 2012):

$$\max_{Z} \quad L_0, \tag{6.1}$$

$$\text{subject to} \quad \text{MES equations for stage 1, P, N}, \tag{6.2}$$

$$\mathbf{x}^{\mathrm{E}}_{1} \leq \mathbf{x}^{\mathrm{E}}_{\mathrm{P}} \leq \mathbf{x}^{\mathrm{E}}_{\mathrm{N}}, \tag{6.3}$$

where variables and abbreviations are used according to Chapter 3 and Z summarizes all variables, i.e., compositions and flowrates at the pinch (P), the first stage (1), and the last stage (N). A detailed description of the problem formulation is provided by Krämer (2012). This optimization problem is valid only for ternary mixtures, as it can only distin-

guish between stable, unstable, and tangential pinch-points, but does not work in combination with saddle pinch points which is a phenomena occurring for isothermal mixtures with more than three components. Appropriate optimization-based problem formulations for mixtures with more than three components still need to be developed. Nevertheless, the ternary example allows for a preliminary investigation of the performance of such a concept which is based on general-purpose numerical algorithms.

The case study is solved using global optimization with ANTIGONE (Misener & Floudas, 2014) in GAMS[1] as well as the solution procedure suggested as part of this thesis in Chapter 3. Both concepts find the identical solution and results are summarized in Table 6.1. The solution by ANTIGONE on a standard personal computer takes 29 seconds, whereas the solution procedure suggested in Chapter 3 is almost hundred times faster and only takes 0.3 seconds. In consequence, a considerably quick screening of alternative solvent candidates could not be attempted using global optimization techniques. However, regarding computer technology, formulation techniques, or performance of optimization algorithms, there is still room for improvement. Therefore, given some improvements in any of these fields, direct solution by global optimization techniques could be a rewarding alternative, because a quick modification of any of the shortcut models is possible.

6.2 Robust optimization-based design of rigorous models

Rigorous models for separation columns, where each stage is modeled by the full set of MESH equations, are both popular and important for the optimal design of unit operations and flowsheets (Cremaschi, 2015). In conceptual process design, optimization with rigorous models is usually the final step (cf. Figure 1.4). For pinch-based shortcut methods, reliable solution for absorption, extraction, and distillation columns is accomplished successfully by the suggested solution procedures. For rigorous models, on the other hand, a reliable solution is still not guaranteed despite their importance in conceptual process design.

Some efforts have already been made on the optimization-based solution of rigorous models. Often, optimization is initialized by the solution of a rigorous model operating close to minimum reflux or solvent ratio (Bauer & Stichlmair, 1996; Skiborowski et al., 2015). The number of stages necessary to establish this favorable operation directly presents an upper bound for the total number of stages. This is particularly valuable for the efficient optimization regarding the number of stages by MINLP superstructure tech-

[1] GAMS: General Algebraic Modeling System, www.gams.com

niques, where an upper bound needs to be defined *a priori*. Furthermore, the operating point at minimum solvent or reflux ratio can be conveniently initialized by pinch-based shortcut methods. There is, however, neither a shortcut method available to estimate an appropriate upper bound for the number of stages, nor is there any concept reliably established to identify the actual stage-to-stage trajectory of a column section.

An interesting first attempt to identify the trajectories within the column section relies on the RBM (Brüggemann, 2005; Kossack et al., 2006). The RBM identifies not only an estimate of the minimum reflux ratio, but the outer surfaces of the rectification bodies also represent an approximation of possible stage-to-stage trajectories. For ternary mixtures, the outer surfaces of rectification bodies are straight lines. Then, piecewise linearization can directly be used to approximate possible stage-to-stage trajectories (Kossack et al., 2006). This concept is, however, limited to ternary mixtures, because for mixtures with four or more components the outer surfaces of rectification bodies are hyperplanes and piecewise linearization cannot identify the unique stage-to-stage trajectory (Bausa et al., 1998). Furthermore, this concept requires *a priori* knowledge on a sufficient number of stages to approximate each line segment, but an upper bound for the total number of stages is not available.

In the following, a new concept for the reliable solution of rigorous models is suggested for further research. The concept also builds on the solution of the pinch-based shortcut method. Then, the improvement of the shortcut result determines both an upper bound for the sufficient number of stages as well as an accurate estimate for the actual stage-to-stage trajectory. This can directly be used to initialize the rigorous model of a column section operating close to minimum solvent or reflux ratio. The new concept is illustrated for the absorption of the ternary mixture of argon (AR), ethylene-oxide (EO), and water (W), which was already introduced for illustration in Chapter 2. Table 6.2 provides a set of specifications for the illustrating case study. Pressure, compositions, and temperatures of both, the feed and the solvent stream, are given. The desired purity of ethylene-oxide in the cleaned gas is set to $y_{1,\mathrm{EO}} = 1\,\text{mol-}\%$.

The steps of the new concept are illustrated in Figure 6.1. Starting from the result of the pinch-based shortcut in Figure 6.1(a), the stepwise addition of stages to the pinch-based shortcut model (cf. Section 2.3.4) yields the accurate solution for twelve additional stages in Figure 6.1(b). A detailed discussion on these two steps can be found in Chapter 2 associated to Figures 2.5 and 2.8. According to Figure 2.6, the improvement of the solution identifies six stages to be sufficient to determine accurate results. With twelve stages, the stage-to-stage calculation from both column ends towards the pinch almost touch the pinch. Therefore, the two stage-to-stage trajectories approaching the pinch from both

Table 6.2.: Specifications for the illustrating case study. Adiabatic and isobaric absorption at 0.1 MPa is assumed. Desired purity of ethylene-oxide in cleaned gas is 1 mol-%.

concentration	$\mathbf{y}_{N+1}$	$\mathbf{x}_0$	temperature	
argon	0.5	0	T_0	373K
ethylene-oxide	0.5	0	T_{N+1}	373K
water	0	1		

column ends are almost connected. The trajectories are only separated by a pinch and a small distance which depends on the desired accuracy and total number of stages. When the pinch is ignored and a continuous trajectory is demanded according to a rigorous model of such a column section, only a small correction is necessary to achieve a continuous trajectory. Following this design procedure, the solution of the rigorous model can be accomplished reliably.

The final step then represents optimization regarding total costs, which is the sum of capital expenditures (CAPEX) and operating expenditures (OPEX). All costs are estimated in AspenPlus v.8.8 with the embedded Aspen Process Economic Analyzer (APEA). OPEX covers solvent costs, which is assumed to be 0.1 ct/kg. CAPEX is determined using standard geometry for 'RadFrac' column section given by AspenPlus 8.8 for a sieve tray column. CAPEX, OPEX, and total costs for this task subject to the structural degree of freedom, the total number of stages, are depicted in Figure 6.2. Twelve stages were identified to be sufficient by the improvement of the pinch-based shortcut model in the previous step. Thus, the column operates close to minimum solvent ratio and OPEX is close to the minimum. When the number of stages is reduced, OPEX increases, because a higher solvent demand is required. CAPEX, however, shows a minimum, because for a low number of stages high solvent demand requires a large column diameter, or for a high number of stages a large column height is required. Total cost show an optimum for a total number of eight stages. The stage-to-stage trajectory of an optimized absorption column represents the last step of the new concept as depicted in Figure 6.1(d).

In conclusion, reliable solution of rigorous models is accomplished based on pinch-based shortcut methods. Pinch-based shortcut methods can be solved reliably for a favorable operating point at minimum solvent or reflux ratio. The improvement of the pinch-based shortcut solution by adding additional stages presents a unique approach to determine not only an upper value for the required number of stages, but also a good estimate

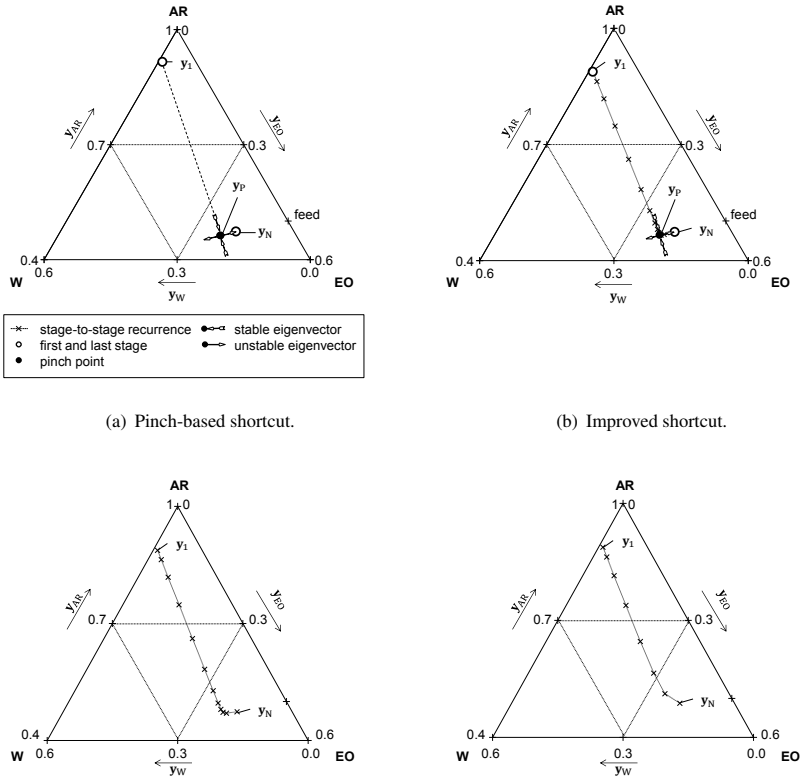

(a) Pinch-based shortcut.

(b) Improved shortcut.

(c) Rigorous model.

(d) Optimized model.

Figure 6.1.: New concept for the robust process optimization using rigorous models; (a) Operation at minimum solvent demand is estimated with the basic shortcut, (b) the improvement identifies a sufficient number of stages, (c) which then allows to solve the rigorous model of a column, (d) before the optimal configuration is determined.

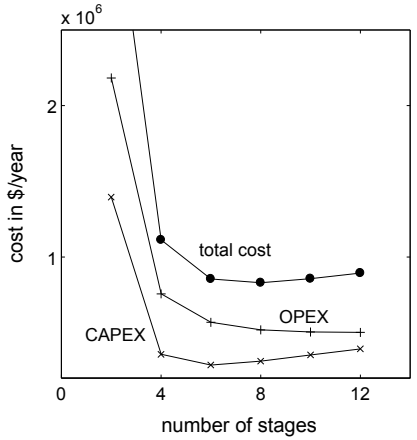

Figure 6.2.: CAPEX, OPEX and total cost for different number of stages.

for the continuous stage-to-stage trajectory of a column operating at minimum solvent or reflux ratio. The estimate can be used for the initialization of the rigorous model of a column section, which can finally be solved and optimized regarding total costs. Hence, starting with a pinch-based method, the optimal solution for rigorous models can be accomplished reliably.

6.3 Integrating diffusion limitations in pinch-based methods

Liquid-liquid solvent extraction is often strongly influenced by transport limitations (Mohanty, 2000). Transport limitations are caused by a number of diffusion-controlled phenomena such as rise, formation, or coalescence of drops, which ultimately can be responsible for a significant deviation from the equilibrium. The final extractor design therefore should preferably rely on non-equilibrium models which could otherwise lead to inaccurate results and wrong conclusions.

For the modeling of mass transfer limitations, various approaches involving different levels of complexity are available (Mohanty, 2000). Simple approaches only rely on efficiencies for the separation device, whereas complex approaches involve CFD (computational fluid dynamics) modeling techniques (e.g., Vedantam et al. (2012)). As efficiencies are empirical with no relation to the actual separation phenomena, almost no

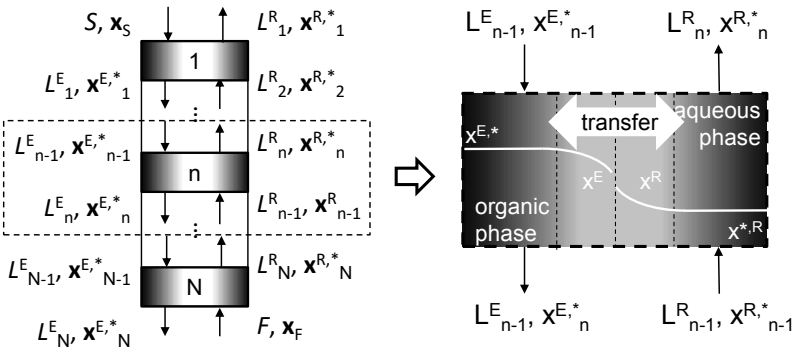

Figure 6.3.: Counter-current cascade of an extraction column and non-equilibrium stage model. According to the two-film theory, equilibrium occurs at the phase interface, and non-equilibrium is caused by mass-transfer limitations in the bulk phases.

extrapolation is possible. CFD-models, on the other hand, provide an in-depth analysis but demand significant computational resources. A good compromise is the two-film model (Lewis & Whitman, 1924), where the most important controlling transport limitations are captured and described by correlations.

The integration of transport limitations increases the complexity of the separation model which is why transport limitations are often avoided in the early phase of conceptual process design. Pinch-based shortcut methods, on the other hand, simplify the separation model while still capturing the full thermodynamic complexity of a mixture. In consequence, non-equilibrium modeling could be integrated into the pinch-based shortcut method directly, allowing to capture complex transport limitations in the early phase of conceptual process design, while the complexity of the overall model is still manageable because the shortcut model is used. In the following, the integration of a non-equilibrium model into the shortcut is briefly discussed for the ternary extraction of itaconic acid from water using 3-methyltetrahydrofuran (3-MTHF) as a solvent. The model for non-equilibrium is briefly introduced followed by a discussion and comparison of the results calculated with the pinch-based shortcut using the equilibrium and non-equilibrium. This survey closes with conclusions on the potential of integrating non-equilibrium modeling in conceptual process design by pinch-based methods.

In Figure 6.3, the schematic of a counter-current column is illustrated. At the interface of the extract and raffinate phase, thermodynamic equilibrium between extract and raffinate phase ($\mathbf{x}^{\mathrm{E}}, \mathbf{x}^{\mathrm{R}}$) is assumed, whereas the mass transport limitations cause non-equilibrium between compositions in the bulk phases ($\mathbf{x}^{\mathrm{E},*}, \mathbf{x}^{\mathrm{R},*}$). The bulk phases enter or leave the stages, which are ordered in a counter-current arrangement. The conservation of mass for each stage and each phase then yields for any stage n

$$0 = L_n^{\mathrm{E}} x_n^{\mathrm{E},*} - L_{n-1,i}^{\mathrm{E}} x_{n-1,i}^{\mathrm{E},*} - l_{n,i}^{\mathrm{E}}, \qquad i = 1,...,C, \tag{6.4}$$

$$0 = L_{n,i}^{\mathrm{R}} x_{n,i}^{\mathrm{R},*} - L_{n+1}^{\mathrm{R}} x_{n+1}^{\mathrm{R},*} + l_{n,i}^{\mathrm{R}}, \qquad i = 1,...,C, \tag{6.5}$$

$$0 = l_{n,i}^{\mathrm{E}} - l_{n,i}^{\mathrm{R}}, \qquad i = 1,...,C, \tag{6.6}$$

where the mass transfer from one phase into the other is described by $\mathbf{l}_n^{\mathrm{E}}$ or $\mathbf{l}_n^{\mathrm{R}}$. For a better readability, the indices n are omitted in the following.

According to the two-film theory (Lewis & Whitman, 1924), the deviation from the thermodynamic equilibrium at the phase interface drives the separation, while diffusive flows ($\mathbf{J}$) in a thin film between the bulk-phases and the interface limit or enhance convective flow. The net flow rate, which is determined by diffusion and convection, is described by

$$l_i^o = J_i^o + x_i^o \sum_{i=1}^{C} l_i^o, \qquad i = 1,...,C, \quad o = \mathrm{E},\mathrm{R}. \tag{6.7}$$

The diffusive part is often described with reasonable accuracy by Fick's law,

$$J_i^o = \frac{\rho_i^o}{M_i^o} k_i^o A \Delta x_i^o, \qquad i = 1,...,C, \quad o = \mathrm{E},\mathrm{R}, \tag{6.8}$$

where $\mathbf{k}$ summarizes transport coefficients, A the area of mass exchange, and Δx the difference of the concentration for each phase.

Diffusive flows from one phase into the other are mainly influenced by the choice of the extractor device. Here, a sieve tray column is investigated according to the non-equilibrum model proposed by Skelland & Conger (1973) and Lao et al. (1989). According to their model, three phenomena control the diffusive mass transport: First, formation (f) of bubbles above the sieve tray, second, rise (r) of bubbles through the continuous phase, and

last, coalescence (c) under the next sieve tray,

$$J_i^o = J_i^{\mathrm{r},o} + J_i^{\mathrm{f},o} + J^{\mathrm{c},o}, \qquad i = 1,...,C-1, \quad o = \mathrm{E},\mathrm{R}, \tag{6.9}$$

$$J_i^{\mathrm{E}} = J_i^{\mathrm{R}}. \tag{6.10}$$

The phenomena of formation and rise account for ninety percent of the phase transport which allows to discard coalescence (Lao et al., 1989).

The modeling of diffusive flows according to Eq. 6.8-6.10 require correlations for transport coefficients, area of mass exchange, and concentration gradient during formation and rise of drops, which are described in the model of Lao et al. (1989) and are here written for short:

$$k_i^{\mathrm{f,o}} = f(x_i^{o,*}, D^0, U_s, U_{\mathrm{O}}, d_{\mathrm{T}}, \rho, \eta), \qquad i = 1,...,C-1, \quad o = \mathrm{E},\mathrm{R}, \tag{6.11}$$

$$k_i^{\mathrm{r,o}} = f(x_i^{o,*}, D^0, U_s, U_{\mathrm{O}}, d_{\mathrm{T}}, \rho, \eta), \qquad i = 1,...,C-1, \quad o = \mathrm{E},\mathrm{R}, \tag{6.12}$$

$$A_n^{\mathrm{f,o}} = f(d_{\mathrm{T}}, N_{\mathrm{O}}), \qquad o = \mathrm{E},\mathrm{R}, \tag{6.13}$$

$$A_n^{\mathrm{r,o}} = f(d_{\mathrm{K}}, d_{\mathrm{D}}, h_{\mathrm{B}}, h_{\mathrm{C}}), \qquad o = \mathrm{E},\mathrm{R}, \tag{6.14}$$

$$\Delta x_i^{\mathrm{r},o} = f(x_i^o, x_i^{o,*}), \qquad i = 1,...,C-1, \quad o = \mathrm{E},\mathrm{R}, \tag{6.15}$$

$$\Delta x_i^{\mathrm{f},o} = f(x_i^o, x_i^{o,*}), \qquad i = 1,...,C-1, \quad o = \mathrm{E},\mathrm{R}. \tag{6.16}$$

These equations add up to multiple additional equations in order to describe the necessary transport coefficients, $\mathbf{k}$, exchange area, A, and concentration differences, $\Delta\mathbf{x}$, which can be functions of diffusion coefficients, $\mathbf{D}$, velocities, U, diameter, d, height, h, density, ρ, and viscosity, η. The comprehensive summary of this non-equilibrium model can be found in Appendix C.

The specifications and results for this case study are summarized in Table 6.3 for an equilibrium-based and non-equilibrium based calculation. Figure 6.4 illustrates the results in a ternary diagram. Circles mark the composition of the first, last and pinch stage calculated with the shortcut model. The pinch point, which is marked as solid circle, experiences liquid-liquid equilibrium because by assuming an infinite number of stages, an infinite number of time to overcome transport limitations is available. The pinch is therefore located on the binodal-line of the miscibility gap. For this example, a stable pinch controls the separation and the composition of the last stage equals the composition of the pinch stage. The first stage, however, shows distinct deviation between the composition at the interface and the composition in the bulk phase.

Figure 6.5 shows for the first stage the concentrations in both bulk phases and at the

Table 6.3.: Specifications and results for shortcut calculation with equilibrium and non-equilibrium-based model. Isothermal temperature at 298 K is assumed.

component	$\mathbf{x}_F$	$\mathbf{x}_S$	$\mathbf{x}_I^R$	$\mathbf{x}_I^E$	$\mathbf{x}_N^E$	$\mathbf{x}_N^R$	flow ratio	
shortcut: equilibrium								
itaconic acid	**0.01**	**0**	**0.005**	0.021	0.050	0.011	S/F	0.052
water	**0.99**	**0**	0.986	0.487	0.539	0.978	L_1^R/F	0.947
3-MTHF	**0**	**1**	0.009	0.491	0.411	0.011	L_N^E/F	0.105
shortcut: non-equilibrium								
itaconic acid	**0.01**	**0**	**0.005**	0.019	0.050	0.011	S/F	0.050
water	**0.99**	**0**	0.987	0.531	0.539	0.978	L_1^R/F	0.947
3-MTHF	**0**	**1**	0.008	0.450	0.411	0.011	L_N^E/F	0.103

interface for the three components itaconic acid, water, and 3-MTHF. At the interface liquid-liquid equilibrium applies, whereas between the interface and the bulk phases transport limitations cause the deviation from the equilibrium

In conclusion, non-equilibrum thermodynamic modeling can be integrated into pinch-based shortcut methods. For the complex non-equilibrium model, good initial values can be retrieved from a preliminary shortcut calculation based on an equilibrium model. Compared to non-equilibrium modeling with rigorous models, the complexity only increases little, because pinch-based methods only require non-equilibrium modeling for the first and the last stage, while the pinch always experiences equilibrium. In subsequent steps, additional stages can be added to the shortcut method according to the previous Section 6.2, not only to improve the accuracy, but also to achieve a robust design of rigorous separation models with non-equilibrium thermodynamic modeling.

Finally, the complex design task for separations which experience distinct deviations from the equilibrium highlights the universal opportunities of pinch-based shortcut methods. The detailed picture of the thermodynamic behavior of any mixture can be covered by pinch-based methods. Thereby, the simplicity of pinch-based shortcut methods, which only covers a limited number of stages and therefore requires less equations than a rigorous model, can be very suitable to integrate the complexity of non-equilibrium modeling, where for each stage directly multiple additional equations need to be considered. In combination with efficient solution strategies for pinch-based methods suggested as part of

this thesis, and in combination with the robust design for rigorous models according to the previous Chapter 6.2, the shortcut allows the reliable design of such complex separation models.

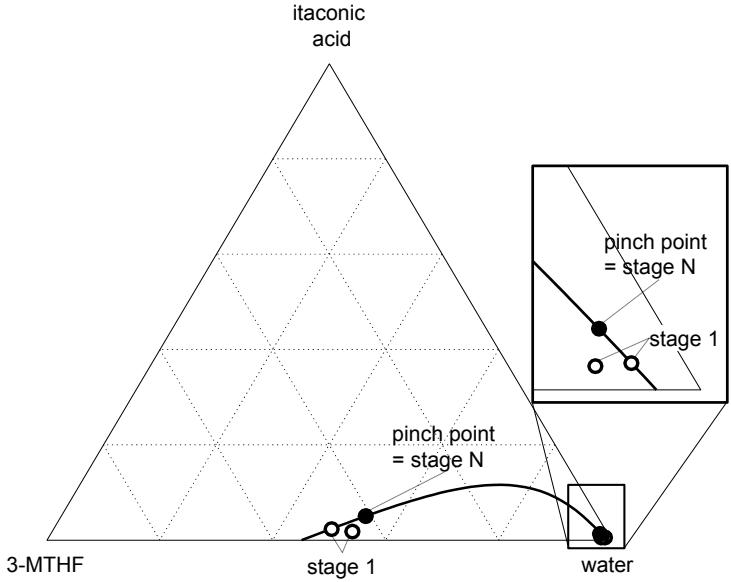

Figure 6.4.: Results for pinch-based shortcut using the non-equilibrium model. The solid line is the liquid-liquid equilibrium at the phase interface. Concentrations away from the solid line represent the bulk phase.

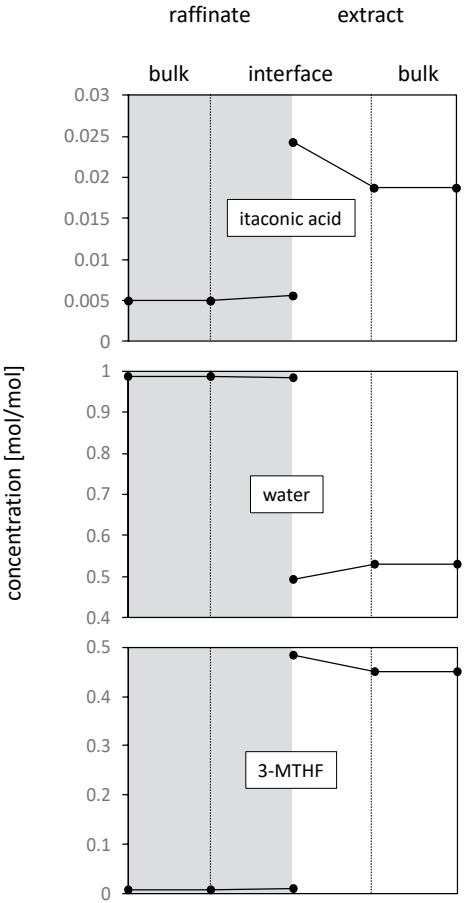

Figure 6.5.: Concentration on the last stage in the two bulk phases and at the interface for itaconic acid, water, and 3-MTHF.

Chapter 7

Conclusions

The conceptual design of energy-efficient processes builds on two paradigms, either the analysis of existing or the synthesis of new processes. Both concepts involve the comparison of a large number of alternatives, which preferably requires simple methods to allow for automated evaluation. Furthermore, processes of different types need to be compared based on a thermodynamically sound objective such as minimum energy demand of a process. One class of design tools which combines all of these requirements are pinch-based shortcut methods.

Pinch-based shortcut methods are well-known for the conceptual process design, and there have been many research efforts in the last decades, most of them focusing on the design of rectification columns. However, some limitations remained unsolved such as the detection of tangential pinch points, simultaneous calculation of outlet streams, as well as the assessment of the inaccuracy, which could be large. In consequence, the extension of these methods to different fields of application stagnated, and pinch-based shortcut methods for the design of absorption or extraction columns were scarce, limited to ternary mixtures, and simplified themodynamic modeling. All of these limitations could be related to the lack of a consistent pinch-based model for general counter-current separation columns.

The novel model is systematically derived by building on analogies between pinch points and fixed points of discrete dynamic systems. Four types of fixed point behavior are identified which are distinguished by the number of stable and unstable eigenvalues. Thereby, tangential pinch points are reliably identified. The pinch-based shortcut model is simple, because it involves the evaluation of only three separation stages within the

model. In particular, the first stage and the last stage are required to balance inlet and outlet streams, and the pinch stage to identify operation at vanishing driving force, i.e., minimum solvent or energy demand. For the approximation of all other necessary stages, a linear approximate by the direction of eigenvectors is employed. The novel shortcut outperforms existing shortcut methods which are not based on pinch points in terms of accuracy. Even though the proposed shortcut model using three stages can show some deviation due to the linear approximation, the accuracy can be arbitrarily refined by adding additional stages. This leads not only to an accurate solution, but allows the transition from the shortcut approximation to the rigorous solution.

The shortcut model facilitates the implementation of tailored solution procedures, which directly allow to screen alternatives represented by different solvents or operating conditions. The suggested procedures for the design of absorption and extraction columns perfectly complement with existing pinch-based methods for rectification columns and heat integration. The combination of pinch-based methods ultimately allows for the comprehensive evaluation of hybrid absorption-rectification and extraction-rectification processes including optimization of the operating point. Altogether, screening of solvents based on optimized process performance is accomplished, targeting minimum operating costs. For different case studies from the fields of absorption and extraction, energy-efficient solvents and their corresponding optimal flowsheet configurations are identified.

The novel pinch-based shortcut methods can be applied to any separation task involving absorption or extraction columns. Regarding the number of components or thermodynamic property modeling, there are no limitations when using the shortcut methods. Therefore, the pinch-based methods can directly be used to screen and benchmark arbitrary solvents and processes. The general model carries over to rectification columns which could allow to determine feasibility, detect tangential pinch points, or improve the accuracy, which is currently not implemented for the pinch-based design of rectification columns. In summary, identification of energy-efficient processes, initialization of rigorous models, as well as screening of operating points, solvents, or processes can directly be addressed.

Finally, the shortcut methods present an effective tool for process analysis and process synthesis. In order to actively support the design of energy-efficient processes, researchers and design engineers are invited to use the Energy-Efficiency Toolbox or any of the software implementations developed as part of this thesis, which are published on the web page of the research group at AVT–Process Systems Engineering, RWTH Aachen University.

Appendix A

General linear approximate solution of the stage-to-stage recurrence

Figure 2.1 illustrates the schematic of the counter-current absorption column. On each stage n, thermodynamic equilibrium between vapor and liquid phase is assumed. It is described by the set of equations

$$0 = y_{n,i} - K(x_{n,i}, y_{n,i}, T_n, p)x_{n,i}, \qquad i = 1,...,C, \tag{A.1}$$

$$0 = 1 - \sum_{i=1}^{C} y_{n,i}. \tag{A.2}$$

If pressure p and C constituents of the liquid composition $\mathbf{x}_n$ are specified, the $C+1$ equations (A.1), (A.2) allow to calculate the unknowns $\mathbf{y}_n$ and T_n if the assumption of the implicit function theorem holds. The equilibrium functions can be written compactly as a set of $C+1$ non-linear equations involving the functions $\mathbf{y}(p,\mathbf{x}_n)$ and $T(p,\mathbf{x}_n)$,

$$\mathbf{0} = \mathbf{F}(p, \mathbf{x}_n, \mathbf{y}(p,\mathbf{x}_n), T(p,\mathbf{x}_n)). \tag{A.3}$$

Inserting these functions for the vapor compositions $\mathbf{y}$ and the boiling temperature T as well as the physical property functions, Eqs (2.6)-(2.8), into the the mass and enthalpy

balances of the stage-to-stage recurrence, Eqs. (2.1)-(2.5), we obtain

$$0 = L_0 x_{0,i} + V_{n+1}\mathbf{y}(p, x_{n+1,i}) - V_1 y_{1,i} - L_n x_{n,i}, \qquad i = 1,...,C, \tag{A.4}$$

$$0 = 1 - \sum_{i=1}^{C} x_{n+1,i}, \tag{A.5}$$

$$\begin{aligned} 0 = {} & L_0 h^{\mathrm{L}}(\mathbf{x}_0, p, T_0) + V_{n+1} h^{\mathrm{V}}(\mathbf{y}(p, \mathbf{x}_{n+1}), p, T(p, \mathbf{x}_{n+1})) - \\ & V_1 h^{\mathrm{V}}(\mathbf{y}_1, p, T_1) - L_n h^{\mathrm{L}}(\mathbf{x}_n, p, T_n). \end{aligned} \tag{A.6}$$

The variables can be separated into design-specific parameters $\phi = (p, \mathbf{x}_0^{\mathrm{T}}, T_0, L_0, \mathbf{y}_1^{\mathrm{T}}, T_1, V_1,)^{\mathrm{T}}$ which are assumed to be given, and variables which represent the next iterate of the recurrence, $\psi = (\mathbf{x}_{n+1}^{\mathrm{T}}, L_n, V_{n+1})^{\mathrm{T}}$. Thus, for given C constituents of the liquid composition $\mathbf{x}_n$, the $C+2$ equations (A.4)-(A.6) allow to calculate the $C+2$ variables ψ. This problem is written as

$$\mathbf{0} = \mathbf{G}(\phi, \mathbf{x}_n, \psi(\phi, \mathbf{x}_n)), \tag{A.7}$$

for short.

Next, the first-order differential $\frac{\partial \phi}{\partial \mathbf{x}_n}$ is calculated by total differentiation of Eq. (A.7),

$$\mathbf{0} = \frac{\partial \mathbf{G}}{\partial L_n}\frac{\mathrm{d}L_n}{\mathrm{d}x_{n,i}} + \frac{\partial \mathbf{G}}{\partial V_{n+1}}\frac{\mathrm{d}V_{n+1}}{\mathrm{d}x_{n,i}} + \sum_{j=1}^{C}\frac{\partial \mathbf{G}}{\partial x_{n+1,j}}\frac{\mathrm{d}x_{n+1,j}}{\mathrm{d}x_{n,i}} + \frac{\partial \mathbf{G}}{\partial x_{n,i}} \qquad i = 1,...,C. \tag{A.8}$$

Rearrangement leads to

$$-\frac{\partial \mathbf{G}}{\partial x_{n,i}} = \frac{\partial \mathbf{G}}{\partial L_n}\frac{\partial L_n}{\partial x_{n,i}} + \frac{\partial \mathbf{G}}{\partial V_{n+1}}\frac{\partial V_{n+1}}{\partial x_{n,i}} + \sum_{j=1}^{C}\frac{\partial \mathbf{G}}{\partial x_{n+1,j}}\frac{\partial x_{n+1,j}}{\partial x_{n,i}} \qquad i = 1,...,C. \tag{A.9}$$

For given partial derivatives $\frac{\partial \mathbf{G}}{\partial \mathbf{x}}$, $\frac{\partial \mathbf{G}}{\partial L_n}$, $\frac{\partial \mathbf{G}}{\partial V_{n+1}}$, and $\frac{\partial \mathbf{G}}{\partial \mathbf{x}_{n+1}}$ the set of linear equations (A.9) can be solved for $\frac{\partial L_n}{\mathbf{x}_n}$, $\frac{\partial V_{n+1}}{\partial \mathbf{x}_n}$, and $\frac{\partial \mathbf{x}_{n+1}}{\partial \mathbf{x}_n}$.

The desired first-order differential $\frac{\partial \mathbf{x}_{n+1}}{\partial \mathbf{x}_n}$ is calculated as a $C \times C$ matrix. However, due to the summation constraint for the mole fractions $\mathbf{x}$, only $C-1$ lines and rows of the matrix are independent and are thus further considered (Poellmann et al., 1994).

The first-order differential is evaluated at the pinch for $n = \mathrm{P}$. The differential can be

approximated by a difference quotient, i.e.,

$$\left.\frac{\partial \mathbf{x}_{\mathrm{n}+1}}{\partial \mathbf{x}_{\mathrm{n}}}\right|_{\mathrm{P}} \approx \frac{\mathbf{x}_{n+1}-\mathbf{x}_{\mathrm{P}}}{\mathbf{x}_{n}-\mathbf{x}_{\mathrm{P}}}, \tag{A.10}$$

which results in a good approximaiton accuracy, if n and $n+1$ are very close to the pinch. Rearrangement of Eq. (A.10) leads to a linear affine discrete dynamical system (Sandefur, 1990),

$$\mathbf{x}_{n+1}-\mathbf{x}_{\mathrm{P}} = \left.\frac{\partial \mathbf{x}_{\mathrm{n}+1}}{\partial \mathbf{x}_{\mathrm{n}}}\right|_{\mathrm{P}} (\mathbf{x}_{n}-\mathbf{x}_{\mathrm{P}}). \tag{A.11}$$

The discrete system represents an iteration scheme. Starting from Eq. (A.11) and building the recurrence leads to

$$\mathbf{x}_{n+1}-\mathbf{x}_{\mathrm{P}} = \left(\frac{\partial \mathbf{x}_{n+1}}{\partial \mathbf{x}_{n}}\right)^{1}_{\mathrm{P}} (\mathbf{x}_{n}-\mathbf{x}_{\mathrm{P}}), \tag{A.12}$$

$$\mathbf{x}_{n+2}-\mathbf{x}_{\mathrm{P}} = \left(\frac{\partial \mathbf{x}_{n+1}}{\partial \mathbf{x}_{n}}\right)^{2}_{\mathrm{P}} (\mathbf{x}_{n}-\mathbf{x}_{\mathrm{P}}), \tag{A.13}$$

$$\mathbf{x}_{n+3}-\mathbf{x}_{\mathrm{P}} = \left(\frac{\partial \mathbf{x}_{n+1}}{\partial \mathbf{x}_{n}}\right)^{3}_{\mathrm{P}} (\mathbf{x}_{n}-\mathbf{x}_{\mathrm{P}}), \tag{A.14}$$

$$\ldots$$

$$\mathbf{x}_{n+l}-\mathbf{x}_{\mathrm{P}} = \left(\frac{\partial \mathbf{x}_{n+1}}{\partial \mathbf{x}_{n}}\right)^{l}_{\mathrm{P}} (\mathbf{x}_{n}-\mathbf{x}_{\mathrm{P}}). \tag{A.15}$$

The iteration sheme allows to calculate iterate $\mathbf{x}_{n+l}$ from an initial composition $\mathbf{x}_n$ after l iterations. Rewritten, a composition $\mathbf{x}_n$ could be calculated from an initial composition $\mathbf{x}_k$, where then the number of iterations l is $n-k$,

$$\mathbf{x}_{n}-\mathbf{x}_{\mathrm{P}} = \left(\frac{\partial \mathbf{x}_{n+1}}{\partial \mathbf{x}_{n}}\right)^{n-k}_{\mathrm{P}} (\mathbf{x}_{k}-\mathbf{x}_{\mathrm{P}}). \tag{A.16}$$

In the following, eigenvalues and eigenvectors of the matrix $\frac{\partial \mathbf{x}_{n+1}}{\partial \mathbf{x}_{n}}$ are used to derive a more convenient right hand side of Eq. (A.16). This is achieved by a basis $\mathbf{U}$ represented by a matrix of eigenvectors $\mathbf{e}$,

$$\mathbf{U} = (\mathbf{e}_1, \mathbf{e}_2, ..., \mathbf{e}_{C-1}). \tag{A.17}$$

The matrix $\frac{\partial \mathbf{x}_{n+1}}{\partial \mathbf{x}_n}$ is regular, which allows to express the matrix by its eigenvalues λ,

$$\left(\frac{\partial \mathbf{x}_{n+1}}{\partial \mathbf{x}_n}\right)^{n-k} = \mathbf{U}\ \mathrm{diag}(\lambda_1, ..., \lambda_{C-1})^{n-k}\ \mathbf{U}^{-1}, \tag{A.18}$$

$$= \mathbf{U}\ \mathrm{diag}(\lambda_1^{n-k}, ..., \lambda_{C-1}^{n-k})\ \mathbf{U}^{-1}. \tag{A.19}$$

Furthermore, any vector can be described by a basis of eigenvectors (Teschl & Teschl, 2013),

$$(\mathbf{x}_k - \mathbf{x}_\mathrm{P}) = \mathbf{U}\ \mathbf{c}, \tag{A.20}$$

where $\mathbf{c}$ are factors corresponding to the eigenvectors.

Finally, substituting Eqs. (A.19) and (A.20) into Eq. (A.16) yields

$$\mathbf{x}_n - \mathbf{x}_\mathrm{P} = \mathbf{U}\ \mathrm{diag}(\lambda_1^{n-k}, ..., \lambda_{C-1}^{n-k})\ \mathbf{U}^{-1}\ \mathbf{U}\ \mathbf{c}, \tag{A.21}$$

$$= \mathbf{U}\ \mathrm{diag}(\lambda_1^{n-k}, ..., \lambda_{C-1}^{n-k})\ \mathbf{c}, \tag{A.22}$$

$$= \sum_{j=1}^{C-1} c_j \lambda_j^{n-k} \mathbf{e}_j, \tag{A.23}$$

which represents the general solution of Eq. (A.11) for an affine linear discrete dynamical system (Sandefur, 1990).

Appendix B

Thermodynamic models

Thermodynamic models are required for the description of the equilibrium and the energy balance. All model equations are implemented in C/C++ in the *props* package according to Figure 5.1 and agree with AspenPlus® thermodynamic property modeling.

Vapor pressure (p_i^S) is a function of temperature (T) and described with Antoine's extended equation,

$$\ln(p_i^S) = c_{1,i} + \frac{c_{2,i}}{T + c_{3,i}} + c_{4,i} \cdot T + c_{5,i} \cdot \ln(T) + c_{6,i} \cdot T^{c_{7,i}}, \tag{B.1}$$

where i represents the model component.

Supercritical components are described by Henry's coefficients, which are described by a temperature dependent polynomial,

$$\ln(H_i) = \ln \frac{H_i^*}{\gamma_i^\infty}, \tag{B.2}$$

$$\ln(H_i^*) = a_i + \frac{b_i}{T} + c_i \ln(T) + d_i \cdot T + \frac{d_i}{T^2}, \tag{B.3}$$

where γ_i^∞ is obtained form the appropriate activity coefficient model.

In this work, activity coefficients γ_i are modeled with the non-random-two-liquid model (NRTL, Renon & Prausnitz (1968)) which allows to describe non-ideal interactions of

binary liquid mixtures,

$$\ln(\gamma_i) = x_j^2 \left[\tau_{j,i} \left(\frac{G_{j,i}}{x_i + x_j \cdot G_{j,i}} \right)^2 + \frac{\tau_{i,j} \cdot G_{i,j}}{\left(x_j + x_i \cdot G_{i,j} \right)^2} \right] \tag{B.4}$$

$$\ln(\gamma_j) = x_i^2 \left[\tau_{i,j} \left(\frac{G_{i,j}}{x_j + x_i \cdot G_{i,j}} \right)^2 + \frac{\tau_{j,i} \cdot G_{j,i}}{\left(x_i + x_j \cdot G_{j,i} \right)^2} \right]$$

$$\ln(G_{i,j}) = -\alpha_{i,j} \cdot \tau_{i,j}$$

$$\ln(G_{j,i}) = -\alpha_{j,i} \cdot \tau_{j,i}$$

$$\tau_{i,j} = c_{1,i,j} + \frac{c_{2,i,j}}{T} + c_{3,i,j} \cdot \ln(T) + c_{4,i,j} \cdot T$$

$$\tau_{j,i} = c_{1,j,i} + \frac{c_{2,j,i}}{T} + c_{3,j,i} \cdot \ln(T) + c_{4,j,i} \cdot T$$

$$\alpha_{i,j} = c_{5,i,j} + c_{6,i,j} \cdot T$$

$$\alpha_{j,i} = c_{5,j,i} + c_{6,j,i} \cdot T\,.$$

The mole-based volume $\ln(v_i^{\mathrm{m}})$ is described with the DIPPR polynomial number 105,

$$\ln(v_i^{\mathrm{m}}) = \frac{c_{2,i}^{1+\left(1-\frac{T}{c_{3,i}}\right)^{c_{4,i}}}}{c_{1,i}}. \tag{B.5}$$

Heat of vaporization H_i^{vap} is described by the DIPPR polynomial number 106,

$$\ln(H_i^{\mathrm{vap}}) = c_{1,i} \cdot \left(1 - T_{\mathrm{r},i}\right)^{\left(c_{2,i} + c_{3,i} \cdot T + c_{4,i} \cdot T_{\mathrm{r},i}^2 + c_{5,i} \cdot T_{\mathrm{r},i}^3\right)}, \quad T_{\mathrm{r},i} = \frac{T}{T_{\mathrm{c},i}}, \tag{B.6}$$

using the critical temperature T_{c} as a reference.

Heat capacities $c_{\mathrm{p,i}}$ are described by the NASA polynomials,

$$c_{\mathrm{p},i} = c_{1,i} + c_{2,i} \cdot T + c_{3,i} \cdot T^2 + c_{4,i} \cdot T^3 + c_{5,i} \cdot T^4\,. \tag{B.7}$$

Appendix C

Non-equilibrium model

Transport limitations in extraction columns can be described by Fick's law according to Eq. 6.8. In the following, equations to describe the concentration gradient, transport coefficients, and mass exchange as a function of drop velocities, geometry of the extractor device, and correlations for the diffusion and drop sizes are summarized. Parameters for pure component are obtained from literature and integrated according to their concentration by mixing rules. The non-equilibrium model in a staged column is taken from Lao et al. (1989) with some updates on the correlations, if more recent correlations existed.

Concentration gradient

The concentration gradient in a staged extraction column is approximated from the concentration difference on two adjacent stages. According to Lao et al. (1989), the gradient can be approximated according to

$$\Delta x_{i,n}^{\text{rise,E}} = x_{i,n}^{\text{E},*} - \frac{x_{i,n+1}^{\text{E}} + x_{i,n}^{\text{E}}}{2}, \qquad i = 1,...C-1, \quad n = 1,...,N, \tag{C.1}$$

$$\Delta x_{i,n}^{\text{rise,R}} = \frac{x_{i,n-1}^{\text{R}} + x_{i,n}^{\text{R}}}{2} - x_{i,n}^{\text{R},*}, \qquad i = 1,...C-1, \quad n = 1,...,N, \tag{C.2}$$

$$\Delta x_{i,n}^{\text{form,E}} = x_{i,n}^{\text{E},*} - x_{n+1,i}^{\text{E}}, \qquad i = 1,...C-1, \quad n = 1,...,N, \tag{C.3}$$

$$\Delta x_{i,n}^{\text{form,R}} = x_{n+1,i}^{\text{R}} - x_{i,n}^{\text{R},*}, \qquad i = 1,...C-1, \quad n = 1,...,N. \tag{C.4}$$

At the first stage, the previous composition $\mathbf{x}_0^{\text{E}}$ is set to the composition of the solvent $\mathbf{x}_{\text{S}}$, and at the last stage the composition of the following stage $\mathbf{x}_{K+1}^{\text{E}}$ is set to the composition of the feed $\mathbf{x}_{\text{F}}$.

Exchange area

During the formation of drops, the exchange area is determined from size and number of drops. Under the assumption of a spherical drop, the size of the drops is determined according to its diameter (d_T). The total number of drops is determined by the number of openings of the sieve tray (N_O),

$$A^\mathrm{form} = N_\mathrm{O} \pi d_\mathrm{T}^2. \tag{C.5}$$

Mass exchange occurs while the drops rise as well as in the hold-up (ϕ), which therefore describes the area of mass exchange. The height of drop rise within one stage is calculated from the height of one stage (h_B) without the height of coalescence (h_C). The effective area is calculated from the total area of the column (d_K) without the sink (d_D),

$$A^\mathrm{rise} = \frac{6\phi}{d_\mathrm{T}} \left(\frac{\pi d_\mathrm{K}^2}{4} - \frac{\pi d_\mathrm{D}^2}{4}\right)(h_\mathrm{B} - h_\mathrm{C}). \tag{C.6}$$

Transport coefficients

Transport coefficients are described by Maxwell-Stefan's law (Krishna, 1977),

$$k_{i,n}^{\mathrm{rise,form},o} = [\mathbf{R}_n^{\mathrm{rise,form}}]^{-1} [\Gamma_n^o][\Theta_n^{\mathrm{rise,form},o}]. \tag{C.7}$$

Binary transport coefficients are summarized in a matrix $\mathbf{R}_n^{\mathrm{rise,form}}$, non-ideality of the transport by binary activity coefficients in Γ, and all other non-idealities in Θ, which allows the integration of actual measurements, if measurements are available. Here, the transport is assumed to be ideal,

$$k_{i,n}^{\mathrm{rise,form},o} = [\mathbf{R}_n^{\mathrm{rise,form}}]^{-1}. \tag{C.8}$$

The matrix is determined from binary transport coefficients (Krishna, 1977),

$$\begin{aligned} R_{n,i,j}^{\mathrm{rise,form},o} = &\left(\frac{x_{n,i}^o}{k_{i,j=C}^{\mathrm{B,rise,form},o}} + \sum_{k=1,k\neq i}^{C} \frac{x_n^o, k}{k_{n,k}^{\mathrm{B,rise,form},o}}\right)\delta_{i,j} \\ &- x_{n,i}^o \left(\frac{1}{k_{n,i,j}^{\mathrm{B,rise,form}}} - \frac{1}{k_{n,i,j=C}^{\mathrm{B,rise,form}}}\right), \qquad n = 1,...,N, \quad i = 1,...,C-1, \end{aligned} \tag{C.9}$$

where δ denotes the Kronecker delta.

The binary transport coefficients are determined from correlations. For the phase of formation of drops, the correlation of Popovich et al. (1964) is used,

$$k_{n,i,j}^{\mathrm{B,form},o} = \sqrt{\frac{D_{n,i,j}^{o} U_{\mathrm{O},n}}{d_{\mathrm{T},n}}}, \qquad o = \mathrm{E},\mathrm{R}, \tag{C.10}$$

which is a function of the diffusion coefficient ($D_{i,j}$), the diameter of the drop (d_{T}), and the velocity at the opening of one stage (U_{O}).

For the phase of rising drops, correlations distinguish between the extract and raffinate phase. For the extract phase, the correlations of Handlos & Baron (1957) apply,

$$k_{n,i,j}^{\mathrm{B,rise,E}} = \frac{0.00375 U_{s,n}}{1 + \eta_n^{\mathrm{E}} / \eta_n^{\mathrm{R}}}, \tag{C.11}$$

which is a function of the velocity (U_s) of a single drop and the viscosity (η). For the raffinate phase the correlation of Ruby & Elgin (1955) are used which are taken from Lao et al. (1989),

$$k_{n,i,j}^{\mathrm{B,rise,R}} = 0.725 \left(\frac{d_{\mathrm{T},n} U_{s,n} \rho_n^{\mathrm{R}}}{\eta_n^{\mathrm{R}}}\right)^{-0.43} \left(\frac{\eta_n^{\mathrm{R}}}{\rho_n^{\mathrm{R}} D_{n,i,j}^{\mathrm{R}}}\right)^{-0.58}, \tag{C.12}$$

and represent a function of the diameter of the drop, the velocity of a single drop, diffusion, viscosity, and density (ρ).

Drop Velocities

The velocities of the swarm of drops,

$$U_{s,n} = \bar{U}_{c,n}(1 - \phi_n), \tag{C.13}$$

is determined from the characteristic velocity of a single drop ($\bar{U}_{c,n}$), which can be determined from single drop measurements and the hold-up (ϕ) (Lo et al., 1983). The hold-up is a function of the velocity of the extract and raffinate phase ($U_n^{\mathrm{E}}, U_n^{\mathrm{R}}$) which can be determined according to

$$0 = U_{s,n}\phi_n(1 - \phi_n) - U_n^{\mathrm{E}}(1 - \phi_n) - f_{\mathrm{A}} U_n^{\mathrm{R}} \phi_n. \tag{C.14}$$

When single drop measurements are not available, the velocity of the single drop can be

estimated according to Lo et al. (1983)

$$\bar{U}_{c,n} = C'\left(\frac{\gamma \Delta\rho_n g}{(\rho^{\mathrm{R}})_n^2}\right)^{\frac{1}{4}}. \tag{C.15}$$

The factor C' depends on the hole diameter and is set to $C' = 1.7$ for a diameter of d_O = 5 mm (Lao et al., 1989).

The averaged velocity in the stage opening U_{O} is between $0.15\,\mathrm{m\,s^{-1}}$ to $0.3\,\mathrm{m\,s^{-1}}$ (Skelland, A. H. P (1974)) and is here set to

$$U_{\mathrm{O}} = 0.2\,\mathrm{m\,s^{-1}}. \tag{C.16}$$

The velocity of the extract and raffinate phase can be calculated from the geometry of the column and the flow rates,

$$U_n^o = \frac{M_n^o}{\rho_n^o}\frac{4L_n^o}{\pi(d_{\mathrm{K}}^2 - d_{\mathrm{K}}^2)}, \qquad o = \mathrm{E,R}. \tag{C.17}$$

In order to avoid flooding and circulation of drops, the velocities should be within some bound. When a bound is violated, a different geometry of the extractor represented by a different diameter should be considered. The maximum velocity in the column should follow (Glanz, 1998)

$$U_{\max} < 40\,\mathrm{m^3\,m^{-2}\,h^{-1}}, \tag{C.18}$$

and the velocity in the sink should be smaller than the stationary drop velocity (Frank, 2008),

$$\min_n U_{\mathrm{D},n} = \max_n U_{c,n}, \tag{C.19}$$

where the velocities are calculated according to

$$U_{\mathrm{D},n} = \frac{L_n^{\mathrm{R}} M_n^{\mathrm{R}}}{\rho_n^{\mathrm{R}}}\frac{4}{\pi d_{\mathrm{D}}^2}, \tag{C.20}$$

$$U_{c,n} = \frac{g d_{\mathrm{T}}^2 \Delta\rho_n}{18\eta_n^{\mathrm{R}}}. \tag{C.21}$$

Geometries

The geometry of the sieve tray column is described by the height of one stage, the height

of coalescence, the diameter of the column, the diameter of the opening of a stage, and the number of holes in a sieve tray. The optimal number of holes for each sieve tray are calculated according to Lo et al. (1983) by

$$\tilde{N}_{\mathrm{O},n} = \left(\frac{L_n^{\mathrm{E}} M_n^{\mathrm{E}}}{\rho_n^{\mathrm{E}}}\right) \frac{4}{\pi d_{\mathrm{O}}^2 U_{\mathrm{O}}}. \tag{C.22}$$

Since the sieve trays will practically have a constant number of holes, the number of holes is set to

$$N_{\mathrm{O},n} = \min_n \tilde{N}_{\mathrm{O}_n}. \tag{C.23}$$

The diameter of the column

$$d_{\mathrm{K}} = \sqrt{\frac{\max_n 4(L_n^{\mathrm{R}} M_n^{\mathrm{R}}/\rho_n^{\mathrm{R}} + L_n^{\mathrm{E}} M_n^{\mathrm{E}}/\rho_n^{\mathrm{E}})}{\pi \cdot 0.826 \cdot U_{\max}}}, \qquad n \in [1, N], \tag{C.24}$$

is a function of the flow rates, density and maximum velocity according to Eq. (C.18).

The diameter of the sieve tray opening (d_{O}) is usually between 3 mm and 8 mm and should not violate

$$\frac{1}{2}\left(\frac{\gamma}{\Delta\rho g}\right)^{1/2} < d_{\mathrm{O}} < \pi\left(\frac{\gamma}{\Delta\rho g}\right)^{1/2}. \tag{C.25}$$

Here, the diameter is set to 5 mm.

The height of one stage is set to

$$\Delta h_{\mathrm{B}} = 0.46\,\mathrm{m}, \tag{C.26}$$

which is the lower bound for a sieve tray column (Lo et al., 1983).

The height of the coalescence is calculated from correlations of Major & Hertzog (1955) which are taken from Pilhofer (1981),

$$\begin{aligned} h_{\mathrm{C},n} = {} & \frac{\rho_n^{\mathrm{E}} U_{\mathrm{O}}^2}{2\Delta\rho_n g(1 - 0.71/\log(\mathrm{Re}_{\mathrm{O},n}))} \\ & + \frac{2.47\rho_n^{\mathrm{R}} U_{\mathrm{D}_n}^2}{\Delta\rho_n g} + \frac{14.72\gamma(\eta_n^{\mathrm{E}})^{0.4}(\eta_n^{\mathrm{R}})^{0.2}}{\Delta\rho_n g d_{\mathrm{O}}^{1.4}}. \end{aligned} \tag{C.27}$$

Mixture Properties

Drop diameter and diffusion coefficients represent characteristic properties of the investigated mixture. The properties are obtained from single drop or pure component measurements, or correlations.

The diameter of the single drop is taken from correlations of Kumar & Hartland (1982),

$$\frac{d_{\mathrm{T},n}}{d_{\mathrm{O}}} = a \cdot \left(\frac{U_{\mathrm{O}}^2 \Delta\rho_n d_{\mathrm{O}}}{\gamma}\right)^b \left(\frac{\Delta\rho_n d_{\mathrm{O}}^2 g}{\gamma}\right)^c. \tag{C.28}$$

The parameters a, b, and c are determined as a function of the Weber number,

$$\mathrm{We}_{\mathrm{O},n} < 2: \quad a = 1.591; b = -0.068; c = -0.278, \tag{C.29}$$

$$\mathrm{We}_{\mathrm{O},n} \geq 2: \quad a = 1.546; b = -0.021; c = -0.214. \tag{C.30}$$

Here, a single diameter for the drops is assumed instead of a population of drop sizes. The diffusion coefficient is calculated acording to correlations of Siddiqi & Lucas (1986),

$$D_{i,j,n}^{o,0} = 9.89 \cdot 10^{-8} \eta_{n,j}^{-0.907} \left(\frac{M_i}{\rho_i}\right)^{-0.45} \left(\frac{M_j}{\rho_j}\right)^{0.265} \cdot T. \tag{C.31}$$

Mixing rules

Mixing rules are applied to determine properties for the binary mixture based on pure component properties for the diffusion coefficients, molar mass, density, and viscosity. For the diffusion coefficient, mixing rules from Wesselingh & Krishna (2006) are applied,

$$D_{n,i,j}^{o} = \left(D_{n,i,j}^{o,0}\right)^{\left(\frac{1+\bar{x}_{n,j}^{o} - \bar{x}_{n,i}^{o}}{2}\right)} \left(D_{n,i,j}^{o,0}\right)^{\left(\frac{1+\bar{x}_{n,i}^{o} - \bar{x}_{n,j}^{o}}{2}\right)}, \tag{C.32}$$

$$\bar{x}_{n,i}^{o} = \frac{x_{n,i}^{o}}{x_{n,i}^{o} + x_{n,j}^{o}}, \tag{C.33}$$

$$\bar{x}_{n,j}^{o} = \frac{x_{n,i}^{o}}{x_{n,i}^{o} + x_{n,j}^{o}}. \tag{C.34}$$

Molar mass and density of the mixture are determined according to Poling et al. (2001)

$$M_n^o = \sum_{i=1}^{C} x_{n,i}^o M_i, \tag{C.35}$$

$$\rho_n^o = \sum_{i=1}^{C} \frac{x_{n,i}^o M_i}{M_n^o} \frac{1}{\rho_i}. \tag{C.36}$$

The viscosity of the mixture is determined by the correlation of Grunberg & Nissan (1949),

$$\log \eta_n^o = \sum_{i=1}^{C} x_{n,i}^o \log \eta_i + \frac{1}{2} \sum_{i=1}^{C} \sum_{j=1}^{C} x_{n,i}^o x_{n,j}^o G_{i,j}. \tag{C.37}$$

The matrix **G** summarizes non-idealites which allow to fit the viscosity with experimental data. Here, non-idealities are discarded and the viscosity is described only by the viscosity of water and solvent; the viscosity of the diluted solutes are discarded.

Bibliography

Achenie, L. E. K., Gani, R., & Venkatasubramanian, V. (Eds.) (2003). Computer aided molecular design: Theory and practice. Volume 12 of *Computer-aided chemical engineering*. (1st ed.). Amsterdam and Boston: Elsevier.

Adjiman, C. S., Galindo, A., & Jackson, G. (2014). Molecules matter: The expanding envelope of process design. In M. Eden, J. D. Siirola, & G. Towler (Eds.), *Proceedings of the 8th International Conference on Foundations of Computer-Aided Process Design* (pp. 55–62). Burlington: Elsevier Science Volume 34 of *Computer Aided Chemical Engineering*.

Agrawal, R. (1996). Synthesis of distillation column configurations for a multicomponent separation. *Industrial & Engineering Chemistry Research*, *35*, 1059–1071.

Alevizou, E. I., & Voutsas, E. C. (2014). Evaluation of COSMO-RS model in binary and ternary mixtures of natural antioxidants, ionic liquids and organic solvents. *Fluid Phase Equilibria*, *369*, 55–67.

Amale, A. S., & Lucia, A. (2008). Non-pinched, minimum energy distillation designs. *Chemical Engineering Research and Design*, *86*, 892–903.

Amaran, S., Sahinidis, N. V., Sharda, B., & Bury, S. J. (2014). Simulation optimization: A review of algorithms and applications. *4OR*, *12*, 301–333.

Audet, C., & Dennis, J. E. (2002). Analysis of generalized pattern searches. *SIAM Journal on Optimization*, *13*, 889–903.

Austin, N. D., Sahinidis, N. V., & Trahan, D. W. (2016). Computer-aided molecular design: An introduction and review of tools, applications, and solution techniques. *Chemical Engineering Research and Design*, *116*, 2–26.

Babi, D. K., Cruz, M. S., & Gani, R. (2016). Fundamentals of process intensification: A process systems engineering view. In J. G. Segovia-Hernández, & A. Bonilla-Petriciolet (Eds.), *Process Intensification in Chemical Engineering* (pp. 7–33). Springer International Publishing.

Bahadori, A., & Vuthaluru, H. B. (2010). A new method for prediction of absorption/stripping factors. *Computers & Chemical Engineering*, *34*, 1731–1736.

Bardow, A., Steur, K., & Gross, J. (2010). Continuous-molecular targeting for integrated solvent and process design. *Industrial & Engineering Chemistry Research*, *49*, 2834–2840.

Barnicki, S. D., & Fair, J. R. (1990). Separation system synthesis: A knowledge-based approach. 1. liquid mixture separations. *Industrial & Engineering Chemistry Research*, *29*, 421–432.

Barnicki, S. D., & Fair, J. R. (1992). Separation system synthesis: A knowledge-based approach. 2. gas/vapor mixtures. *Industrial & Engineering Chemistry Research*, *31*, 1679–1694.

Barnicki, S. D., & Siirola, J. J. (2004). Process synthesis prospective. *Computers & Chemical Engineering*, *28*, 441–446.

Bauer, M., & Stichlmair, J. (1996). Superstructures for the mixed integer optimization of nonideal and azeotropic distillation processes. *Computers & Chemical Engineering*, *20*, 25–30.

Bausa, J. (2001). Näherungsverfahren für den konzeptionellen entwurf und die thermodynamische analyse von destillativen trennprozessen. Volume 692 of *Fortschritt-Berichte // VDI Reihe 3, Verfahrenstechnik*. VDI Verlag.

Bausa, J., & Marquardt, W. (2000). Quick and reliable phase stability test in VLLE flash calculations by homotopy continuation. *Computers & Chemical Engineering*, *24*, 2447–2456.

Bausa, J., Watzdorf, R. v., & Marquardt, W. (1998). Shortcut methods for nonideal multicomponent distillation: I. simple columns. *AIChE Journal*, *44*, 2181–2198.

Beneke, D. A., Kim, S. B., & Linninger, A. A. (2011). Pinch point calculations and its implications on robust distillation design. *Chinese Journal of Chemical Engineering*, *19*, 911–925.

Benson, S. W., & Buss, J. H. (1958). Additivity rules for the estimation of molecular properties. thermodynamic properties. *The Journal of Chemical Physics*, *29*, 546.

Beyn, W.-J., Effenberger, C., & Kressner, D. (2011). Continuation of eigenvalues and invariant pairs for parameterized nonlinear eigenvalue problems. *Numerische Mathematik*, *119*, 489–516.

Beyn, W. J., L Champneys, A., Doedel, E., Kuznetsov, Y. U., Govaerts, W., & Sandstede, B. (2002). Numerical continuation, and computation of normal forms. In B. Hasselblatt, & A. B. Katok (Eds.), *Handbook of dynamical systems* (pp. 149–219). Amsterdam: N.H. North Holland.

Bhattacharyya, D., & Miller, D. C. (2017). Post-combustion CO2 capture technologies — a review of processes for solvent-based and sorbent-based CO2 capture. *Current Opinion in Chemical Engineering*, *17*, 78–92.

Bonet, J., Plesu, V., Bonet-Ruiz, A., Tuluc, A., Iancu, P., Tohaneanu, M. C., & Llorens, J. (2015). Fast solvent screening for counter-current liquid–liquid extraction columns. *Clean Technologies and Environmental Policy*, *17*, 1227–1238.

Bongartz, D., Doré, L., Eichler, K., Grube, T., Heuser, B., Hombach, L., Schiebahn, S., & Mitsos, A. (2016). Comparison of options for transportation fuels produced from renewable hydrogen. *in preparation*, .

Bonvin, D., Georgakis, C., Pantelides, C. C., Barolo, M., Grover, M. A., Rodrigues, D., Schneider, R., & Dochain, D. (2016). Linking models and experiments. *Industrial & Engineering Chemistry Research*, *55*, 6891–6903.

Brüggemann, S. (2005). Rapid screening of conceptual design alternatives for distillation processes. Volume 841 of *Berichte aus dem Lehrstuhl für Prozesstechnik*. Düsseldorf: VDI Verlag.

Brüggemann, S., & Marquardt, W. (2004). Shortcut methods for nonideal multicomponent distillation: 3. Extractive distillation columns. *AIChE Journal*, *50*, 1129–1149.

Brüggemann, S., & Marquardt, W. (2011a). Conceptual design of distillation processes for mixtures with distillation boundaries: I. Computational assessment of split feasibility. *AIChE Journal*, *57*, 1526–1539.

Brüggemann, S., & Marquardt, W. (2011b). Conceptual design of distillation processes for mixtures with distillation boundaries. II. Optimization of recycle policies. *AIChE Journal*, *57*, 1540–1556.

Brunet, J. C., & Liu, Y. A. (1993). Studies in chemical process design and synthesis. 10. An expert system for solvent-based separation process synthesis. *Industrial & Engineering Chemistry Research*, *32*, 315–334.

Bundesministerium für Umwelt, Naturschutz und Reaktorsicherheit (2012). Energiemanagementsysteme in der Praxis, ISO 50001: Leitfaden für Unternehmen und Organisationen.

Bunse, K., Vodicka, M., Schönsleben, P., Brülhart, M., & Ernst, F. O. (2011). Integrating energy efficiency performance in production management – gap analysis between industrial needs and scientific literature. *Journal of Cleaner Production*, *19*, 667–679.

Bureš, M., Majer, V., & Zábranský, M. (1981). Modification of Benson method for estimation of ideal-gas heat capacities. *Chemical Engineering Science*, *36*, 529–537.

Burger, J., Kaul, M., & Hasse, H. (2016). Slope curve method for the analysis of separations in extraction columns of infinite height. *Chemical Engineering Science*, *143*, 105–113.

Burger, J., Papaioannou, V., Gopinath, S., Jackson, G., Galindo, A., & Adjiman, C. S. (2015). A hierarchical method to integrated solvent and process design of physical CO2 absorption using the SAFT-c Mie approach. *AIChE Journal*, *61*, 3249–3269.

Caballero, J. A. (2015). Logic hybrid simulation-optimization algorithm for distillation design. *Computers & Chemical Engineering*, *72*, 284–299.

Caballero, J. A., & Grossmann, I. E. (2008). An algorithm for the use of surrogate models in modular flowsheet optimization. *AIChE Journal*, *54*, 2633–2650.

Caballero, J. A., & Grossmann, I. E. (2014). Optimal synthesis of thermally coupled distillation sequences using a novel MILP approach. *Computers & Chemical Engineering*, *61*, 118–135.

Chen, Y., Eslick, J. C., Grossmann, I. E., & Miller, D. C. (2015). Simultaneous process optimization and heat integration based on rigorous process simulations. *Computers & Chemical Engineering*, *81*, 180–199.

Choi, S. H., Harney, D. A., & Book, N. L. (1996). A robust path tracking algorithm for homotopy continuation. *Computers & Chemical Engineering*, *20*, 647–655.

Clausen, L. R., Elmegaard, B., & Houbak, N. (2010). Technoeconomic analysis of a low CO2 emission dimethyl ether (DME) plant based on gasification of torrefied biomass. *Energy*, *35*, 4831–4842.

Cremaschi, S. (2015). A perspective on process synthesis: Challenges and prospects. *Computers & Chemical Engineering*, *81*, 130–137.

Davison, B. H., & Thompson, J. E. (1993). Continuous direct solvent extraction of butanol in a fermenting fluidized-bed bioreactor with immobilizedclostridium acetobutylicum. *Applied Biochemistry and Biotechnology*, *39-40*, 415–426.

Doherty, M. F. (1985). Properties of liquid-vapour composition surfaces for multicomponent mixtures with constant latent heat. *Chemical Engineering Science*, *40*, 1979–1980.

Doherty, M. F. (2008). Perry's Chemical Engineers' Handbook: Distillation. (8th ed.). McGraw-Hill.

Dörr, M., Wahren, S., & Bauernhansl, T. (2013). Methodology for energy efficiency on process level. *Procedia CIRP*, *7*, 652–657.

Douglas, J. M. (1985). A hierarchical decision procedure for process synthesis. *AIChE Journal*, *31*, 353–362.

Douglas, J. M. (1988). Conceptual Design of Chemical Processes. McGraw-Hill chemical engineering series. New York: McGraw-Hill.

Douglas, J. M. (1995). Synthesis of separation system flowsheels. *AIChE Journal*, *41*, 2522–2536.

Dowidat, C., Kalliski, M., Schembecker, G., & Bramsiepe, C. (2016). Synthesis of batch heat exchanger networks utilizing a match ranking matrix. *Applied Thermal Engineering*, *100*, 78–83.

Dowling, A. W., & Biegler, L. T. (2015). A framework for efficient large scale equation-oriented flowsheet optimization. *Computers & Chemical Engineering*, *72*, 3–20.

Drumm, C. (2014). Energy efficiency management: Energieeffizienz-management und -benchmarking für die prozessindustrie. Technische Informationsbibliothek Universitätsbibliothek Hannover.

Drumm, C., Busch, J., Dietrich, W., Eickmans, J., & Jupke, A. (2013). Structese® – energy efficiency management for the process industry. *Chemical Engineering and Processing: Process Intensification*, *67*, 99–110.

Duran, M. A., & Grossmann, I. E. (1986). A mixed-integer nonlinear programming algorithm for process systems synthesis. *AIChE Journal*, *32*, 592–606.

Eckert, F., & Klamt, A. (2002). Fast solvent screening via quantum chemistry: COSMO-RS approach. *AIChE Journal*, *48*, 369–385.

Eden, M. R., Jørgensen, S. B., Gani, R., & El-Halwagi, M. (2002). Property integration—a new approach for simultaneous solution of process and molecular design problems. In *European Symposium on Computer Aided Process Engineering-12, 35th European Symposium of the Working Party on Computer Aided Process Engineering* (pp. 79–84). Elsevier Volume 10 of *Computer Aided Chemical Engineering*.

Edmister, W. C. (1957). Absorption and stripping-factor functions for distillation calculation by manual- and digital-computer methods. *AIChE Journal*, *3*, 165–171.

Espinosa, J., Brüggemann, S., & Marquardt, W. (2005). Application of the rectification body method to batch rectification. In L. Puigjaner, & A. Espuña (Eds.), *European Symposium on Computer-Aided Process Engineering* (pp. 757–762). Elsevier Volume 20 of *Computer-aided chemical engineering*.

Fahmi, I., Nuchitprasittichai, A., & Cremaschi, S. (2014). A new representation for modeling biomass to commodity chemicals development for chemical process industry. *Computers & Chemical Engineering*, *61*, 77–89.

Fatih Demirbas, M. (2009). Biorefineries for biofuel upgrading: A critical review. *Applied Energy*, *86*, S151–S161.

Felbab, N. (2012). An efficient method of constructing pinch point curves and locating azeotropes in nonideal distillation systems. *Industrial & Engineering Chemistry Research*, *51*, 7035–7055.

Felbab, N., Hildebrandt, D., & Glasser, D. (2011). A new method of locating all pinch points in nonideal distillation systems, and its application to pinch point loci and distillation boundaries. *Computers & Chemical Engineering*, *35*, 1072–1087.

Floudas, C. A. (1999). Recent advances in global optimization for process synthesis, design and control: Enclosure of all solutions. *Computers & Chemical Engineering*, *23*, S963–S973.

Floudas, C. A. (2000). Global optimization in design and control of chemical process systems. *Journal of Process Control*, *10*, 125–134.

Floudas, C. A., Akrotirianakis, I. G., Caratzoulas, S., Meyer, C. A., & Kallrath, J. (2005). Global optimization in the 21st century: Advances and challenges. *Computers & Chemical Engineering*, *29*, 1185–1202.

Franceschini, G., & Macchietto, S. (2008). Model-based design of experiments for parameter precision: State of the art. *Chemical Engineering Science*, *63*, 4846–4872.

Frank, T. C. (2008). Perry's Chemical Engineers' Handbook: Liquid-liquid extraction and other liquid-liquid operations and equipment. Volume 15. McGraw-Hill.

Furman, K. C., & Sahinidis, N. V. (2004). Approximation algorithms for the minimum number of matches problem in heat exchanger network synthesis. *Industrial & Engineering Chemistry Research*, *43*, 3554–3565.

Gani, R. (2004). Computer-aided methods and tools for chemical product design. *Chemical Engineering Research and Design*, *82*, 1494–1504.

Gani, R., Hytoft, G., Jaksland, C., & Jensen, A. K. (1997). An integrated computer aided system for integrated design of chemical processes. *Computers & Chemical Engineering*, *21*, 1135–1146.

Gani, R., Jiménez-González, C., & Constable, D. J. (2005). Method for selection of solvents for promotion of organic reactions. *Computers & Chemical Engineering*, *29*, 1661–1676.

Gatti, M., Martelli, E., Marechal, F., & Consonni, S. (2014). Review, modeling, heat integration, and improved schemes of Rectisol®-based processes for CO2 capture. *PRES'13 Process Integration*, *70*, 1123–1140.

Geilen, F. M. A., Engendahl, B., Harwardt, A., Marquardt, W., Klankermayer, J., & Leitner, W. (2010). Selective and flexible transformation of biomass-derived platform chemicals by a multifunctional catalytic system. *Angewandte Chemie*, *122*, 5642–5646.

Geiser, E., Przybilla, S. K., Friedrich, A., Buckel, W., Wierckx, N., Blank, L. M., & Bolker, M. (2016). Ustilago maydis produces itaconic acid via the unusual intermediate trans-aconitate. *Microbial biotechnology*, *9*, 116–126.

Glanz, S. (1998). Synthese und strukturoptimierung von prozessen zur trennung heterogener flussigkeitsgemische. Volume Nr. 563 of *Fortschritt-Berichte VDI. Reihe 3, Verfahrenstechnik*. Dusseldorf: VDI Verlag.

Gmehling, J. (2009). Present status and potential of group contribution methods for process development. *The Journal of Chemical Thermodynamics*, *41*, 731–747.

Gmehling, J., & Schedemann, A. (2014). Selection of solvents or solvent mixtures for liquid–liquid extraction using predictive thermodynamic models or access to the Dortmund Data Bank. *Industrial & Engineering Chemistry Research*, *53*, 17794–17805.

Groot, W. J., Schoutens, G. H., van Beelen, P. N., van den Oever, C. E., & Kossen, N. W. F. (1984). Increase of substrate conversion by pervaporation in the continuous butanol fermentation. *Biotechnology Letters*, *6*, 789–792.

Groot, W. J., Soedjak, H. S., Donck, P. B., Lans, R., Luyben, K., & Timmer, J. M. K. (1990). Butanol recovery from fermentations by liquid-liquid extraction and membrane solvent extraction. *Bioprocess Engineering*, *5*, 203–216.

Groot, W. J., van der Lans, R., & Luyben, K. (1989). Batch and continuous butanol fermentations with free cells: Integration with product recovery by gas-stripping. *Applied Microbiology and Biotechnology*, *32*, 305–308.

Groot, W. J., van der Lans, R., & Luyben, K. (1992). Technologies for butanol recovery integrated with fermentations. *Process Biochemistry*, *27*, 61–75.

Grossmann, I. E. (2002). Review of nonlinear mixed-integer and disjunctive programming techniques. *Optimization and Engineering*, *3*, 227–252.

Grossmann, I. E., & Biegler, L. T. (2004). Part II. Future perspective on optimization. *Computers & Chemical Engineering*, *28*, 1193–1218.

Grossmann, I. E., & Guillén-Gosálbez, G. (2010). Scope for the application of mathematical programming techniques in the synthesis and planning of sustainable processes. *Computers & Chemical Engineering*, *34*, 1365–1376.

Grossmann, I. E., & Ruiz, J. P. (2012). Generalized disjunctive programming: A framework for formulation and alternative algorithms for MINLP optimization. In J. Lee, & S. Leyffer (Eds.), *Mixed Integer Nonlinear Programming* (pp. 93–115). New York, NY: Springer New York Volume 154 of *The IMA Volumes in Mathematics and its Applications*.

Grunberg, L., & Nissan, A. H. (1949). Mixture law for viscosity. *Nature*, *164*, 799–800.

Handlos, A. E., & Baron, T. (1957). Mass and heat transfer from drops in liquid-liquid extraction. *AIChE Journal*, *3*, 127–136.

Hansen, J. (2006). The threat to the planet. *New York Rev. Books*, *53*, 12–16.

Harmsen, J. (2013). Industrial process scale-up: A practical innovation guide from idea to commercial implementation. Oxford: Elsevier.

Harwardt, A. (2013). Systematic design of separations for processing of biorenewables. Volume 936 of *Berichte aus der Aachener Verfahrenstechnik - Prozesstechnik*. (Als ms. gedr ed.). Düsseldorf: VDI-Verl.

Harwardt, A., Kossack, S., & Marquardt, W. (2008). Optimal column sequencing for multicomponent mixtures. In *18th European Symposium on Computer Aided Process Engineering* Computer Aided Chemical Engineering (pp. 91–96). Elsevier.

Hasan, M. M. F., Baliban, R. C., Elia, J. A., & Floudas, C. A. (2012). Modeling, simulation, and optimization of postcombustion CO2 capture for variable feed concentration and flow rate. 1. chemical absorption and membrane processes. *Industrial & Engineering Chemistry Research*, *51*, 15642–15664.

Henao, C. A., & Maravelias, C. T. (2011). Surrogate-based superstructure optimization framework. *AIChE Journal*, *57*, 1216–1232.

Hoell, D., Mensing, T., Roggenbuck, R., Sakuth, M., Sperlich, E., Urban, T., Neier, W., & Strehlke, G. (2000). 2-butanone. In *Ullmann's Encyclopedia of Industrial Chemistry*. Weinheim, Germany: Wiley-VCH Verlag GmbH & Co. KGaA.

Holland, S. T., Tapp, M., Hildebrandt, D., Glasser, D., & Hausberger, B. (2004). Novel separation system design using "moving triangles". *Computers & Chemical Engineering*, *29*, 181–189.

Hunter, T. G., & Nash, A. W. (1935). Liquid-liquid extraction systems. *Industrial & Engineering Chemistry*, *27*, 836–845.

International Organization for Standardization (2015). Petroleum products - fuels (class F) - specifications of dimethyl ether (DME).

IPCC (2007). Summary for policymakers. In S. Solomon, D. Qin, M. Manning, Z. Chen, M. Marquis, K. B. Averyt, M. Tignor, & H. L. Miller (Eds.), *Climate Change 2007: The Physical Science Basis.*. United Kingdom and New York, NY, USA: Cambridge University Press.

Ishii, S., Taya, M., & Kobayashi, T. (1985). Production of butanol by clostridium acetobutylicum in extractive fermentation system. *Journal of Chemical Engineering of Japan*, *18*, 125–130.

Jaksland, C. A., Gani, R., & Lien, K. M. (1995). Separation process design and synthesis based on thermodynamic insights. *Chemical Engineering Science*, *50*, 511–530.

Jiménez-Islas, H., Martínez-González, G. M., Navarrete-Bolaños, J. L., Botello-Álvarez, J. E., & Oliveros-Muñoz, J. M. (2013). Nonlinear homotopic continuation methods: A chemical engineering perspective review. *Industrial & Engineering Chemistry Research*, *52*, 14729–14742.

Kallrath, J. (2000). Mixed integer optimization in the chemical process industry. *Chemical Engineering Research and Design*, *78*, 809–822.

Kallrath, J. (2005). Solving planning and design problems in the process industry using mixed integer and global optimization. *Annals of Operations Research*, *140*, 339–373.

Kamath, R. S., Grossmann, I. E., & Biegler, L. T. (2010). Aggregate models based on improved group methods for simulation and optimization of distillation systems. *Computers & Chemical Engineering*, *34*, 1312–1319.

Kicherer, A., Schaltegger, S., Tschochohei, H., & Pozo, B. F. (2007). Eco-efficiency. *The International Journal of Life Cycle Assessment*, *12*, 537–543.

Kim, S. B., Ruiz, G. J., & Linninger, A. A. (2010). Rigorous separation design. 1. Multicomponent mixtures, nonideal mixtures, and prefractionating column networks. *Industrial & Engineering Chemistry Research*, *49*, 6499–6513.

Kister, H. Z. (2008). Equipment for distillation, gas absorption, phase dispersion, and phase separation. Volume 14 of *Perry's chemical engineers' handbook*. New York: McGraw-Hill.

Klamt, A. (1995). Conductor-like screening model for real solvents: A new approach to the quantitative calculation of solvation phenomena. *The Journal of Physical Chemistry*, *99*, 2224–2235.

Klamt, A., Eckert, F., & Arlt, W. (2010). COSMO-RS: An alternative to simulation for calculating thermodynamic properties of liquid mixtures. *Annual review of chemical and biomolecular engineering*, *1*, 101–122.

Klatt, K.-U., & Marquardt, W. (2009). Perspectives for process systems engineering—personal views from academia and industry. *Computers & Chemical Engineering*, *33*, 536–550.

Klement, T., & Buchs, J. (2013). Itaconic acid–a biotechnological process in change. *Bioresource technology*, *135*, 422–431.

Klemeš, J. J., & Kravanja, Z. (2013). Forty years of heat integration: Pinch analysis (PA) and mathematical programming (MP). *Current Opinion in Chemical Engineering*, *2*, 461–474.

Knapp, J. P., & Doherty, M. F. (1994). Minimum entrainer flows for extractive distillation: A bifurcation theoretic approach. *AIChE Journal*, *40*, 243–268.

Köhler, J., Poellmann, P., & Blass, E. (1995). A review on minimum energy calculations for ideal and nonideal distillations. *Industrial & Engineering Chemistry Research*, *34*, 1003–1020.

Kong, L., Sen, S. M., Henao, C. A., Dumesic, J. A., & Maravelias, C. T. (2016). A superstructure-based framework for simultaneous process synthesis, heat integration, and utility plant design. *Computers & Chemical Engineering*, .

Kongpanna, P., Babi, D. K., Pavarajarn, V., Assabumrungrat, S., & Gani, R. (2016). Systematic methods and tools for design of sustainable chemical processes for CO2 utilization. *Computers & Chemical Engineering*, *87*, 125–144.

Kossack, S. (2010). A systematic synthesis framework for the conceptual design of distillation processes. Volume Nr. 914 of *Berichte aus der Aachener Verfahrenstechnik - Prozesstechnik*. Düsseldorf: VDI.

Kossack, S., Kraemer, K., & Marquardt, W. (2006). Efficient optimization-based design of distillation columns for homogenous azeotropic mixtures. *Industrial & Engineering Chemistry Research*, *45*, 8492–8502.

Kossack, S., Krämer, K., Gani, R., & Marquardt, W. (2008). A systematic synthesis framework for extractive distillation processes. *Chemical Engineering Research and Design*, *86*, 781–792.

Krämer, K. (2012). Optimization-based synthesis of hybrid separation processes. Volume 934 of *Fortschritt-Berichte VDI / Reihe 3 Verfahrenstechnik*. Aachen: Hochschulbibliothek der Rheinisch-Westfälischen Technischen Hochschule Aachen.

Krämer, K., Harwardt, A., Bronneberg, R., & Marquardt, W. (2011a). Separation of butanol from acetone–butanol–ethanol fermentation by a hybrid extraction–distillation process. *Computers & Chemical Engineering*, *35*, 949–963.

Krämer, K., Harwardt, A., Skiborowski, M., Mitra, S., & Marquardt, W. (2011b). Shortcut-based design of multicomponent heteroazeotropic distillation. *Special Issue on Distillation & Absorption*, *89*, 1168–1189.

Krämer, K., Kossack, S., & Marquardt, W. (2009). Efficient optimization-based design of distillation processes for homogeneous azeotropic mixtures. *Industrial & Engineering Chemistry Research*, *48*, 6749–6764.

Krause, U. (1999). Differenzengleichungen und diskrete dynamische systeme: Eine einführung in theorie und anwendungen. Stuttgart: Teubner.

Kravanja, Z., & Grossmann, I. E. (1990). Prosyn—an MINLP process synthesizer. *Computers & Chemical Engineering*, *14*, 1363–1378.

Kravanja, Z., & Grossmann, I. E. (1993). Prosyn — an automated topology and parameter process synthesizer. *Computers & Chemical Engineering*, *17*, S87–S94.

Kremser, A. (1930). Theoretical analysis of absorption process. *Natural Petroleum News*, (pp. 43–49).

Krishna, R. (1977). A generalized film model for mass transfer in non-ideal fluid mixtures. *Chemical Engineering Science*, *32*, 659–667.

Krishna, R., & Wesselingh, J. A. (1997). The maxwell-stefan approach to mass transfer. *Chemical Engineering Science*, *52*, 861–911.

Kumar, A., & Hartland, S. (1982). Prediction of drop size produced by a multiorifice distributor. *Transactions of the Institution of Chemical Engineers*, (pp. 35–39).

Kurkijärvi, A., Lehtonen, J., & Linnekoski, J. (2014). Novel dual extraction process for acetone–butanol–ethanol fermentation. *Separation and Purification Technology*, *124*, 18–25.

Lao, M., Kingsley, J. P., Krishnamurthy, R., & Taylor, R. (1989). A nonequilibrium stage model of multicomponent separation processes VI: simulation of liquid-liquid extraction. *Chemical Engineering Communications*, *86*, 73–89.

Lee, J. W., Brüggemann, S., & Marquardt, W. (2003). Shortcut method for kinetically controlled reactive distillation systems. *AIChE Journal*, *49*, 1471–1487.

Lee, U., Mitsos, A., & Han, C. (2016). Optimal retrofit of a CO2 capture pilot plant using superstructure and rate-based models. *International Journal of Greenhouse Gas Control*, *50*, 57–69.

Lehmann, A., & Maranas, C. D. (2004). Molecular design using quantum chemical calculations for property estimation. *Industrial & Engineering Chemistry Research*, *43*, 3419–3432.

Levy, S. G., & Doherty, M. F. (1986). A simple exact method for calculating tangent pinch points in multicomponent nonideal mixtures by bifurcation theory. *Chemical Engineering Science*, *41*, 3155–3160.

Levy, S. G., van Dongen, D. B., & Doherty, M. F. (1985). Design and synthesis of homogeneous azeotropic distillations. 2. Minimum reflux calculations for nonideal and azeotropic columns. *Industrial & Engineering Chemistry Fundamentals*, *24*, 463–474.

Lewis, W. K., & Whitman, W. G. (1924). Principles of gas absorption. *Industrial & Engineering Chemistry*, *16*, 1215–1220.

Linnhoff, B., & Hindmarsh, E. (1983). The pinch design method for heat exchanger networks. *Chemical Engineering Science*, *38*, 745–763.

Liu, J., Fan, L. T., Seib, P., Friedler, F., & Bertok, B. (2004). Downstream process synthesis for biochemical production of butanol, ethanol, and acetone from grains: generation of optimal and near-optimal flowsheets with conventional operating units. *Biotechnology progress*, *20*, 1518–1527.

Lo, T. C., Baird, Malcolm H. I, & Hanson, C. (1983). Handbook of Solvent Extraction. New York: Wiley.

Lucia, A., Amale, A., & Taylor, R. (2008). Distillation pinch points and more. *Computers & Chemical Engineering*, *32*, 1342–1364.

Lutze, P., Gani, R., & Woodley, J. M. (2010). Process intensification: A perspective on process synthesis. *Chemical Engineering and Processing: Process Intensification*, *49*, 547–558.

Major, C. J., & Hertzog, R. R. (1955). Flow capacities of sieve-plate liquid-extraction columns. *Chem. Eng. Prog.*, *1*.

Marcilla, A., Gómez, A., Reyes, J. A., & Olaya, M. M. (1999). New method for quaternary systems liquid−liquid extraction tray to tray design. *Industrial & Engineering Chemistry Research*, *38*, 3083–3095.

Marquardt, W. (2005). Model-based experimental analysis of kinetic phenomena in multiphase reactive systems. *Chemical Engineering Research and Design*, *83*, 561–573.

Marquardt, W., Harwardt, A., Hechinger, M., Kraemer, K., Viell, J., & Voll, A. (2010). The biorenewables opportunity - toward next generation process and product systems. *AIChE Journal*, *56*, 2228–2235.

Marquardt, W., Kossack, S., & Kraemer, K. (2008). A framework for the systematic design of hybrid separation processes. *Chinese Journal of Chemical Engineering*, *16*, 333–342.

Masurel, E., Authier, O., Castel, C., & Roizard, C. (2015). Screening method for solvent selection used in tar removal by the absorption process. *Environmental technology*, *36*, 2556–2567.

McCabe, W. L., & Thiele, E. W. (1925). Graphical design of fractionating columns. *Industrial & Engineering Chemistry*, *17*, 605–611.

Minotti, M., Doherty, M. F., & Malone, M. F. (1996). A geometric method for the design of liquid liquid extractors. *Industrial & Engineering Chemistry Research*, (pp. 2672–2681).

Minotti, M., Doherty, M. F., & Malone, M. F. (1998). Design for simultaneous reaction and liquid−liquid extraction. *Industrial & Engineering Chemistry Research*, *37*, 4748–4755.

Misener, R., & Floudas, C. A. (2014). ANTIGONE: Algorithms for continuous/integer global optimization of nonlinear equations. *Journal of Global Optimization*, (pp. 503–526).

Mohanty, S. (2000). Modeling of liquid-liquid extraction column: a review. *Reviews in Chemical Engineering*, *16*.

Mohd Ali, J., Hussain, M. A., Tade, M. O., & Zhang, J. (2015). Artificial intelligence techniques applied as estimator in chemical process systems – a literature survey. *Expert Systems with Applications*, *42*, 5915–5931.

Morar, M., & Agachi, P. S. (2010). Review: Important contributions in development and improvement of the heat integration techniques. *Computers & Chemical Engineering*, *34*, 1171–1179.

Nadgir, V. M., & Liu, Y. A. (1983). Studies in chemical process design and synthesis: Part V: A simple heuristic method for systematic synthesis of initial sequences for multicomponent separations. *AIChE Journal*, *29*, 926–934.

Ng, L. Y., Chong, F. K., & Chemmangattuvalappil, N. G. (2015). Challenges and opportunities in computer-aided molecular design. *Special Issue: Selected papers from the 8th International Symposium on the Foundations of Computer-Aided Process Design (FOCAPD 2014), July 13-17, 2014, Cle Elum, Washington, USA*, *81*, 115–129.

Notz, R., Tönnies, I., Mangalapally, H. P., Hoch, S., & Hasse, H. (2011). A short-cut method for assessing absorbents for post-combustion carbon dioxide capture. *International Journal of Greenhouse Gas Control*, *5*, 413–421.

Nuchitprasittichai, A., & Cremaschi, S. (2013). Optimization of CO2 capture process with aqueous amines - a comparison of two simulation–optimization approaches. *Industrial & Engineering Chemistry Research*, *52*, 10236–10243.

Otto, A. (2015). Chemische, verfahrenstechnische und ökonomische Bewertung von Kohlendioxid als Rohstoff in der chemischen Industrie. Jülich: Forschungszentrum Jülich.

Oudshoorn, A., van der Wielen, L. A. M., & Straathof, A. J. J. (2009). Assessment of options for selective 1-butanol recovery from aqueous solution. *Industrial & Engineering Chemistry Research*, *48*, 7325–7336.

Pajula, E., Seuranen, T., Koiranen, T., & Hurme, M. (2001). Synthesis of separation processes by using case-based reasoning. *Computers & Chemical Engineering*, *25*, 775–782.

Papadopoulos, A. I., Badr, S., Chremos, A., Forte, E., Zarogiannis, T., Seferlis, P., Papadokonstantakis, S., Galindo, A., Jackson, G., & Adjiman, C. S. (2016). Computer-aided molecular design and selection of CO2 capture solvents based on thermodynamics, reactivity and sustainability. *Mol. Syst. Des. Eng.*, *1*, 313–334.

Papadopoulos, A. I., & Linke, P. (2005). A unified framework for integrated process and molecular design. *Chemical Engineering Research and Design*, *83*, 674–678.

Papadopoulos, A. I., & Linke, P. (2006). Multiobjective molecular design for integrated process-solvent systems synthesis. *AIChE Journal*, *52*, 1057–1070.

Papoulias, S. A., & Grossmann, I. E. (1983). A structural optimization approach in process synthesis. *Computers & Chemical Engineering*, *7*, 707–721.

Penner, D., Redepenning, C., Mitsos, A., & Viell, J. (2017). Conceptual design of methyl ethyl ketone production via 2,3-butanediol for fuels and chemicals. *Industrial & Engineering Chemistry Research*, *56*, 3947–3957.

Pérez, R. Y. U. (2005). Targeting and conceptual design of heteroazeotropic distillation processes. Volume Nr. 845 of *Fortschritt-Berichte VDI. Reihe 3, Verfahrenstechnik*. Düsseldorf: VDI Verlag.

Peschel, A., Jörke, A., Sundmacher, K., & Freund, H. (2012). Optimal reaction concept and plant wide optimization of the ethylene oxide process. *Chemical Engineering Journal*, *207-208*, 656–674.

Petlyuk, F., Danilov, R., & Burger, J. (2015). A novel method for the search and identification of feasible splits of extractive distillations in ternary mixtures. *Distillation and Absorption*, *99*, 132–148.

Petlyuk, F. B., & Danilov, R. (2001). Theory of distillation trajectory bundles and its application to the optimal design of separation units: Distillation trajectory bundles at finite reflux. *Chemical Engineering Research and Design*, *79*, 733–746.

Petlyuk, F. B., Danilov, R. Y., & Serafimov, L. A. (2008). Trees of reversible distillation trajectories and the structure of trajectory bundles for sections of adiabatic columns. *Theoretical Foundations of Chemical Engineering*, *42*, 795–804.

Pfennig, A. (2004). Thermodynamik der gemische. Berlin, Heidelberg: Springer Berlin Heidelberg.

Pilhofer, T. (1981). Optimum design of unpulsed sieve-plate extraction columns. *Chemical Engineering Communications*, *11*, 241–254.

Pleşu, V., Bonet Ruiz, A. E., Bonet, J., Llorens, J., & Iancu, P. (2015). Shortcut assessment of alternative distillation sequence schemes for process intensification. *Computers & Chemical Engineering*, *83*, 58–71.

Poellmann, P., Glanz, S., & Blass, E. (1994). Calculating minimum reflux of nonideal multicomponent distillation using eigenvalue theory. *Computers & Chemical Engineering*, *18*, S49–S53.

Poling, B. E., Prausnitz, J. M., & O'Connell, J. P. (2001). The properties of gases and liquids. (5th ed.). New York: McGraw-Hill.

Popovich, A., Jervis, R., & Trass, O. (1964). Mass transfer during single drop formation. *Chemical Engineering Science*, *19*, 357–365.

Press, W. H. (2007). Numerical recipes: The art of scientific computing. (3rd ed.). Cambridge, UK and New York: Cambridge University Press.

Pretel, E. J., López, P. A., Bottini, S. B., & Brignole, E. A. (1994). Computer-aided molecular design of solvents for separation processes. *AIChE Journal*, *40*, 1349–1360.

Qi, W., & Malone, M. F. (2011). Semibatch reactive distillation for isopropyl acetate synthesis. *Industrial & Engineering Chemistry Research*, *50*, 1272–1277.

Qureshi, N., & Ezeji, T. C. (2008). Butanol, 'a superior biofuel' production from agricultural residues (renewable biomass): Recent progress in technology. *Biofuels, Bioproducts and Biorefining*, *2*, 319–330.

Qureshi, N., Hughes, S., Maddox, I. S., & Cotta, M. A. (2005). Energy-efficient recovery of butanol from model solutions and fermentation broth by adsorption. *Bioprocess and biosystems engineering*, *27*, 215–222.

Qureshi, N., Maddox, I. S., & Friedl, A. (1992). Application of continuous substrate feeding to the abe fermentation: Relief of product inhibition using extraction, perstraction, stripping, and pervaporation. *Biotechnology Progress*, *8*, 382–390.

Recker, S., Skiborowski, M., Redepenning, C., & Marquardt, W. (2015). A unifying framework for optimization-based design of integrated reaction–separation processes. *Computers & Chemical Engineering*, *81*, 260–271.

Redepenning, C., & Marquardt, W. (2016). Pinch-based shortcut method for the conceptual design of adiabatic absorption columns. *AIChE Journal*, *86*, 991.

Redepenning, C., Penner, D., & Marquardt, W. (2014). Optimierungsbasierter Entwurf von Extraktionskolonnen mit Nicht-Gleichgewichtsmodellen. *Chemie Ingenieur Technik*, *86*, 1497.

Redepenning, C., Recker, S., & Marquardt, W. (2016). Pinch-based shortcut method for the conceptual design of isothermal extraction columns. *AIChE Journal*, *34*, 1003.

Redepenning, C., Skiborowski, M., & Marquardt, W. (2013). Shortcut method for the design of extraction columns for multi-component mixture separations. *Comput Aided Chem Eng*, (pp. 1039–1044).

Renon, H., & Prausnitz, J. M. (1968). Local compositions in thermodynamic excess functions for liquid mixtures. *AIChE Journal*, *14*, 135–144.

Roffler, S., Blanch, H. W., & Wilke, C. R. (1987a). Extractive fermentation of acetone and butanol: Process design and economic evaluation. *Biotechnology Progress*, *3*, 131–140.

Roffler, S. R., Blanch, H. W., & Wilke, C. R. (1987b). In-situ recovery of butanol during fermentation. *Bioprocess Engineering*, *2*, 1–12.

Rong, B.-G. (2014). A systematic procedure for synthesis of intensified nonsharp distillation systems with fewer columns. *Chemical Engineering Research and Design*, *92*, 1955–1968.

Rooks, R. E., Julka, V., Doherty, M. F., & Malone, M. F. (1998). Structure of distillation regions for multicomponent azeotropic mixtures. *AIChE Journal*, *44*, 1382–1391.

Ruby, C. L., & Elgin, J. C. (1955). Mass transfer between liquid drops and a continous liquid phase in a countercurrent fluidized system: Liquid-liquid extraction in a spray tower. *Chem. Eng. Prog. Symp.*, (pp. 16–17).

Ruiz Beviá, F., Prats Rico, D., & Marcilla Gomis, A. (1984). Liquid-liquid extraction: A graphical method for equilibrium stage calculations for quaternary systems. *Fluid Phase Equilibria*, *15*, 257–265.

Ryll, O., Blagov, S., & Hasse, H. (2012). ∞/∞-analysis of homogeneous distillation processes. *Chemical Engineering Science*, *84*, 315–332.

Salem, A. S. H., Hamad, E. Z., & Al-Naafa, M. A. (1994). Quaternary liquid-liquid equilibrium of n-heptane-toluene-o-xylene-propylene carbonate. *Industrial & Engineering Chemistry Research*, *33*, 689–692.

Saling, P., Kicherer, A., Dittrich-Krämer, B., Wittlinger, R., Zombik, W., Schmidt, I., Schrott, W., & Schmidt, S. (2002). Eco-efficiency analysis by BASF: The method. *The International Journal of Life Cycle Assessment*, *7*, 203–218.

Sandefur, J. T. (1990). Discrete dynamical systems: Theory and applications. Oxford [England] and New York: Clarendon Press and Oxford University Press.

Sanders, J., Clark, J. H., Harmsen, G. J., Heeres, H. J., Heijnen, J. J., Kersten, S., van Swaaij, W., & Moulijn, J. A. (2012). Process intensification in the future production of base chemicals from biomass. *Chemical Engineering and Processing: Process Intensification*, *51*, 117–136.

Scheffczyk, J., Fleitmann, L., Schwarz, A., Lampe, M., Bardow, A., & Leonhard, K. (2016a). COSMO-CAMD: A framework for optimization-based computer-aided molecular design using COSMO-RS. *Chemical Engineering Science*, .

Scheffczyk, J., Redepenning, C., Jens, C. M., Winter, B., Leonhard, K., Marquardt, W., & Bardow, A. (2016b). Massive, automated solvent screening for minimum energy demand in hybrid extraction-distillation using COSMO-RS. *Chemical Engineering Research and Design*, *115*, 433–442.

Schweitzer, P. A. (1988). Handbook of separation techniques for chemical engineers. Volume Sec. 1.9. (2nd ed.). New York: McGraw-Hill.

Seider, W. D., Seader, J. D., Lewin, D. R., & Widagdo, S. (2010). Product and process design principles: Synthesis, analysis and design. (3rd ed.). Chichester: John Wiley.

Sharma, I., Hoadley, A. F., Mahajani, S. M., & Ganesh, A. (2016). Multi-objective optimisation of a Rectisol™ process for carbon capture. *Journal of Cleaner Production*, *119*, 196–206.

Siddiqi, M. A., & Lucas, K. (1986). Correlations for prediction of diffusion in liquids. *The Canadian Journal of Chemical Engineering*, *64*, 839–843.

Siirola, J. J. (1996). Strategic process synthesis: Advances in the hierarchical approach. *Computers & Chemical Engineering*, *20*, S1637–S1643.

Skelland, A. H. P., & Conger, W. L. (1973). A rate approach to design of perforated-plate extraction columns. *Industrial & Engineering Chemistry Process Design and Development*, *12*, 448–454.

Skelland, A. H. P (1974). Diffusional Mass Transfer. New York: Wiley.

Skiborowski, M. (2015). Optimization-based methods for the conceptual design of separation processes for azeotropic mixtures. Volume 946 of *Fortschritt-Berichte VDI : Reihe 3, Verfahrenstechnik*. (Als ms. gedr ed.). Düsseldorf.

Skiborowski, M., Bausa, J., & Marquardt, W. (2016). A unifying approach for the calculation of azeotropes and pinch points in homogeneous and heterogeneous mixtures. *Industrial & Engineering Chemistry Research*, *55*, 6815–6834.

Skiborowski, M., Harwardt, A., & Marquardt, W. (2015). Efficient optimization-based design for the separation of heterogeneous azeotropic mixtures. *Computers & Chemical Engineering*, *72*, 34–51.

Smith, B. D., & Brinkley, W. K. (1960). General short-cut equation for equilibrium stage processes. *AIChE Journal*, *6*, 446–450.

Smith, R. (2016). Chemical process design and integration. (Second edition ed.). Chichester, West Sussex, United Kingdom: John Wiley & Sons, Inc.

Statistisches Bundesamt (30.10.2015). Energieverbrauch in der Industrie im Jahr 2014 geringfügig gestiegen.

Stavrou, M., Lampe, M., Bardow, A., & Gross, J. (2014). Continuous molecular targeting–computer-aided molecular design (CoMT-CAMD) for simultaneous process and solvent design for CO2 capture. *Industrial & Engineering Chemistry Research*, *53*, 18029–18041.

Steffens, M. A., Fraga, E. S., & Bogle, I. (1999). Multicriteria process synthesis for generating sustainable and economic bioprocesses. *Computers & Chemical Engineering*, *23*, 1455–1467.

Steffens, M. A., Fraga, E. S., & Bogle, I. D. L. (2000). Synthesis of bioprocesses using physical properties data. *Biotechnology and Bioengineering*, *68*, 218–230.

Stephanopoulos, G., & Han, C. (1996). Intelligent systems in process engineering: A review. *Computers & Chemical Engineering*, *20*, 743–791.

Struebing, H., Ganase, Z., Karamertzanis, P. G., Siougkrou, E., Haycock, P., Piccione, P. M., Armstrong, A., Galindo, A., & Adjiman, C. S. (2013). Computer-aided molecular design of solvents for accelerated reaction kinetics. *Nature chemistry*, *5*, 952–957.

Sun, L., & Smith, R. (2013). Rectisol wash process simulation and analysis. *Journal of Cleaner Production*, *39*, 321–328.

Tawarmalani, M., & Sahinidis, N. V. (2005). A polyhedral branch-and-cut approach to global optimization. *Mathematical Programming*, *103*, 225–249.

Taylor, R., Krishna, R., & Kooijman, H. (2003). Real-world modeling of distillation. *Chem. Eng. Prog.*, (pp. 28–39).

Teschl, G., & Teschl, S. (Eds.) (2013). Mathematik für informatiker. Springer.

Trespalacios, F., & Grossmann, I. E. (2014). Review of mixed-integer nonlinear and generalized disjunctive programming methods. *Chemie Ingenieur Technik*, *86*, 991–1012.

Ulonska, K., Voll, A., & Marquardt, W. (2016). Screening pathways for the production of next generation biofuels. *Energy & Fuels*, *30*, 445–456.

Umeda, T., Niida, K., & Shiroko, K. (1979). A thermodynamic approach to heat integration in distillation systems. *AIChE Journal*, *25*, 423–429.

Underwood, A. J. V. (1949). Fractional distillation of multicomponent mixtures. *Industrial & Engineering Chemistry*, *41*, 2844–2847.

Urdaneta, R. Y., Bausa, J., Brüggemann, S., & Marquardt, W. (2002). Analysis and conceptual design of ternary heterogeneous azeotropic distillation processes. *Industrial & Engineering Chemistry Research*, *41*, 3849–3866.

U.S. Energy Information Administration (2017). International energy statistics.

van Gerven, T., & Stankiewicz, A. (2009). Structure, energy, synergy, time - the fundamentals of process intensification. *Industrial & Engineering Chemistry Research*, *48*, 2465–2474.

Vedantam, S., Wardle, K. E., Tamhane, T. V., Ranade, V. V., & Joshi, J. B. (2012). CFD simulation of annular centrifugal extractors. *International Journal of Chemical Engineering*, *2012*, 1–31.

Viswanathan, J., & Grossmann, I. E. (1990). A combined penalty function and outer-approximation method for MINLP optimization. *Computers & Chemical Engineering*, *14*, 769–782.

Voll, A., & Marquardt, W. (2012). Reaction network flux analysis: Optimization-based evaluation of reaction pathways for biorenewables processing. *AIChE Journal*, *58*, 1788–1801.

Wallert, C. (2008). Konzeptioneller entwurf und wirtschaftliche bewertung hybrider trennprozesse mit näherungsverfahren. Volume 889 of *Berichte aus dem Lehrstuhl für Prozesstechnik, RWTH Aachen*. Düsseldorf: VDI-Verlag.

Wankat, P. C. (2007). Separation process engineering. (2nd ed.). Upper Saddle River, NJ: Prentice Hall.

von Watzdorf, R., Bausa, J., & Marquardt, W. (1999). Shortcut methods for nonideal multicomponent distillation: 2. complex columns. *AIChE Journal*, *45*, 1615–1628.

Wesselingh, J. A., & Krishna, R. (2006). Mass transfer in multicomponent mixtures. Delft: VSSD.

Westerberg, A. W. (2004). A retrospective on design and process synthesis. *Computers & Chemical Engineering*, *28*, 447–458.

Widagdo, S., & Seider, W. D. (1996). Azeotropic distillation. *AIChE Journal*, *42*, 96–130.

Xiu, Z.-L., & Zeng, A.-P. (2008). Present state and perspective of downstream processing of biologically produced 1,3-propanediol and 2,3-butanediol. *Applied microbiology and biotechnology*, *78*, 917–926.

Yang, X., Dong, H.-G., & Grossmann, I. E. (2012). A framework for synthesizing the optimal separation process of azeotropic mixtures. *AIChE Journal*, *58*, 1487–1502.

Yuan, Z., & Chen, B. (2012). Process synthesis for addressing the sustainable energy systems and environmental issues. *AIChE Journal*, *58*, 3370–3389.

Yuan, Z., Chen, B., & Gani, R. (2013). Applications of process synthesis: Moving from conventional chemical processes towards biorefinery processes. *Computers & Chemical Engineering*, *49*, 217–229.

Zhang, Y., Zhang, S., & Benson, T. (2015). A conceptual design by integrating dimethyl ether (DME) production with tri-reforming process for CO2 emission reduction. *Fuel Processing Technology*, *131*, 7–13.

Zhou, T., Lyu, Z., Qi, Z., & Sundmacher, K. (2015). Robust design of optimal solvents for chemical reactions—a combined experimental and computational strategy. *Chemical Engineering Science*, *137*, 613–625.

Online-Buchshop für Ingenieure

VDI nachrichten

BUCHSHOP

Online-Shops

Fachliteratur und mehr - jetzt bequem online recherchieren & bestellen unter: www.vdi-nachrichten.com/Der-Shop-im-Ueberblick

Täglich aktualisiert: Neuerscheinungen VDI-Schriftenreihen

Im Buchshop von vdi-nachrichten.com finden Ingenieure und Techniker ein speziell auf sie zugeschnittenes, umfassendes Literaturangebot.

Mit der komfortablen Schnellsuche werden Sie in den VDI-Schriftenreihen und im Verzeichnis lieferbarer Bücher unter 1.000.000 Titeln garantiert fündig.

Im Buchshop stehen für Sie bereit:

VDI-Berichte und die Reihe **Kunststofftechnik:**

Berichte nationaler und internationaler technischer Fachtagungen der VDI-Fachgliederungen

Fortschritt-Berichte VDI:

Dissertationen, Habilitationen und Forschungsberichte aus sämtlichen ingenieurwissenschaftlichen Fachrichtungen

Newsletter „Neuerscheinungen":

Kostenfreie Infos zu aktuellen Titeln der VDI-Schriftenreihen bequem per E-Mail

Autoren-Service:

Umfassende Betreuung bei der Veröffentlichung Ihrer Arbeit in der Reihe Fortschritt-Berichte VDI

Buch- und Medien-Service:

Beschaffung aller am Markt verfügbaren Zeitschriften, Zeitungen, Fortsetzungsreihen, Handbücher, Technische Regelwerke, elektronische Medien und vieles mehr – einzeln oder im Abo und mit weltweitem Lieferservice

Die Reihen der Fortschritt-Berichte VDI:

1 Konstruktionstechnik/Maschinenelemente
2 Fertigungstechnik
3 Verfahrenstechnik
4 Bauingenieurwesen
5 Grund- und Werkstoffe/Kunststoffe
6 Energietechnik
7 Strömungstechnik
8 Mess-, Steuerungs- und Regelungstechnik
9 Elektronik/Mikro- und Nanotechnik
10 Informatik/Kommunikation
11 Schwingungstechnik
12 Verkehrstechnik/Fahrzeugtechnik
13 Fördertechnik/Logistik
14 Landtechnik/Lebensmitteltechnik
15 Umwelttechnik
16 Technik und Wirtschaft
17 Biotechnik/Medizintechnik
18 Mechanik/Bruchmechanik
19 Wärmetechnik/Kältetechnik
20 Rechnerunterstützte Verfahren (CAD, CAM, CAE CAQ, CIM ...)
21 Elektrotechnik
22 Mensch-Maschine-Systeme
23 Technische Gebäudeausrüstung

ISBN 978-3-18-3**95503**-9